

Role of Thioredoxin-Interacting Protein (TXNIP) in Regulating Redox Balance and
Mitochondrial Function in Skeletal Muscle

by

Karen Lynn DeBalsi

Department of Pharmacology and Cancer Biology
Duke University

Date: _____

Approved:

Deborah Muoio, Supervisor

Christopher Newgard

Donald McDonnell

Jeff Rathmell

Rosalind Coleman

Dissertation submitted in partial fulfillment of
the requirements for the degree of Doctor
of Philosophy in the Department of
Pharmacology and Cancer Biology in the Graduate School
of Duke University

2013

ABSTRACT

Role of Thioredoxin-Interacting Protein (TXNIP) in Regulating Redox Balance and Mitochondrial Function in Skeletal Muscle

by

Karen Lynn DeBalsi

Department of Pharmacology and Cancer Biology
Duke University

Date: _____

Approved:

Deborah Muoio, Supervisor

Christopher Newgard

Donald McDonnell

Jeff Rathmell

Rosalind Coleman

An abstract of a dissertation submitted in partial fulfillment of the requirements for the degree of Doctor of Philosophy in the Department of Pharmacology and Cancer Biology in the Graduate School of Duke University

2013

Copyright by
Karen Lynn DeBalsi
2013

Abstract

The Muoio lab studies the interplay between lipid whole body energy balance, mitochondrial function and insulin action in skeletal muscle. Data from our lab suggests that lipid-induced insulin resistance in skeletal muscle may stem from excessive incomplete oxidation of fatty acids, which occurs when high rates of β -oxidation exceed TCA cycle flux (Koves et al., 2005; Koves et al., 2008). Most notably, we have shown that mice with a genetically engineered decrease in mitochondrial uptake and oxidation of fatty acids are protected against diet-induced insulin resistance (Koves et al., 2008). This suggests that an excessive and/or inappropriate metabolic burden on muscle mitochondria provokes insulin resistance. Our working model predicts that: 1) high rates of incomplete β -oxidation reflect a state of “mitochondrial stress,” and 2) that energy-overloaded mitochondria generate a yet unidentified signal that mediates insulin resistance. One possibility is that this putative “mitochondrial-derived signal” stems from redox imbalance and disruptions in redox sensitive signaling cascades. Therefore, we are interested in identifying molecules that link redox balance, mitochondrial function and insulin action in skeletal muscle. The work described herein identifies thioredoxin-interacting protein (TXNIP) as an attractive candidate that regulates both glucose homeostasis and mitochondrial fuel selection,

TXNIP is a redox sensitive, α -arrestin protein that has been implicated as a negative regulator of glucose control. Mounting evidence suggested that TXNIP might play a key role in regulating mitochondrial function; however, the molecular nature of this relationship was poorly defined. Previous studies in TXNIP knockout mice reported that deficiency of this protein compromises oxidative metabolism, increases glycolytic activity and promotes production of reactive oxygen species (ROS), while also affording protection against insulin resistance. Therefore, we hypothesized that TXNIP might serve as a nutrient sensor that couples cellular redox status to the adjustments in mitochondrial function. We tested this hypothesis by exploiting loss of function models to evaluate the effects of TXNIP deficiency on mitochondrial metabolism and respiratory function.

In chapter 3, we comprehensively evaluated oxidative metabolism, substrate selection, respiratory kinetics and redox balance in mice with total body and skeletal muscle-specific TXNIP deficiency. Targeted metabolomics, comprehensive bioenergetics analysis, whole-body respirometry and conventional biochemistry showed that TXNIP deficiency results in reduced exercise tolerance with marked impairments in skeletal muscle oxidative metabolism. The deficits in substrate oxidation were not secondary to decreased mitochondrial mass or increased H₂O₂ emitting potential from the electron transport chain. Instead, the activities of several mitochondrial dehydrogenases involved in branched-chain amino acid and ketone catabolism, the

tricarboxylic acid (TCA) cycle and fatty acid β -oxidation were significantly diminished in TXNIP null muscles. These deficits in mitochondrial enzyme activities were accompanied by decreased protein abundance without changes in mRNA expression. Taken together, these results suggest that in skeletal muscle TXNIP plays an essential role in maintaining protein synthesis and/or stability of a subset of mitochondrial dehydrogenase enzymes that permit muscle use of alternate fuels under conditions of glucose deprivation.

Based on these conclusions, we questioned whether additional regulatory mechanisms could contribute to the reduced oxidative metabolism in the absence of TXNIP. Several metabolic enzymes of the TCA cycle have been shown to be redox-sensitive protein targets regulated by the thioredoxin (TRX1/TRX2) and glutathione (GSH) redox-mediated circuits. TXNIP has been shown to respond to oxidative stress by shuttling to the mitochondria where it binds to TRX2 and/or other proteins, thus affecting downstream signaling pathways, such as the apoptotic cascade. Therefore, we speculated whether there was a role for redox imbalance in mediating the mitochondrial phenotype of the TXNIP knockout (TKO) mice. In chapter 4, we present preliminary evidence that increased glucose uptake promotes non-mitochondrial ROS production, causing a shift in redox balance, decreased GSH/GSSG, and S-glutathionylation of α -ketoglutarate dehydrogenase (α -KGD). This post-translational modification protects the protein from permanent oxidative damage, but at the cost of reversible loss of activity

and subsequent disruption of TCA cycle flux that contributes, in part, to the diminished oxidative metabolism observed in the TXNIP deficient mice.

In aggregate, this work sheds new light onto the physiological role of TXNIP in skeletal muscle as it pertains to substrate metabolism and fuel switching in response to nutrient availability. This work has important implications for metabolic diseases such as obesity and type 2 diabetes, which are characterized by marked disruptions in fuel selection.

Dedication

This work is dedicated to the three most influential women in my life: my mother, Cecilia DeBalsi, my godmother, Norine Camara, and my late grandmother, Deomar Camara. Without the unwavering support, love and dedication of these women, I would not be where I am today.

Contents

Abstract.....	iv
List of Tables	xv
List of Figures	xvi
List of Acronyms and Abbreviations	xviii
Acknowledgements	xxii
1. Introduction.....	1
1.1 Background and Rationale.....	1
1.2 Oxidative Stress and Redox Signaling	5
1.3 The Thioredoxin (TXN) and Glutathione (GSH) Redox-Mediated Networks.....	6
1.4 Thioredoxin Interacting Protein (TXNIP).....	7
1.4.1 Description, Structure and Tissue Distribution of TXNIP	7
1.4.2 TXNIP in Disease Pathogenesis	10
1.4.3 Transcriptional Regulation of TXNIP	11
1.5 TXNIP in Metabolic Regulation	13
1.5.1 Peripheral Glucose and Lipid Metabolism and the Fasting Phenotype in Mouse Models of TXNIP Ablation.....	13
1.5.2 TXNIP in Metabolic Syndrome and the Pathogenesis of Type 2 Diabetes Mellitus (T2DM)	17
1.6 Metabolic Regulation by TXNIP is both Redox-Dependent and Redox- Independent	22
1.6.1 Redox-Dependent Regulation.....	22
1.6.2 Redox-Independent Regulation.....	25

1.7	Known and Candidate TXNIP Binding Proteins.....	29
1.8	Regulation of TXNIP.....	32
1.9	Project Summary and Goals	36
2.	Materials and Methods	39
2.1	Reagents.....	39
2.2	Animals.....	39
2.3	Metabolic Phenotype Parameters	40
2.3.1	Glucose Tolerance Test (GTT).....	40
2.3.2	Serum Metabolic Substrates	40
2.3.2.1	Triacylglycerides (TAG)	40
2.3.2.2	Non-Esterified Fatty Acids (NEFA).....	41
2.3.2.3	β -Hydroxybutyrate (BHB).....	42
2.3.3	Blood Glucose and Blood Lactate.....	42
2.3.4	Lactate Dehydrogenase (LDH) Assay.....	42
2.4	Exercise Studies	43
2.5	Mitochondrial Isolation from Mouse Tissue.....	44
2.5.1	Protease Preparation from Gastrocnemius Muscle.....	44
2.5.2	Mechanical Preparation from Gastrocnemius Muscle	45
2.5.3	Mechanical Preparation from Liver	46
2.6	Mouse Embryonic Fibroblasts (MEFs).....	47
2.6.1	Isolation and Culture.....	47
2.7	Substrate Oxidation	48

2.7.1	Isolated Mitochondria	48
2.7.1.1	Pyruvate and Palmitate Oxidation.....	48
2.7.1.2	Leucine Oxidation	49
2.7.2	Whole Muscle	50
2.7.3	MEFs	51
2.7.3.1	Palmitate Oxidation.....	51
2.7.3.2	Leucine Oxidation	52
2.8	Mitochondrial Content / Mass.....	52
2.9	Respirometry / Electron Transport Chain (ETC) Function	52
2.9.1	Isolated Mitochondrial Oxygen Consumption.....	52
2.9.2	Permeabilized Muscle Fiber Bundles (PmFB).....	53
2.9.2.1	Preparation of the PmFB.....	53
2.9.2.2	Mitochondrial Respiration in PmFB	54
2.9.2.3	H ₂ O ₂ Emission in PmFB	55
2.10	Targeted Metabolic Profiling.....	56
2.11	Enzyme Activity Assays.....	56
2.11.1	Citrate Synthase.....	56
2.11.2	Short-Chain Hydroxyacyl-CoA Dehydrogenase (SCHAD)	58
2.11.3	β-Hydroxybutyrate Dehydrogenase (BDH1).....	59
2.11.4	Branched-Chain Ketoacid Dehydrogenase (BCKAD)	59
2.11.5	Isocitrate Dehydrogenase (ICD2 & ICD3)	60
2.11.6	Succinate Dehydrogenase (SDHA).....	61

2.11.7	Pyruvate Dehydrogenase (PDH)	62
2.11.8	Aconitase	62
2.11.9	α -Ketoglutarate Dehydrogenase (α -KGD)	63
2.12	Analysis of mRNA Expression.....	63
2.13	Protein Expression	64
2.14	GSH/GSSG Assay	65
2.14.1.1	Muscle Tissue	65
2.14.1.2	MEFs	67
2.15	NADH and NADPH.....	68
2.16	Statistical Analysis	68
3.	Targeted Metabolomics Connects TXNIP to Adaptive Fuel Selection and Regulation of Specific Mitochondrial Oxidoreductase Enzymes in Skeletal Muscle.....	69
3.1	Introduction	69
3.2	Results.....	72
3.2.1	TXNIP Deficiency Disrupts Whole Body Energy Metabolism.....	72
3.2.2	TXNIP Deficiency Compromises Exercise Tolerance	75
3.2.3	TXNIP Deficiency Diminishes Substrate Oxidation in Muscle but Not Liver Mitochondria.....	78
3.2.4	TXNIP Deficiency Does Not Affect Mitochondrial Content or Respiratory Function	80
3.2.5	TXNIP Deficiency Disrupts Redox Balance Without Affecting Mitochondrial ROS Emission.....	83
3.2.6	Targeted Metabolomics Revealed Several Muscle-Specific Roadblocks in Mitochondrial Carbon Flux.....	86

3.2.7	TXNIP Deficiency Results in Muscle-Specific Deficits in Multiple Dehydrogenase Enzymes	91
3.3	Discussion	95
4.	TXNIP Deficiency Compromises Skeletal Muscle Redox Balance Leading to Glutathionylation and Reduced Activity of α -Ketoglutarate Dehydrogenase	106
4.1	Introduction	106
4.2	Results	107
4.2.1	TXNIP Deficiency Disrupts Redox Balance in Skeletal Muscle	107
4.2.2	Pharmacologically Depleting GSH and Increasing H ₂ O ₂ in L6 Cells Diminishes Fat and Leucine Oxidation	110
4.2.3	N-acetylcysteine (NAC) Partially Rescues Oxidative Failure in TXNIP Deficient MEFs	112
4.2.4	Rescue of Substrate Oxidation with NAC <i>in vivo</i> is Inconclusive	114
4.2.5	TXNIP Deficiency Reduces the Activities of TCA Cycle Enzymes in Skeletal Muscle	115
4.2.6	The Reduced Activity of α -Ketoglutarate Dehydrogenase is Secondary to Glutathionylation	117
4.3	Discussion	118
5.	Conclusions, Remaining Questions and Future Directions	122
5.1	How Does TXNIP Regulate the Mitochondrial Dehydrogenases?	124
5.1.1	Does TXNIP and/or TXN Stabilize the Mitochondrial Dehydrogenases? ...	124
5.1.2	Is Stability Modulated through Direct Binding of TXNIP or TXN to the Mitochondrial Dehydrogenases?	125
5.1.3	Is Translation of the Mitochondrial Dehydrogenases Promoted through mRNA Binding of TXNIP?	128

5.2	Imbalances in Cellular Energetic Metabolites and the Redox State	131
5.2.1	The State of the Reducing Equivalents	131
5.2.2	What is the Source of ROS and Does It Contribute to the TKO Metabolic Phenotype?	135
5.2.3	How is the Insulin-Signaling Cascade Augmented in the TKO Skeletal Muscle?	137
5.2.4	Are Other Mitochondrial Proteins S-Glutathionylated?	141
5.3	Why is PDH Activity Decreased in Heart but Not Skeletal Muscle in the Absence of TXNIP?.....	142
5.4	What Effects Would a High Fat Diet Have on TKO Mice?	146
5.4.1	Muscle Insulin Resistance, Lipid Oversupply and Mitochondrial Stress....	146
5.4.2	TXNIP Expression Increases in Association with Fat, Incomplete Fat Oxidation and Decreases in Response to Pharmacological Inhibition of Fat Oxidation	150
5.4.3	Are TKO Mice More Susceptible to Diet-Induced Mitochondrial Dysfunction?	152
5.4.4	Does Mitochondrial Dysfunction in TKO Mice Exacerbate or Protect Against Diet-Induced Defects in the Proximal Arm of the Insulin-Signaling Cascade?	154
5.5	Summary	156
	References.....	157
	Biography	182

List of Tables

Table 1: Mitochondrial Dehydrogenase Activity	92
---	----

List of Figures

Figure 1-1: The Glutathione / Thioredoxin Regulatory Networks.....	7
Figure 1-2: Structure of the N-terminal domain of human TXNIP.....	9
Figure 1-3: TXNIP mRNA expression tissue distribution.....	10
Figure 1-4: Summary of TXNIP Transcriptional Regulation and Function.....	13
Figure 3-1: TXNIP Deficiency Alters Whole Body Energy Metabolism.....	75
Figure 3-2: TXNIP Deficiency Decreases Exercise Tolerance	78
Figure 3-3: Mitochondrial Substrate Oxidation in Skeletal Muscle and Liver	79
Figure 3-4: Mitochondrial Content and Respiratory Function in Skeletal Muscle	83
Figure 3-5: Redox Imbalance In TXNIP Deficient Skeletal Muscles	85
Figure 3-6: Targeted Metabolic Profiling of Skeletal Muscle and Serum	90
Figure 3-7: Targeted Metabolic Profiling of Liver	90
Figure 3-8: Expression of Mitochondrial Dehydrogenase Enzymes in Skeletal Muscle and Liver	94
Figure 3-9: TXNIP Deficiency Disrupts Mitochondrial Fuel Selection.....	99
Figure 3-10: TXNIP Preserves Skeletal Muscle Mitochondrial Capacity to Switch Substrates During Glucose Deprivation.	104
Figure 4-1: Redox Imbalance in TXNIP Deficient Skeletal Muscle	109
Figure 4-2: Decrease in GSH Concentration after 24 h Treatment with BSO	110
Figure 4-3: Depletion of GSH and Addition of H ₂ O ₂ Diminishes Substrate Oxidation in L6 Cells	112
Figure 4-4: NAC Partially Rescues Oxidative Failure in TXNIP Deficient MEFs.....	114
Figure 4-5: NAC Supplementation Has Mixed Results on Substrate Oxidation <i>in vivo</i>	115

Figure 4-6: TXNIP Deficiency Disrupts Two TCA Cycle Enzymes Susceptible to Redox Regulation in Skeletal Muscle	116
Figure 4-7: Reversing S-glutathionylation Completely Rescues the Activity of α -ketoglutarate dehydrogenase	118
Figure 5-1: The Malate-Aspartate Shuttle.....	133
Figure 5-2: Models of Lipid Dysregulation and Skeletal Muscle Insulin Resistance	149
Figure 5-3: TXNIP Expression Increases in Association with Fat, Incomplete Fat Oxidation and Decreases in Response to Pharmacological Inhibition of Fat Oxidation	151

List of Acronyms and Abbreviations

ACS	acyl-CoA synthetase
AARDC1-5	α -arrestin proteins 1-5
α -KGD	alpha-ketoglutarate dehydrogenase
ASK1	apoptosis signaling kinase 1
BCAA	branched-chain amino acid
BCKAD	branched-chain ketoacid dehydrogenase
BDH1	beta-hydroxybutyrate dehydrogenase
BHB	beta-hydroxybutyrate
BSA	bovine serum albumin
BSO	buthione sulfoximine
ChoRE	carbohydrate response element
DAG	diacylglycerol
DMEM	Dulbecco's Modified Eagle Medium
EDL	extensor digitorum longus
ETC	electron transport chain
FCHL	familial combined hyperlipidemia
GSH	reduced glutathione
GSIS	glucose stimulated insulin secretion
GSSG	oxidized glutathione

GTT	glucose tolerance test
ICD2	isocitrate dehydrogenase 2 (NADP ⁺ -dependent)
ICD3	isocitrate dehydrogenase 3 (NAD ⁺ -dependent)
IR	insulin receptor
IRS-1	insulin receptor substrate-1
JAB1	jun activating binding protein
KHB	Krebs Henseleit buffer
LCFA-CoA	long-chain fatty acid acyl-CoA
LDH	lactate dehydrogenase
M2VP	1-methyl-2-vinyl-pyridium trifluoromethane sulfonate
MEFs	mouse embryonic fibroblasts
NAD ⁺	nicotinamide adenine dinucleotide
NADH	nicotinamide adenine dinucleotide, reduced
NADP ⁺	nicotinamide adenine dinucleotide phosphate
NADPH	nicotinamide adenine dinucleotide phosphate, reduced
NEFA	non-esterified fatty acids
NLRP3	NLR protein 3
OXPHOS	oxidative phosphorylation
PBS	phosphate buffered saline
PBS/P-S	phosphate buffered saline with penicillin and streptomycin

PDH	pyruvate dehydrogenase
PmFB	permeabilized muscle fiber bundles
PPAR γ	peroxisome-activated receptor- γ
RER	respiratory exchange ratio
ROS	reactive oxygen species
SCHAD	short-chain hydroxyacyl-CoA dehydrogenase
SDHA	succinate dehydrogenase
SDS	sodium dodecyl sulfate
SET	sucrose, EDTA, tris-HCl buffer
STZ	streptozotocin
T2DM	type 2 diabetes mellitus
TAG	triacylglycerides
TBP-2 ^{-/-}	thioredoxin binding protein 2 targeted inactivation mouse
TCA	tricarboxylic acid cycle
TKO	thioredoxin interacting protein knockout mouse (whole-body)
TXN1	thioredoxin (cytosolic isoform)
TXN2	thioredoxin (mitochondrial isoform)
TXNIP	thioredoxin interacting protein
TXNIP ^{fl/fl}	thioredoxin interacting protein floxed control
TXNIP ^{skm-/-}	muscle-specific thioredoxin interacting protein knockout mouse

TXNIP-null thioredoxin interacting protein targeted gene deletion mouse

UV ultraviolet light

UTR untranslated region

Acknowledgements

Pursuit of a Ph.D. is a long process, often beginning earlier in life than one actually realizes. Success requires unmitigated support from others. Oddly, I believe that reinforcement comes from those who believed...and from those who didn't. Therefore, at this time I would like to acknowledge both.

First, I would like to thank the members of my current lab. To my P.I., Debbie Muoio, thank you (and "meow"☺) for the opportunity to study in your lab and for never settling despite my many protestations, to Tim Koves, thank you for your patience and advice, to April Wittmann and Dorothy Slentz, thank you for your willingness to teach, to Kari Wong and Mike Davies, thank you for keeping it real and fun. Most of all, I would like to thank my lab wife, Sarah Seiler, without whom I would not have made it. I will miss the laughter, the complaining, the baked goods and the evil scheming. Although it is time for us to part, remember that we will always have Wrightsville Beach ☺.

Second, I would like to thank my committee members, Chris Newgard, Rosalind Coleman, Donald McDonnell, Jeff Rathmell and Debbie Muoio for their guidance.

Third, I would like to thank my previous mentors, Jeff Bowen, Ed Brush and Merri Krevosky, for preparing me for this journey.

Mostly, I would like to thank all of my family for their love and support of my many endeavors: my parents, Ralph and Cecilia DeBalsi; my brothers, Tony and Jason DeBalsi; my godfather, Paul Camara; my godmother and her husband, Norine and Joe Camara; my favorite nephew, Marlo DeBalsi, my sisters-in-law, Sherrilyn and Edie DeBalsi; my cousin John Terceira; my late aunts, Daguimar and Adeline, and to whom I miss the most, my late grandmother Deomar Camara. You are always with me!

Lastly, those who don't believe often provide the greatest motivation, so I would like to thank my high school chemistry teacher, Mrs. Ladetto, who told me that I was "not cut out for the sciences" and should choose a different career path. I often thought of this when I wanted to give up on my dream, so to you I say with the utmost sincerity, "HA!"

1. Introduction

Herein, I provide a general background and rationale for this thesis project followed by a comprehensive review of TXNIP. Details are provided about oxidative stress and the thioredoxin and glutathione redox-regulating circuits. The structure, transcriptional regulation and function of TXNIP in the pathogenesis of various diseases are also discussed. There is a particular emphasis on metabolism and insulin resistance, including the known redox-dependent and -independent ways by which TXNIP may modulate these disease states. Finally, this section concludes with what is currently known about TXNIP regulation followed by a project summary and goals statement.

1.1 *Background and Rationale*

Mitochondrial dysfunction is a hallmark in nearly all pathological and toxicological conditions (Pieczenik and Neustadt, 2007). Conditions range from exercise intolerance to sarcopenia, neurodegenerative diseases including Alzheimer's and Parkinson's, inherited diseases such as from Kearns-Sayre syndrome and MERRF (myoclonic epilepsy and ragged-red fibers) and acquired diseases including cancer, cardiovascular disease and diabetes, the latter of which is a focal point of the Muoio lab. A major symptom of metabolic disorders such as diabetes and obesity is peripheral insulin resistance, which occurs when there are impairments in insulin-stimulated uptake, storage and disposal of glucose, particularly in skeletal muscle.

The etiology of insulin resistance has been linked to metabolic insults such as overnutrition, dyslipidemia and mitochondrial malfunction. One theory of lipid-induced skeletal muscle insulin resistance proposes that increased systemic lipid delivery, coupled with reduced mitochondrial fat oxidation due to “mitochondrial respiratory dysfunction,” leads to rising intracellular fatty acid metabolites, such as long-chain acyl-CoAs (LCFA-CoAs), diacylglycerol (DAG) and ceramides. These cytosolic lipids are thought to activate serine/threonine kinases, such as protein kinase C (PKC), resulting in constitutive serine phosphorylation of the insulin receptor (IR) and insulin receptor substrate-1 (IRS-1) proteins, and thus inhibition of PI3K-Akt activity and GLUT4 translocation (Itani et al., 2002; Morino et al., 2006; Petersen and Shulman, 2002). However, other lines of evidence suggest that mitochondrial dysfunction might occur as a late-stage consequence of overnutrition and/or insulin resistance rather than a root cause. Data from our lab suggests that diet-induced and genetic forms of insulin resistance stem from high rates of incomplete fat oxidation, which occurs when high rates of β -oxidation exceeds TCA cycle flux, as evidenced by high intramuscular levels of LCFA-carnitine esters and reduced TCA cycle intermediates (Koves et al., 2005; Koves et al., 2008). Moreover, two genetically engineered models of reduced mitochondrial metabolism actually enhance insulin action. For example, malonyl-CoA decarboxylase knockout (*mcd*^{-/-}) mice have reduced β -oxidation, due to high levels of malonyl-CoA and are protected against high fat-induced glucose intolerance (Koves et al., 2008). In a

second model, ablation of apoptosis-inducing factor (AIF), the primary physiological role of which is the maintenance of a fully functional electron transport chain, results in decreased mitochondrial oxidative phosphorylation (OXPHOS), but protection from obesity and insulin resistance (Pospisilik et al., 2007). Therefore, one would hypothesize that an excessive and/or inappropriate metabolic load on muscle mitochondria, rather than oxidative potential, would provoke insulin resistance. The current working hypothesis of the Muoio lab is two-fold: 1) high rates of incomplete β -oxidation reflect a state of “mitochondrial stress,” and 2) that energy-overloaded mitochondria generate a yet unidentified signal that mediates insulin resistance. This proposed “mitochondrial-derived signal” could stem from disturbances in substrate selection, anaplerotic and/or cataplerotic carbon flux, production of reactive oxygen species (ROS), redox imbalance or possibly, disruptions in redox sensitive signaling cascades (Muoio and Neuffer, 2012). Therefore, we are interested in identifying molecules that link redox balance, mitochondrial function and insulin action in skeletal muscle.

TXNIP is an α -arrestin protein involved in redox sensing and metabolic control, which is described in depth in subsequent sections. Briefly, TXNIP is an endogenous negative regulator of thioredoxin (TXN) activity and sensitizes the cell to oxidative stress (Nishiyama et al., 1999). Moreover, the few mouse strains with natural or targeted deletions of TXNIP have hypertriglyceridemia, hypercholesterolemia and increased secretion of liver lipoproteins (Oka et al., 2006b). In addition to lipid metabolism, TXNIP

is also involved in glucose homeostasis. A role for TXNIP as a negative regulator of glucose metabolism is supported by reports showing that TXNIP mRNA expression is elevated in muscle of insulin resistant and diabetic humans (Parikh et al., 2007). Moreover, silencing TXNIP expression in human adipocytes and skeletal muscle myocytes enhanced glucose uptake, whereas TXNIP overexpression inhibited glucose uptake. Revealed to be reciprocally regulated by insulin and glucose, TXNIP is proposed to function as a homeostatic switch that regulates glucose uptake in peripheral tissue (Parikh et al., 2007). Emerging evidence has suggested a link between TXNIP and mitochondrial function. For instance, TXNIP knockout mice have an increased dependence on glycolysis, with high levels of circulating free fatty acids and ketones, thus suggesting decreased oxidation of these substrates and compromised TCA cycle and respiratory function (Bodnar et al., 2002; Donnelly et al., 2004; Hui et al., 2004; Sheth et al., 2005). Although speculation as to the complex molecular mechanisms underlying the regulatory capacity of TXNIP in mitochondrial function has been widespread, rigorous experimental evaluation has been lacking.

Since TXNIP, with its connection to redox biology, metabolic control and insulin action, appeared to be one of the aforementioned molecules of interest occupying a crucial position for mitochondrial regulation, we chose to investigate its physiological role in regulating skeletal muscle mitochondrial metabolism. We hypothesized that TXNIP would directly regulate mitochondrial function at the level of bioenergetics,

oxidative metabolism, redox balance and substrate selection. In this work, we share our results in undertaking this challenge.

1.2 Oxidative Stress and Redox Signaling

Reactive oxygen species (ROS) are produced by all aerobic organisms. Levels of ROS generated in excessive quantities can result in oxidative stress (Nordberg and Arner, 2001). Within physiological concentrations, however, ROS are involved in intracellular signaling and redox regulation, functioning as secondary messengers (Thannickal and Fanburg, 2000) or altering control of transcription factors (Dalton et al., 1999; Morel and Barouki, 1999). Primary sources of intracellular ROS are: 1) mitochondrial-derived through leakage from the electron transport chain (ETC) or 2) cytosol-derived through excessive stimulation of NADPH oxidases (Valko et al., 2007). When endogenous antioxidant networks are unable to compensate for increased concentrations of ROS, redox systems become imbalanced leading to tissue and cellular damage, such as mutations in DNA, lipid peroxidation and formation of disulfide bonds in proteins (Melov, 2000; Nordberg and Arner, 2001). Ultimately, this may lead to oxidative stress-related disorders such as diabetes mellitus, cancer, cardiovascular disease, neurodegenerative disease and inflammation (Evans et al., 2002; Kovacic and Somanathan, 2012; Madamanchi and Runge, 2013; Popolo et al., 2013; Valko et al., 2007).

1.3 The Thioredoxin (TXN) and Glutathione (GSH) Redox-Mediated Networks

The TXN and GSH redox-mediated networks are responsible for monitoring and controlling cellular redox balance. Both depend on NADPH and utilize reversible redox-active disulfide/thiol (free sulfhydryl) exchange reactions known as sulfur switches (Jones, 2008; Nordberg and Arner, 2001). In its reduced form, TXN utilizes cysteine residues (Cys-Gly-Pro-Cys) at redox active sites to reduce oxidized disulfide substrates. Thioredoxin reductase then catalyzes the reduction of TXN utilizing an electron transferred by NADPH. In the homologous GSH system, GSH functions as a critical antioxidant by detoxifying H_2O_2 via glutathione peroxidase. The resulting oxidized glutathione (GSSG) is reduced back to GSH via glutathione reductase with the electron/ H^+ donated by NADPH (Fig. 1-1). Additionally, GSSG can react with protein thiols, which can subsequently be reduced by glutaredoxin (not shown).

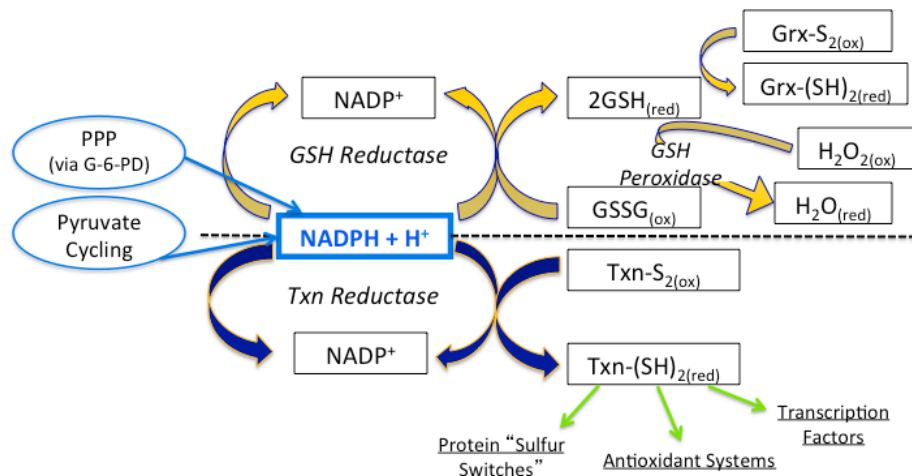


Figure 1-1: The Glutathione / Thioredoxin Regulatory Networks

The GSH/TXN redox regulatory networks both use the reducing power of NADPH, which is provided from the pentose phosphate pathway (PPP) and/or from pyruvate cycling, to either form reduced glutathione (GSH) or reduced thioredoxin (TXN), antioxidants which are involved in downstream pathways as shown.

The exact number of redox-sensitive protein targets regulated by these networks is unknown, but the current list encompasses proteins that function in mitochondrial protein import (Koehler et al., 2006), several metabolic enzymes of the tricarboxylic acid (TCA) cycle and the β -oxidation pathways, and several phosphatases involved in insulin signaling (Jones, 2006).

1.4 Thioredoxin Interacting Protein (TXNIP)

1.4.1 Description, Structure and Tissue Distribution of TXNIP

TXNIP was first reported as an upregulated gene in HL-60 leukemia cells stimulated with 1,25-dihydroxyvitamin D₃ (Chen and DeLuca, 1994). It was later

isolated in a yeast two-hybrid screen to identify TXN-binding proteins (Nishiyama et al., 1999; Yamanaka et al., 2000) and has since been shown to bind to the redox-active site cysteine residues of TXN1 and TXN2 (Patwari et al., 2006), thus serving as an endogenous negative regulator of TXN activity and sensitizing the cell to oxidative stress (Nishiyama et al., 1999).

Structurally, TXNIP has seven conserved domains that it shares with the α -arrestin scaffold family, (Alvarez, 2008). Spindel et al. (2012) identified critical residues and domains that are exposed to mediate protein-protein interactions. The NH₂ domain contains two SH3-binding domains, and the COOH domain contains two PPxY motifs and three SH3 domains (Fig. 1-2). The authors propose the SH3 domains mediate scaffold functions, while the PPxY motifs mediate TXNIP ubiquitination via the E3-ubiquitin ligase Itch (Zhang et al., 2010). Two other redox-sensitive residues are Tyr279, which facilitates interaction with phosphotyrosine phosphatases, such as PTEN and SHP-2 (Spindel et al., 2012), and Cys247, which is used to form the mixed disulfide bond with TXN (Patwari et al., 2006). Taken together, this demonstrates the importance of TXNIP for regulating multiple biological processes in both a redox-dependent and redox-independent manner.

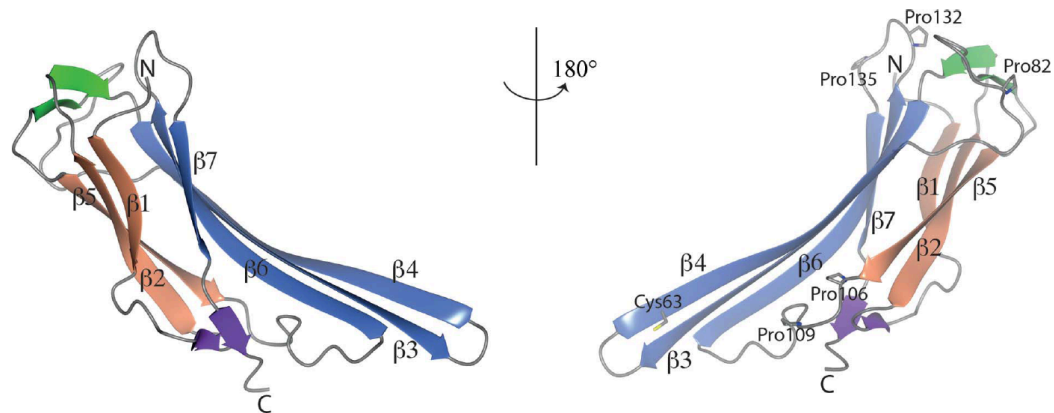


Figure 1-2: Structure of the N-terminal domain of human TXNIP.

The two antiparallel β -sheets (orange and blue), the Cys63 residue for binding to TXN and the SH3 domains are shown as stick structures (Polekhina et al., 2013). PDB Reference: TXNIP, 4gei.

TXNIP protein is ubiquitously expressed in all major metabolic tissues (Junn et al., 2000), however, mRNA levels are highly expressed in oxidative tissues, such as the heart and skeletal muscle, with lesser expression in lipogenic tissues, such as the liver and brain, which may hint at varying functions in different tissues (Fig. 1-3). Additionally, TXNIP protein has been localized to multiple cellular locations, including the cytosol, nucleus and mitochondria (Ago et al., 2008; Junn et al., 2000; Nishiyama et al., 2001; Saxena et al., 2010; World et al., 2011; Zhou et al., 2011).

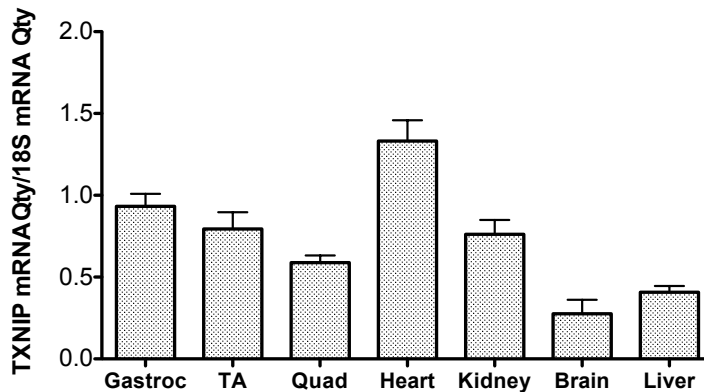


Figure 1-3: TXNIP mRNA expression tissue distribution.

TXNIP mRNA expression measured by qPCR in tissues from wild type mice normalized to 18S mRNA control (n = 4).

1.4.2 TXNIP in Disease Pathogenesis

TXNIP has been implicated in several disease processes, including Type 2 diabetes mellitus (T2DM) (Cha-Molstad et al., 2009; Masson et al., 2009; Minn et al., 2005b; Yoshihara et al., 2010), cancer (Butler et al., 2002; Dutta et al., 2005; Han et al., 2003), apoptosis (Saxena et al., 2010), ROS (Bodnar et al., 2002; Hui et al., 2004; Patwari et al., 2006), inflammation (Davis and Ting, 2010; Lane et al., 2013; Zhou et al., 2010), nonalcoholic steatohepatitis (NASH) (Ahsan et al., 2009), neurodegenerative disorders (Perrone et al., 2012), vascular dysfunction (Schulze et al., 2002; Wang et al., 2004; Xu et al., 2006; Yamawaki et al., 2005) and cardiac hypertrophy (Wang et al., 2002; Yoshioka et al., 2007). With the exception of some of the functions of TXNIP in metabolism, many of these pathologies are redox-dependent and can be partly explained by the negative regulation of TXN by TXNIP. For example, TXNIP has shown to be primarily localized

to the nucleus of pancreatic β -cells under physiological conditions. However, under conditions of oxidative stress, TXNIP shuttles into the mitochondria where it competes with ASK-1 for binding to TXN2, thus allowing for the phosphorylation/activation of ASK-1 and the initiation of the apoptotic cascade (Saxena et al., 2010). Similarly, chronic hyperglycemia or inflammasome activators can lead to oxidative stress, under which the NLR protein 3 (NLRP3) inflammasome binds to TXNIP following its release from TXN. Once bound to TXNIP, the NLRP inflammasome causes procaspase-1 cleavage and interleukin-1 β (IL-1 β) secretion, which is implicated in islet cell dysfunction and the pathogenesis of T2DM (Davis and Ting, 2010; Zhou et al., 2010). However, TXNIP's regulatory functions in metabolism may be both redox-dependent and redox-independent, as a function of its α -arrestin domains, and will be discussed in later chapters.

1.4.3 Transcriptional Regulation of TXNIP

Further clues as to the functions of TXNIP in various tissues and processes involve its diverse transcriptional regulation. TXNIP is upregulated by glucose, which is at least partly mediated by a carbohydrate-response element (ChoRE) in its promoter. ChoRE associates with the MondoA:Mix transcription factor complex, which is activated by glycolytic intermediates such as glucose-6-phosphate (Stoltzman et al., 2008). Further, TXNIP mRNA expression is elevated in muscle of insulin resistant and diabetic humans (Parikh et al., 2007). Expression has shown to be additionally enhanced by

extracellular adenosine-containing molecules that amplify the glucose-signaling pathway (Yu et al., 2009). Other conditions that upregulate TXNIP expression are various stressors, including ROS and paraquat (Joguchi et al., 2002; Junn et al., 2000), ultraviolet light (UV) (Cheng et al., 2004), heat shock factor 1 (HSF1) (Kim et al., 2004), and the HDAC inhibitor suberoylanilide hydroxamic acid (SAHA) (Butler et al., 2002); pharmaceuticals, such as etoposide (Chen et al., 2008a), 5-fluorouracil (Takahashi et al., 2002) and PPAR γ agonist (GW929) (Billiet et al., 2008). In addition, metabolites including ceramides (Chen et al., 2008a), glucocorticoids (Wang et al., 2006), and lipopolysaccharide (Oka et al., 2010) induce TXNIP expression. In juxtaposition, TXNIP is strongly downregulated by insulin (Rani et al., 2010; Shaked et al., 2009). In cardiomyocytes, platelet-derived growth factor (PDGF), biomechanical strain and calcium channel blockers suppress TXNIP (Schulze et al., 2002; Shaked et al., 2009; Yoshioka et al., 2007). Pharmaceuticals and metabolites, such as the anti-diabetic exenatide (Chen et al., 2006), trans-Resveratrol (Nivet-Antoine et al., 2010), glutamine (Kaadige et al., 2009) and inhibitors of oxidative phosphorylation (OXPHOS) including the anti-diabetic drug metformin, an ETC Complex I inhibitor (Chai et al., 2012; Yu et al., 2010), also downregulate TXNIP transcriptional expression. This regulation is summarized below (Fig. 1-4).

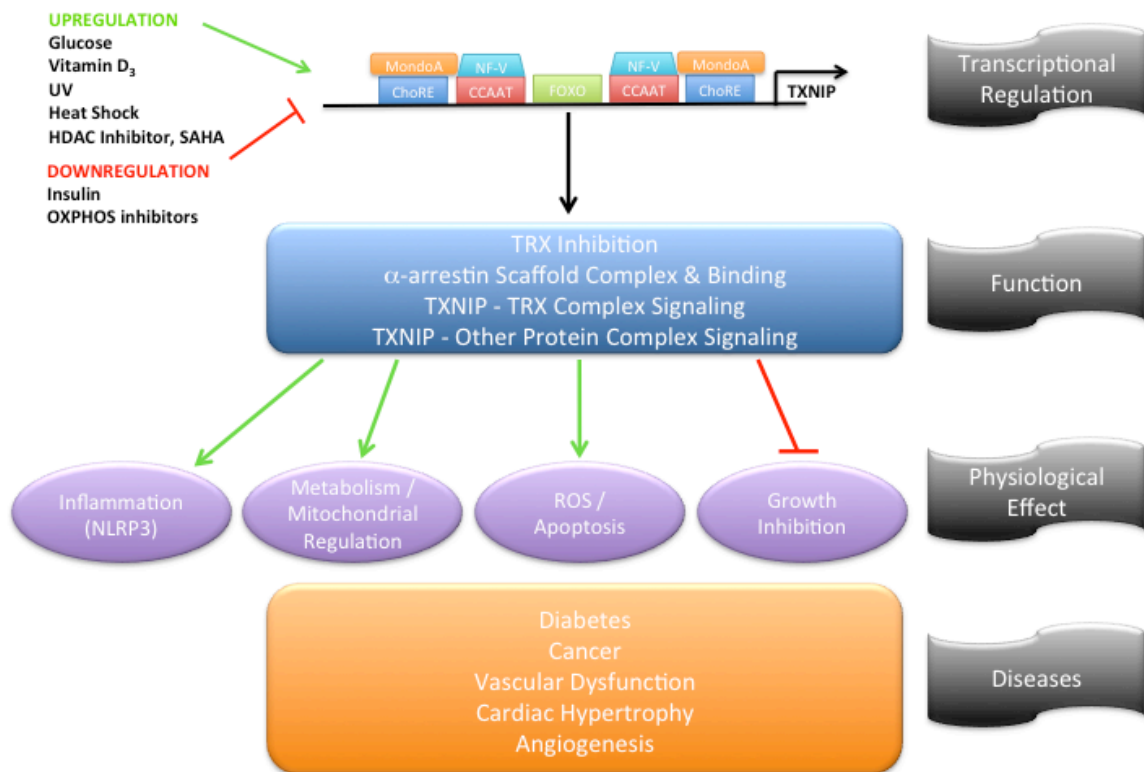


Figure 1-4: Summary of TXNIP Transcriptional Regulation and Function

TXNIP is transcriptionally regulated by diverse factors. As a result TXNIP functions in several ways, including as an inhibitor of TRX, a scaffold and binding complex and a signaling complex with TRX and/or other proteins. These functions are proposed to be the underlying mechanism(s) for the physiological effects of TXNIP and its contribution to disease pathogenesis. Adapted from Spindel et al. (2012).

1.5 TXNIP in Metabolic Regulation

1.5.1 Peripheral Glucose and Lipid Metabolism and the Fasting Phenotype in Mouse Models of TXNIP Ablation

TXNIP was first shown to play a critical role in metabolic control when a mutant mouse strain, HcB-19/Dem (HcB-19) with a nonsense mutation in the TXNIP gene causing a lack of TXNIP expression, resulted in features of familial combined

hyperlipidemia (FCHL) including hypertriglyceridemia, hypercholesterolemia, elevated plasma apolipoprotein B and increased secretion of triglyceride-rich lipoproteins (Bodnar et al., 2002). It was later shown that no association was found between FCHL families and the TXNIP gene (Coon et al., 2004), but the impact of the deficiency of TXNIP on lipid metabolism was clear. In addition to hypertriglyceridemia, HcB-19 mice in the prolonged fasted state (≥ 18 h) have elevated plasma free fatty acids, ketones and lactate with lower pyruvate levels in comparison to wild type controls (Bodnar et al., 2002; Donnelly et al., 2004; Hui et al., 2004; Sheth et al., 2005). Moreover, decreased TCA cycle flux as measured by CO₂ production from isolated liver slices was significantly decreased suggesting mitochondrial dysfunction with TXNIP deficiency (Bodnar et al., 2002).

Subsequently, mice generated with a targeted inactivation of TXNIP (TBP-2^{-/-}) displayed a similar phenotype with even more pronounced abnormalities, such as liver steatosis, severe gastrointestinal bleeding and hepatic-renal dysfunction after 24h fasting, and a predisposition to death under extreme fasting conditions ≥ 48 h (Oka et al., 2006a). The phenotypic presentation in both of these mouse models of TXNIP deficiency points toward impairment in liver fatty acid flux through the TCA cycle, possibly sparing those fatty acids for incorporation into triglycerides and ketones (Bodnar et al., 2002; Donnelly et al., 2004; Oka et al., 2006a; Sheth et al., 2005).

In addition to its function in lipid metabolism, TXNIP is a key regulator in glucose homeostasis. TXNIP is transcriptionally upregulated by glucose (Stoltzman et al., 2008) and its mRNA expression is elevated in muscle of insulin resistant and diabetic humans (Parikh et al., 2007). Moreover, silencing TXNIP expression in human adipocytes and skeletal muscle myocytes enhances glucose uptake, whereas TXNIP overexpression inhibits glucose uptake. Under prolonged fasted conditions, both the HcB-19 and TBP-2^{-/-} mouse models of TXNIP deficiency display higher insulin with lower blood glucose levels in comparison to wild type controls (Bodnar et al., 2002; Donnelly et al., 2004; Hui et al., 2004; Sheth et al., 2005), which was shown to be due to a defect in hepatocyte glucose production (Chutkow et al., 2008) and increased insulin secretion and sensitivity (Hui et al., 2004).

A third and fourth model of TXNIP ablation generated through a Cre-loxP-mediated gene recombination (TKO) and targeted gene deletion (TXNIP-null), respectively, share similar phenotypes to the previous two models (HcB-19 and TBP-2^{-/-}) with the exception of normal insulin levels (Chutkow et al., 2010; Chutkow et al., 2008; Hui et al., 2008). The reason for the varied fasting insulin levels between the models is unknown, but Chutkow et al. (2008) suggest that it could be caused by experimental conditions for fasting and susceptibility or modifier gene effects resulting from strain differences. Nonetheless, in all models in which TXNIP is disrupted, there is consistent enhancement of glucose tolerance, insulin sensitivity and augmented glucose transport

in some peripheral tissues (Chutkow et al., 2010; Chutkow et al., 2008; Hui et al., 2008; Oka et al., 2006a). For instance, TXNIP null mice challenged on a 4-week high fat diet were insulin sensitive and demonstrated augmented glucose uptake into skeletal muscle and white adipose tissue by 30 and 40%, respectively, relative to WT controls (Chutkow et al., 2010). These conditions occurred in spite of a 2-fold increase in adiposity due to hyperphagia. TXNIP deficiency similarly improved glucose intolerance and insulin resistance in the skeletal muscle of diabetic ob/ob mice crossed with TBP-2^{-/-} mice (ob/ob•TBP-2^{-/-}), without amelioration of obesity or obesity-induced adipocytokines (Yoshihara et al., 2010).

Interestingly, the peripheral tissue phenotypes as a result of TXNIP ablation vary. TKO (total body knock-out) mice created by Hui et al. (2008) exhibited increased insulin signaling, insulin sensitivity and glycolysis in oxidative tissues (skeletal muscle and hearts), but not in lipogenic tissues (adipose and liver). This is in contrast to the enhanced glucose uptake reported by Chutkow et al. (2010) in both skeletal muscle and liver of TXNIP null mice, which may be due to strain differences or specific aspects of the gene-targeting approaches. Also in the TKO mice, oxidative tissues displayed impaired mitochondrial glucose and fatty acid oxidation and were predicted to have disrupted mitochondrial respiration, while no comparable studies were conducted with the TXNIP null mice of Chutkow et al (2010). Conversely, in other studies mitochondrial fatty acid oxidation was not impaired in the hearts of

HcB-19 mice, although the TXNIP-deficient hearts preferentially used fatty acids as a substrate over glucose as measured by percentage of acetyl-CoA originated from fats or glucose for the TCA cycle (Sheth et al., 2005). More interestingly, in this same study fatty acid oxidation in skeletal muscle was dramatically increased by 35% in the TXNIP deficient mice as compared to controls, but only in a prolonged fasted state.

In summary, although TXNIP is ubiquitously expressed in all tissues (Junn et al., 2000), existing data suggests that the precise metabolic function of TXNIP varies among tissues and possibly under different physiological conditions (i.e. extreme fasting/starvation). Further, genetic ablation of TXNIP appears to compromise mitochondrial oxidative function across multiple catabolic pathways and impair respiratory/ETC function in some peripheral tissues but systematic comparisons of mitochondrial function in disparate tissues under various physiological states have not been addressed. These studies will be described in chapter 3.

1.5.2 TXNIP in Metabolic Syndrome and the Pathogenesis of Type 2 Diabetes Mellitus (T2DM)

Metabolic syndrome is a cluster of metabolic risk factors, which increase an individual's chances of developing T2DM, cardiovascular disease (CVD) and stroke. Risk factors include impaired glucose tolerance and insulin sensitivity/signaling, hypertension, dyslipidemia, obesity and physical inactivity, and it is estimated that 35% of the US population that is ≥ 20 years of age has some degree of metabolic syndrome

(Alberti et al., 2009). Moreover, TXNIP has been implicated in many aspects of the pathogenesis of this disease.

As previously discussed, all models of TXNIP deficiency have improved glucose tolerance and insulin sensitivity (Chutkow et al., 2010; Chutkow et al., 2008; Hui et al., 2008; Oka et al., 2006a). Insulin signaling through the PI3K/Akt pathway is also augmented. TKO mice demonstrated enhanced insulin signaling in oxidative tissue (skeletal muscle and heart), but not lipogenic tissue (liver and adipose), through constitutively active Akt (Hui et al., 2008). The authors attributed this phosphorylation of Akt to the accumulation of oxidized (inactive) PTEN secondary to impaired TXNIP NADPH-reductive activation of PTEN caused by the accumulation of the competitive inhibitor NADH. This enhanced extrahepatic insulin sensitivity/signaling was maintained even after mice consumed a high fat diet for 12 weeks. Similarly, several insulin signaling-related genes in skeletal muscle, such as *Igf1*, *Igf2bp2*, *Igf2bp4*, *Irs-1*, *Pik3r1*, *Pik3r5*, were upregulated at the mRNA and protein expression levels by TXNIP deficiency in *TBP-2^{-/-}* and *ob/ob•TBP-2^{-/-}* (Yoshihara et al., 2010). Phosphorylation of Akt in response to insulin was shown in the skeletal muscle and heart, but not liver, of these same mice. In agreement with Hui et al. (2008), this suggests TXNIP deficiency, regardless of increased adiposity, results in enhanced insulin signaling/sensitivity in oxidative, but not lipogenic, tissue. In disagreement, however, the enhancement of the

insulin signaling cascade begins upstream of Akt, but the mechanism described by Hui et al. (2008) could synergistically augment the activation of Akt.

Impaired early glucose stimulated insulin secretion (GSIS) in pancreatic β -cells contributes to declining glucose tolerance and the pathogenesis of insulin resistance (Pratley and Weyer, 2001). *In vitro*, insulin negatively regulates TXNIP in human myocytes and adipocytes (Parikh et al., 2007). *In vivo*, both HcB-19 and TBP-2^{-/-} mice in a prolonged fasted state have increased serum insulin and C-peptide levels, which were attributed to an exaggeration of prolonged insulin secretion (Hui et al., 2004; Oka et al., 2009). Hui et al. (2004) also hypothesized that the increased insulin secretion could partly be due to an increase in β -cell mass, but experimental evidence was not provided. In a subsequent study, HcB-19 mice were protected from streptozotocin-induced (STZ) hyperglycemia in part due to a 1.6-fold higher β -cell mass over controls (Masson et al., 2009). Conversely, no significant changes in islet mass were found between TBP-2^{-/-} and WT mice or between ob/ob•TBP-2^{-/-} and ob/ob mice, although glucose stimulated serum insulin levels were heightened with TXNIP deficiency (Yoshihara et al., 2010). Based on *ex vivo* studies in pancreatic islets, the authors attributed the higher insulin levels to enhanced GSIS at high glucose concentrations (16.7mM) compared with basal conditions (2.8mM). In aggregate, these data point to the involvement of TXNIP deficiency in enhanced GSIS and possible protection from diabetes.

Aggravating the pathogenesis of T2DM is the induction of β -cell apoptosis, which also appears to be regulated by TXNIP. *In vitro* incubation of INS-1 cells resulted in an 18-fold increase in TXNIP protein expression and a 12-fold induction of caspase-3 under conditions of glucotoxicity (25mM glucose for 24h) (Chen et al., 2008c). When human TXNIP was overexpressed in an INS-1 cell line, a significant increase in β -cell apoptosis, as measured by mRNA expression of the Bax/Bcl2 ratio and caspase-3 and increased protein expression of activated caspase-9 was reported (Minn et al., 2005a). In a subsequent study by this group, pathway analysis of Affymetrix Gene Chip data in these same cells showed significant upregulation of cell death pathways and down-regulated of pathways involved in proliferation and inhibition of apoptosis, thus consistent with previous findings (Minn et al., 2005b). In a pharmacological assessment, Exenatide (Ex-4), an agonist of glucagon-like peptide-1 receptor and anti-diabetic drug, reduced the mRNA expression of TXNIP in INS-1 cells, thus protecting them from H₂O₂-induced apoptosis (Chen et al., 2006). The authors reported these same observations in primary mouse and human islets. Thus, upregulation of TXNIP does appear to result in the induction of β -cell apoptosis.

In vivo, TXNIP expression was increased in pancreatic islets isolated from 8-week old obese, diabetic BTBR.ob mice as compared to BTBR.lean controls, which correlated with an 8-fold increase in caspase 3 cleavage (Chen et al., 2008c). HcB-19 TXNIP deficient mice were shown to have increased β -cell mass and are resistant to STZ-

induced diabetes (Chen et al., 2008b). Double mutant mice created by crossing the HcB-19 mice with obese, diabetic BTBR.ob mice, resulted in a 3-fold increase in β -cell mass and protection from apoptosis induced through Akt/Bcl-xL signaling. These results were confirmed in a β -cell specific knockout (β TKO) mouse model, which had enhanced β -cell mass and a 50-fold reduction in apoptosis when treated with STZ (Chen et al., 2008b). In sum, TXNIP ablation appears to protect mice from diabetes secondary to prevention of β -cell apoptosis.

Another factor contributing to the loss of β -cell mass in diabetes is the prolonged activation of endoplasmic reticulum (ER) stress pathways, which leads to apoptosis (Corbett, 2008). Initially, overexpression of TXNIP in INS-1 cells did not result in the upregulation of either Bip (immunoglobulin heavy-chain binding protein) or Chop (C/EBP homologous protein), two markers of ER stress, which seemed to negate a regulatory role for TXNIP (Chen et al., 2008c). Conversely, it was simultaneously reported that TXNIP links ER stress, inflammation and β -cell death. The mechanism described involved the upregulation of TXNIP by ER stress through PERK (protein kinase RNA-like endoplasmic reticulum kinase) and IRE-1 (inositol-requiring enzyme 1), two unfolded protein response (UPR) sensors. Activation of this pathway induces transcription of IL-1 β , which activates the NLRP3 inflammasome (Lerner et al., 2012; Osowski et al., 2012).

In aggregate, these animal model studies suggest that TXNIP may be a critical regulatory factor in the progression of metabolic syndrome to T2DM in humans. Clinically, TXNIP expression is upregulated in the skeletal muscle of patients with insulin resistance and T2DM (Parikh et al., 2007) and diabetic patients have higher triacylglyceride concentrations and increased diastolic blood pressure (van Greevenbroek et al., 2007). Evidence also suggests that TXNIP may also contribute to the downstream T2DM-complications seen in these patients. For example, TXNIP expression represents an early change in diabetic neuropathy (Price et al., 2006), diabetic retinopathy (Advani et al., 2009; Devi et al., 2013; Perrone et al., 2009; Perrone et al., 2010) and diabetic nephropathy (Tan et al., 2011).

1.6 Metabolic Regulation by TXNIP is both Redox-Dependent and Redox-Independent

1.6.1 Redox-Dependent Regulation

Previous chapter sections have discussed TXNIP as a metabolic regulator involved in glucose homeostasis, lipid metabolism and possibly mitochondrial function through several catabolic pathways. Additionally, TXNIP forms a redox-sensitive disulfide bond with TXN (Patwari et al., 2006), thus inhibiting TXN and sensitizing the cell to oxidative stress (Nishiyama et al., 2001). Given this, it has been suggested that TXNIP may couple oxidative stress and/or redox imbalance, glucose uptake, insulin

signaling and mitochondrial function in peripheral tissues (Chutkow et al., 2008; Hui et al., 2008; Hui et al., 2004; Muoio, 2007; Schulze et al., 2004; Sheth et al., 2005).

In vitro, overexpression of TXNIP has led to at least a 50% decrease in TXN activity (Nishiyama et al., 2001). When cells were exposed to various stress stimuli, such as H₂O₂, ultraviolet (UV) light, γ -rays, ionomycin and heat shock, TXNIP was significantly induced and the activity of TXN was inhibited as a direct result of its interaction/binding to TXNIP at its catalytically active center (Junn et al., 2000). Application of increasing glucose concentrations to human aortic smooth muscle cells resulted in concentration-dependent decreases in TXN activity, which promoted the formation of ROS that was directly linked to the induction of TXNIP (Schulze et al., 2004). Furthermore, selective silencing of TXNIP via RNAi was able to restore TXN activity even in the presence of hyperglycemia, and *in vivo*, diabetic animals with increased vascular expression of TXNIP and reduced TXN activity could be rescued with insulin treatment. Surprisingly with this exception, no additional evidence has been reported directly connecting the increase in oxidative stress under nutritional overload to inhibition of TXN activity by TXNIP. Conversely, TXN activity and protein levels were unchanged between TXNIP deficient mice and WT controls in liver (Chutkow et al., 2008; Sheth et al., 2005) and heart (Yoshioka et al., 2007). These findings suggest that redox-dependent metabolic regulation by TXNIP may be mediated by interactions and events other than, or in addition to, inhibition of TXN.

In support of this idea, changes in redox state such as imbalances in redox potential, as reflected in changes in the NADH/NAD⁺, NADPH/NADP⁺ and GSH/GSSG ratios, have been suggested to affect glucose uptake and insulin signaling (Evans et al., 2002; Muoio and Newgard, 2006) and could involve TXNIP (Muoio, 2007). In animal models of TXNIP deficiency, redox state has been altered, albeit inconsistently. Based upon the increase in the lactate to pyruvate ratio in TXNIP deficient mice, it was predicted that this would mirror an increased NADH/NAD⁺ ratio (Bodnar et al., 2002) resulting in decreased flux through the TCA cycle and the promotion of triglyceride synthesis. This was later shown to be the case in the livers of TXNIP deficient mice in the fed state, where the NADH/NAD⁺ ratio was 2-fold higher as compared to the WT controls. However, no differences were observed between the genotypes while in a prolonged fasted state, although lactate concentrations remained high (Sheth et al., 2005). In contrast, Hui et al. (2008) predicted an accumulation of NADH in the oxidative tissue of TXNIP KO mice secondary to diminished mitochondrial respiration. However, NADH was not measured experimentally. Attempts to accurately determine the NADPH/NADP⁺ ratios have proven technically challenging (Sheth et al., 2005). Sulfhydryl status in the livers of TXNIP deficient mice as measured by the GSH/GSSG ratio has also been inconsistent. Following prolonged fasting, the hepatic GSH/GSSG ratio was increased by 30% as compared to WT controls in one study (Hui et al., 2004), while found to be unchanged in another (Chutkow et al., 2008).

Due to inconsistencies and lack of experimental evidence on the changes in redox state and sequelae in the absence of TXNIP, particularly in skeletal muscle, we address this in a succeeding chapter. The increased glycolytic activity and decreased flux through the TCA cycle in TXNIP deficient mice, could easily contribute to changes in redox potential and redox status. Further, understanding the redox status is of critical importance, since several mitochondrial enzymes such as the 2-oxoacid dehydrogenases, have shown to be redox-sensitive (Bunik, 2003). Changes in redox status also present opportunities for secondary regulatory mechanisms, such as reversible glutathionylation, which has been shown to occur with TCA cycle enzymes, such as α -ketoglutarate dehydrogenase (α -KGD) (Applegate et al., 2008; Nulton-Persson et al., 2003).

1.6.2 Redox-Independent Regulation

Evidence for redox-independent metabolic regulation by TXNIP is secondary to its role as a member of the arrestin superfamily of proteins. This superfamily consists of the photoreceptor-specific visual arrestins, the structurally similar β -arrestins and the phylogenetically older α -arrestins (Alvarez, 2008; Patwari and Lee, 2012). The β -arrestins function as endocytic adaptors and mediate trafficking of seven-transmembrane receptors (7TMRs), also known as G protein-coupled receptors (GPCRs), through desensitization and degradation (DeWire et al., 2007; Shenoy and Lefkowitz, 2011). β -arrestins also serve as signal transduction scaffolds for various complexes, such

as the mitogen activated protein kinases (MAPKs), the extracellular signal related kinase (ERK), c-Jun N-terminal kinase 3 (JNK3), apoptosis signaling kinase 1 (ASK1) and Akt (DeWire et al., 2007). The α -arrestins or arrestin domain containing proteins (ARRDC) consist of six members in humans, TXNIP and ARRDC1 – 5. In addition to arrestin domains, all contain conserved PPxY motifs, which allow for protein-protein interactions through WW domains (Alvarez, 2008; Spindel et al., 2012). Individual functions differ based upon their varied cellular distribution (Masutani et al., 2012).

Both α - and β -arrestins have been implicated in metabolic regulation. β -arrestin-1 is able to associate with the insulin receptor (IR) and promote receptor endocytosis (Zhao and Pei, 2013), regulate long-term insulin signaling by preventing the degradation of IRS-1 (Usui et al., 2004), mediate GPCR insulin secretion signaling in islets (Dalle et al., 2011) and foster endothelin type A (ETA)-stimulated, but not insulin-stimulated, GLUT4 translocation (Imamura et al., 2001). Most interestingly, β -arrestin-1 knock out (β arr1-ko) mice are susceptible to increased adipose, TAGs and NEFA accumulation with decreased glucose tolerance and insulin sensitivity when fed a high fat diet for 14 weeks (Zhuang et al., 2011b). Under the same diet conditions, transgenic overexpression of β -arrestin-1 in mice resulted in reduced obesity with improved glucose tolerance and insulin sensitivity as compared with WT controls (Zhuang et al., 2011b). In a follow-up study, this same group showed that the diet-induced obesity and adipogenesis was due

to the regulation of β -arrestin-1 by peroxisome-activated receptor- γ (PPAR γ) (Zhuang et al., 2011a).

Although β -arrestin-1 is able to interact with the IR, only β -arrestin-2 directly interacts with downstream factors of insulin signaling cascade (Zhao and Pei, 2013). As with the β arr1-ko mice, β arr2-ko mice demonstrated insulin resistance and glucose intolerance after high fat feeding, however the β arr2-ko mice exhibited impaired insulin sensitivity under re-fed conditions while fed a standard chow diet (Luan et al., 2009). Furthermore, adenoviral administration of β -arrestin-2 was able to rescue insulin sensitivity. The authors also found that insulin triggered the formation of a new β -arrestin-2 signaling complex involving the scaffolding of Akt/Src to the IR, which was deteriorated under β -arrestin-2 deficiency or dysfunction, thus contributing to the insulin resistant phenotype. Lastly, β -arrestin-2 can also mediate glucose uptake and inhibition in soleus muscle via the β_2 -adrenoreceptor when exposed to the β_2 -adrenoreceptor agonists, BRL37344 and clenbuterol (Ngala et al., 2008; Ngala et al., 2009). This contradictory effect is due to different ligand-directed signaling (Ngala et al., 2013).

The α -arrestin protein ARRDC3, also known as thioredoxin-binding protein-2-like inducible membrane protein (TLIMP) was the first to be functionally characterized (Masutani et al., 2012) and linked to cellular growth regulation and PPAR γ activation (Oka et al., 2006b). *In vivo*, it was later revealed that ARRDC3 deficient male mice were

protected from age-induced obesity due to increased energy expenditure through increased activity levels and thermogenesis of brown and white adipose tissue (Patwari et al., 2011). Interestingly another α -arrestin protein, ARRDC4, was identified when quantitative trait loci (QTL) were mapped that contribute to the biological control of voluntary exercise-related traits in an intercrossed line of mice originally generated from a reciprocal cross between mice with a genetic propensity for voluntary exercise and C57BL/6J (Kelly et al., 2012; Kelly et al., 2010). ARRDC4 abundance was significant for running duration, which involves regulation of energy expenditure as with ARRDC3.

Inhibition of glucose uptake and lactate output are common hallmarks of both TXNIP and ARRDC4 deficiency (Patwari et al., 2009; Patwari and Lee, 2012). These paralogs share 63% similarity over their entire open reading frames and are both transcriptionally regulated through carbohydrate response elements (ChoREs) (Stoltzman et al., 2008); however, only TXNIP is able to bind TXN, thus indicating that glucose uptake by TXNIP does not require binding to TXN (Patwari et al., 2009). This idea was experimentally tested by overexpressing the TXNIP mutant (C247S), which is unable to bind to TXN but maintains inhibition of glucose uptake. Moreover, this function is inherent to the arrestin domains and not due to protein-protein interaction through the PPxY motifs in the C-terminal tail domain. Also, although functionally intrinsic to the arrestin domains, regulation of glucose uptake is not shared by ARRDC3. Still unknown was the molecular mechanism by which the arrestin domains regulate

glucose uptake. However, very recent evidence has shown that TXNIP binds directly to the glucose transporter GLUT1 and induces its internalization through clathrin-coated pits (Wu et al., 2013), thus providing evidence for how TXNIP regulates glucose uptake, but contrary evidence has also been reported suggesting TXNIP does not affect GLUT4 localization to the plasma membrane in muscle (Andres et al., 2011).

1.7 Known and Candidate TXNIP Binding Proteins

With the evidence that TXNIP is an α -arrestin protein comes the possibility of regulatory functions secondary to direct protein binding at both its active redox-sensitive cysteine residues and at its α -arrestin domains and/or PPxY motifs. Previous chapters have covered the inhibitory redox-sensitive binding of TXNIP to TXN, but other binding partners have also been uncovered. For instance, TXNIP suppresses promoter activity of cyclin A₂ and Il-3 in transiently transfected 293 cells by forming a transcriptional repressor complex with promyelocytic leukemia zinc-finger (PLZF), Fanconi anemia zinc-finger (FAZF) and histone deacetylase 1 (HDAC1) (Han et al., 2003). What remains unclear is where the co-repressors are binding on TXNIP and if TXN was involved.

The reduced expression of several cyclin-dependent kinase inhibitors, such as p27^{kip}, is found in many types of tumors. The low expression of p27^{kip} is regulated through translocation from the nucleus to the cytoplasm where it undergoes proteasome-mediated degradation. The translocation of p27^{kip} is regulated by the Jun

activating binding protein (JAB1), thus promoting tumor progression (Tomoda et al., 1999). In another transcriptional repressor complex, TXNIP binds to JAB1 to restore the JAB1-induced suppression of the stability of p27^{kip} (Jeon et al., 2005; Yamaguchi et al., 2008). In another scenario, TXNIP decreases the stability of HIF1 α by binding to the β -domain of von Hippel-Lindau protein (pVHL), thus enhancing the nuclear export of pVHL/HIF1 α . In the cytoplasm, the TXNIP/pVHL/HIF1 α complex adds ubiquitin ligase to complete the degradation of HIF1 α (Shin et al., 2008). In a third scenario, TXNIP inhibits the mammalian target of rapamycin (mTOR), a conserved serine-threonine kinase involved in coordinating cell growth and proliferation, by binding to and stabilizing Redd1 protein (Jin et al., 2011). In a fourth scenario in islet cells *in vivo*, TXNIP was shown to bind to Mybbp1, a protein known to inhibit peroxisome proliferator-activated receptor gamma coactivator 1-alpha (PGC-1 α) function and transcription of PGC-1 α target genes (Yoshihara et al., 2010). Finally, TXNIP has recently been revealed to bind to GLUT1 in HepG2 cells, consequently facilitating GLUT1 endocytosis through clathrin-coated pits to partially regulate glucose uptake (Wu et al., 2013). Interestingly, TXNIP also suppressed GLUT1 mRNA levels by an unknown mechanism resulting in extended suppression of GLUT1 protein and glucose uptake. In all cases, it remains unclear if there is any involvement of TXN and/or the redox-sensitive cysteine residues of TXNIP.

The binding of TXNIP to the NLRP3 inflammasome and Dnajb5-HDAC4, a heat shock protein and class II histone deacetylase complex, is redox-dependent and involves TXN. Conditions of oxidative stress are critical for the activation of the NLRP3 inflammasome because this milieu results in the oxidation of TXN and the release of TXNIP. Upon release, the C-terminal arrestin domain of TXNIP binds to the leucine-rich repeats (LRRs) and nucleotide-binding NACHT domain of NLRP3 (Zhou et al., 2011). Remaining unknown is whether there is a ROS-induced conformational change in NLRP3 that allows for TXNIP binding. Ultimately, TXNIP binding causes procaspase-1 activation and IL-1 β secretion, which is implicated in islet cell dysfunction and the pathogenesis of T2DM (Davis and Ting, 2010; Zhou et al., 2010). A key experiment missing from the study was to determine if the binding of NLRP3 could occur with TXNIP mutants that are unable to bind to TXN, thus confirming that the TXNIP-TXN state is required. During oxidative stress in the heart, HDAC4 is oxidized and exported into the cytosol where it is unable to suppress positive mediators of cardiac hypertrophy. To prevent hypertrophy, TXN facilitates the reduction and subsequent binding of Dnajb5 and HDAC4. Lastly, the reduced TXN-Dnajb5-HDAC4 complex binds to TXNIP and importin α_1 , which is required for translocation of the complex into the nucleus (Ago et al., 2008).

Given the association of TXNIP deficiency and lactate production, Yoshioka et al. (2012) measured the quantity and enzymatic activity of pyruvate dehydrogenase, E1

component, subunit α (PDHE1 α) in TKO hearts and WT controls. Although no difference in quantity was found, there was a 54% decrease in PDH activity in the TKO hearts. In a protein interaction immunoprecipitation assay, an interaction between TXNIP and PDHE1 α was identified suggesting that TXNIP directly interacts with PDHE1 α to regulate its activity. However, no mechanism of action was confirmed experimentally. In a proteomic analysis, 21 protein spots were differently expressed between TKO hearts and WT controls. Of these, 13 were identified by mass spectrometry, including β -enolase isoform 1, ATP synthase and NADH dehydrogenase flavoprotein 1 (complex I), suggesting additional TXNIP binding proteins.

1.8 Regulation of TXNIP

Previous chapters have described how TXNIP regulates the functions of many proteins involved in processes from metabolism to cancer. The transcriptional regulation of TXNIP has also been covered, but TXNIP is also subject to regulation at the protein level. Prior reports suggest that TXNIP translocates from the cytoplasm to the nucleus, but no classic nuclear localization signal (NLS) in the TXNIP sequence has been identified. Instead, it appears that importin α -1 (Rch1), a member of the importin system, binds to TXNIP to allow for this nuclear translocation (Nishinaka et al., 2004). The interaction was specific for Rch1, as shRch1 was able to suppress nuclear accumulation of TXNIP. The authors identified that amino acids 1-227 of TXNIP were

required for binding to Rch1, which they hypothesize might require a conformational structure or multiple NLS-like sequences and does not involve TXN.

Other proteins not only regulate TXNIP but also are regulated by TXNIP. For example, one of the conserved functions of the α -arrestin proteins, including TXNIP, and the arrestin-like trafficking adaptors (ARTs) in yeast is the targeting of plasma membrane proteins for endocytosis (Alvarez, 2008). In conjunction with the HECT ubiquitin ligases (Lin et al., 2008) and the ESCRT (endosomal sorting complex) machinery (Rauch and Martin-Serrano, 2011), proteins are targeted for internalization and degradation. All of the α -arrestin proteins, including TXNIP, have been shown to interact with all of the HECT ubiquitin ligases, but to varying degrees (Rauch and Martin-Serrano, 2011). TXNIP has strong binding affinity for Nedd4 and WWP1, with less affinity for WWP2, Itch, Tsg101, ALIX and ubiquitin; but all require the PPxY motifs of TXNIP. Interestingly, the α -arrestin proteins are not only involved in targeting proteins for ubiquitination, but they themselves are also substrates for the HECT ubiquitin ligases. For example, ARRDC3/TLIMP and ARRDC4 recruit Nedd4 E3 ubiquitin ligase to mediate ubiquitination of the β_2 adrenergic receptor and β_4 integrin (Draheim et al., 2010; Nabhan et al., 2010; Shea et al., 2012) similar to the β -arrestins (Shenoy and Lefkowitz, 2011). This does not occur with TXNIP, but TXNIP has been shown to undergo Itch E3 ubiquitin ligase-dependent degradation in cancer cells, the function of which is to modulate ROS-mediated apoptosis (Zhang et al., 2010).

TXNIP has also been shown to be regulated by the AMP-activated protein kinase (AMPK), a protein involved in cellular energy homeostasis sensitive to changes in the AMP/ATP ratio. A decrease in the ratio, indicating a low energy state, causes the activation (phosphorylation) of AMPK and the subsequent phosphorylation of proteins by AMPK in order to activate catabolic pathways to restore ATP levels and energy homeostasis. Reduced phosphorylation at Thr-172 of AMPK and reduced cellular AMP levels were found in the heart and soleus muscle, but not gastrocnemius muscle, of TXNIP KO mice following prolonged (18h) fasting (Andres et al., 2011). Phosphorylation at Ser-485/491 was unaffected. Additionally, no changes were seen in phosphorylated (all sites) AMPK and AMP levels in a fed state. Because these mice have increased glucose uptake and glycolysis (Hui et al., 2008), the expression of glucose transporters, GLUT1 and GLUT4 were examined (Andres et al., 2011). Although GLUT4 protein levels were unchanged at the plasma membrane, GLUT1 protein levels in heart, soleus and gastrocnemius in prolonged fasted mice were decreased. GLUT1 expression was unchanged during the fed state. Because GLUT1 mRNA levels were also diminished in the fasted state, the authors concluded that reduction of GLUT1 protein levels was transcriptionally dependent and independent of AMPK signaling. On the contrary, in rat hepatocytes TXNIP curbed glucose uptake directly by binding and targeting GLUT1 for endocytosis and indirectly by reducing mRNA levels of GLUT1 (Wu et al., 2013). How then does this regulate TXNIP? Well, ultimately this feedback

loop is activated by acute glucose withdrawal, resulting in AMPK activation and Ser-308 phosphorylation on TXNIP. This phosphorylation induces a conformational change that exposes the PPxY motifs of the protein, thus allowing for the binding to an unidentified E3 ubiquitin ligase, which results in the degradation of TXNIP. The degradation of TXNIP relieves the suppression of GLUT1, thereby activating glucose uptake. The two contrary studies (Andres et al., 2011; Wu et al., 2013) may have different results because of the use of different models systems (*in vivo* vs. *in vitro*) and different tissues. Hepatocytes express GLUT1, where muscles primarily express GLUT4, and each appear to be regulated differently by TXNIP.

Another suggested feedback loop is the reciprocal regulation between TXN and TXNIP. In this newly proposed hypothesis, TXNIP partially functions by binding to the reduced form of TXN at its redox-sensitive cysteine residues, and in turn, TXN stabilizes TXNIP by regulating some of its α -arrestin functions (Patwari and Lee, 2012). For example, it was reported that adipogenesis is promoted by the dissociation of TXN from TXNIP and subsequent degradation of TXNIP through interaction with an E3 ubiquitin ligase at its PPxY motifs, as described earlier (Chutkow and Lee, 2011). To test this experimentally the authors used a TXNIP mutant, which suppresses glucose uptake yet does not bind to TXN, to examine the effects on adipogenesis. The mutant was less stable and had reduced ability to inhibit adipogenesis, while the TXNIP-TXN complex with the catalytically active TXN promoted TXNIP stability by preventing its

degradation. This regulation is only afforded to TXNIP and not all α -arrestin proteins because only TXNIP is able to bind to TXN, rendering TXNIP unique among the α -arrestin protein family.

Lastly, TXNIP can be regulated post-transcriptionally by the microRNA, miR-17-5p, which directly interacts with the 3'-untranslated region (UTR) of the TXNIP promoter to destabilize its mRNA and down-regulate TXNIP protein expression in senescent fibroblasts (Zhuo de et al., 2010). MicroRNA, miR-17 post-transcriptionally regulates TXNIP in the endoplasmic reticulum (ER). During the unfolded protein response (UPR), IRE1 α reduces levels of miRNA-17, thus increasing TXNIP mRNA stability and protein translation, which in turn activates the NLRP3 inflammasome (Lerner et al., 2012). Other microRNAs and/or other pathways affected by miR-17 await discovery.

1.9 Project Summary and Goals

Thus far, I have provided an in-depth review of TXNIP in redox sensing and metabolic control. Although some evidence has suggested a link between TXNIP and mitochondrial function, the molecular nature of this relationship remains unclear and experimental evidence lacking. Therefore, we hypothesized that TXNIP had a direct role in regulating mitochondrial function. Contained in this work is the empirical evidence to evaluate this hypothesis.

Our overarching goal was to determine whether TXNIP deficiency causes mitochondrial dysfunction in skeletal muscle, and if so, discover the molecular nature of this dysfunction and pinpoint the molecular lesions in mitochondrial metabolism. Therefore, in chapter 3 using mouse models of total body and muscle-specific TXNIP deficiency we performed systematic analyses of oxidative metabolism and respiratory function in whole animals, isolated muscles, permeabilized myofibers and isolated skeletal muscle mitochondria to determine if TXNIP deficiency leads to global disruptions in oxidative fuel metabolism and bioenergetics. Once substrate oxidative deficiencies were identified, we used targeted metabolomics and conventional biochemical assays to pinpoint specific enzymes disrupting flux through these catabolic pathways. We also asked whether the metabolic and mitochondrial abnormalities correlated with decreased mitochondrial content, major lesions in the electron transport chain (ETC) and/or disrupted redox balance. Ultimately, we were able to identify muscle-specific deficits in multiple dehydrogenase enzymes resulting in the reduced capacity for oxidative metabolism and elevated circulating level of fatty acids, ketones and branched-chain amino acids. The loss of enzymatic activity of these select dehydrogenases was accompanied by and correlated to insufficiencies in protein abundance, without concomitant changes in mRNA expression. Thus, we demonstrate that TXNIP is mandatory for maintaining protein synthesis and/or stability of these enzymes. This implies a novel role of TXNIP in coordinating mitochondrial fuel

switching in response to nutrient availability adding to its physiological relevance as a key metabolic regulator.

In chapter 4, we address the topic of redox imbalance in skeletal muscle in the absence of TXNIP. We hypothesized that due to its multifunctional role in redox metabolism and mitochondrial function, there would be additional regulatory mechanisms contributing to the reduced oxidative metabolism of TXNIP deficient skeletal muscle. To address this hypothesis, we characterized the oxidative milieu by measuring a series of metabolites that provide information on cellular energy charge and oxidative stress. We then sought to determine if and how this imbalance contributed to the diminished oxidative metabolism observed in TXNIP deficient mice through *in vitro* and *in vivo* studies. We conclude with evidence supporting S-glutathionylation as a secondary regulatory mechanism for the protection of the TCA cycle enzyme, α -ketoglutarate dehydrogenase, under oxidative conditions.

In summary, we provide novel evidence for the physiological role of TXNIP in skeletal muscle as it pertains to mitochondrial regulation. We conclude with identifying remaining questions regarding the regulation and physiological role of TXNIP and presenting an experimental plan to address these gaps in the literature.

2. Materials and Methods

This chapter contains the detailed methods for all procedures relative to this dissertation. Versions of some protocols had been previously used in this lab or available in the literature, but all were modified according to my research needs and availability of reagents.

2.1 Reagents

All reagents were purchased from Sigma-Aldrich Chemical Company (St. Louis, MO), unless otherwise noted.

2.2 Animals

Duke University Institutional Animal Care and Use Committee approved all animal studies. Generation of the total body *Txnip* knockout (TKO) and TXNIP^{fl/fl} mice has been previously described (Hui et al., 2008). To generate skeletal muscle specific knockout mice (TXNIP^{SKM-/-}), TXNIP homozygous floxed mice were bred with transgenic mice expressing cre recombinase under control of the mouse myogenin promoter and *MEF2C* (myo-Cre^{Tg/0}), which express Cre recombinase exclusively in skeletal muscle but not heart. TXNIP^{fl/+,cre/f} and TXNIP^{fl/+,f/f} mice from the first cross were interbred to generate the homozygous floxed, myo-cre skeletal muscle specific knock out mice (TXNIP^{SKM-/-}) and the homozygous WT floxed mice (TXNIP^{fl/fl}). All lines have been back-crossed >6 times to the C57B/6J background. Either male TKO mice and WT littermates or male skeletal muscle-specific knockout (TXNIP^{SKM-/-}) mice and flox/flox

(TXNIP^{fl/fl}) littermates were used for all experiments as indicated. Animals were housed in a temperature-controlled environment with a 12-hour light:12-hour dark cycle and allowed *ad libitum* access to standard chow (Purina Rodent Chow no. 5015, Purina Mills, St. Louis, MO, USA) and water. On the day of sacrifice, food was pulled 5-6 h prior to harvesting tissues and blood.

2.3 Metabolic Phenotype Parameters

2.3.1 Glucose Tolerance Test (GTT)

Mice were fasted for 6 h prior to an intraperitoneal injection of 1.75g/kg of glucose. Blood glucose was measured from the tail at 0, 15, 30, 60 and 120 min using a glucometer (BD Medical, Franklin Lakes, NJ).

2.3.2 Serum Metabolic Substrates

EDTA blood was collected after a 6 h food withdrawal at 9, 12 and 18 weeks-of-age and at the time of sacrifice. Samples were centrifuged (4000 x g, 10min, 4°C), plasma collected and stored at -20°C.

2.3.2.1 Triacylglycerides (TAG)

Plasma samples were analyzed for TAGs using the Serum Triglyceride Determination kit (Sigma TR0100), which involves the hydrolysis of triglycerides to glycerol and free fatty acids followed by the enzymatic measurement of the glycerol released. Briefly, a 250mg/dL stock solution of Free Glycerol Reagent (Sigma F6428) was serially diluted 1:1 to prepare a standard curve (125.0000, 62.5000, 31.2500, 7.8125,

3.9063, 1.9531, 0mg/dL) with ddH₂O serving as the blank. Free glycerol readings were obtained on a Spectromax spectrophotometer (Molecular Devices, Silicon Valley, CA) at 540nm by adding 2μL of the blank, standard or sample and 160μL of Free Glycerol Reagent to each well in a 96-well plate. To each well, 40μL of Total Triglyceride Reagent was added followed by gentle agitation, incubation at 37°C for 5 min then reading the plate at 540nm. True triglycerides values were calculated by subtracting “Free Glycerol” from “Total Glycerol” readings.

2.3.2.2 Non-Esterified Fatty Acids (NEFA)

Plasma samples were analyzed for NEFAs using the NEFA C assay kit (Wako Chemicals, Richmond, VA), which involves the measurement of the H₂O₂ by-product of the oxidation of acyl-CoAs, formed from NEFAs in the sample and acyl-CoA synthetase (ACS), coupled to an enzymatic colorimetric reaction. Dilutions (1.00, 0.80, 0.50, 0.20, 0.10, 0.05, 0mM) of the 1mM stock NEFA standard solution (Wako 276-76491) with 0.9% saline were used for the standard curve. Serum samples were diluted 1:2 in saline and 10μL, along with 150μL of Reagent A (Wako 999-34691 & 995-34791), were added to each well of a 96-well plate. The plate was gently agitated and incubated for 10min at 37°C before reading spectrophotometrically at 550nm to obtain the pre-read absorbance. For the final absorbance, this last step was repeated with 50μL of Reagent B (Wako 991-34891 & 993-35191). Subtracting the pre-read absorbance from the final absorbance and correcting for the 1:1 dilution determined the actual NEFA values in mM.

2.3.2.3 β -Hydroxybutyrate (BHB)

The Sarah W. Stedman Nutrition and Metabolism Center Metabolomics Core Facilities at Duke University analyzed plasma samples for ketone bodies (acetone, acetoacetate, β -hydroxybutyrate) using a Hitachi 911 clinical chemistry analyzer.

2.3.3 Blood Glucose and Blood Lactate

At the start of the light cycle (7:00am), mouse cages were changed and food removed. Blood glucose and blood lactate were measured from the tail at 0, 2, 4 and 6 h post food removal using a glucometer (BD Medical, Franklin Lakes, NJ) and the Lactate Plus analyzer (Nova Biomedical, Waltham, MA).

2.3.4 Lactate Dehydrogenase (LDH) Assay

This assay was optimized from previously described methods (Wolterbeek and van der Meer, 2005) to detect lactate produced as a metabolic by-product of glucose oxidation. Therefore, following glucose oxidation in whole muscle, the incubation media (~500 μ L) was collected in 1.7mL microcentrifuge tubes and stored at -20°C. For one 96-well plate, 150mg of NAD⁺ (Sigma N-3014) was added to 20mL of lactate buffer (175mM hydrazine sulfate, 68mM glycine, 2.9mM EDTA, pH 9.5) for a final concentration of 11.3mM NAD⁺. A 12mM solution of L-lactic acid was prepared and serially diluted 1:1 in media for 6, 3, 1.5, 0.75, 0.375 and 0.1875mM solutions to generate the standard curve. To each well was added 20 μ L of sample or standard and 200 μ L of assay buffer. The plate was mixed and pre-read on the SpectroMax spectrophotometer

(Molecular Devices, Silicon Valley, CA) using an endpoint setting at 340nm. 10 μ L of 1000 Units/mL LDH (Sigma 61311) were added to each well and the plate read every minute kinetically for 60 min at 340nm. When values reached a plateau, a final endpoint reading was taken, less the pre-read value, to calculate the concentration of lactate in the sample based on the standard curve.

2.4 Exercise Studies

Before either the high-intensity or endurance exercise challenges, the mice were habituated to the appropriate treadmills for three consecutive days before the day of the test. During this acclimation, the mice were placed on a stationary treadmill set at a 10% incline for 5 min followed by 1 min at each of the following speeds: 6, 9 and 12m/min. The enclosed metabolic high-intensity treadmill protocol began at a speed of 3m/min following a 5 min 0m/min acclimation. The speed increases occurred every 3 min as follows: 15, 18, 21, 24, 27 and 30m/min until exhaustion, as defined by remaining on the shock grid for 10 consecutive seconds. Indirect calorimetry measures, peak VO_2 and respiratory exchange ratio ($\text{RER}=\text{VCO}_2/\text{VO}_2$), were calculated by the Comprehensive Laboratory Animal Monitoring System (CLAMS) attached to the treadmill (Columbus Instruments, Columbus, OH). Measurements were collected every minute throughout the exercise challenge. The endurance protocol was conducted on an open field six-lane treadmill set at a 10% incline. Following the 5 min 0m/min acclimation period, the speed

was raised to 6m/min and increased by 2m/min every 5 minutes until exhaustion, as previously defined. Total distance and time to exhaustion were assessed.

2.5 Mitochondrial Isolation from Mouse Tissue

2.5.1 Protease Preparation from Gastrocnemius Muscle

Mixed gastrocnemius muscles (~300mg) were removed under Nembutal anesthesia (0.1mg/g body weight), weighed, cleaned and stored in 500 μ L of ice-cold KMEM buffer (100mM KCl, 50mM MOPS, 1mM EGTA, 5mM MgSO₄, 1mM ATP, pH 7.4) in a 1.7mL microcentrifuge tube. The muscles were minced 50x then transferred to a 10mL homogenization vial with the addition of another 1mL of KMEM buffer. The suspension was digested with 0.5mg/mL Type XXIV protease (Sigma) for 2 min with periodic light vortexing every 30 s. The digestion was stopped with the addition of 6mL of KMEM buffer with 0.2% BSA. Once settled, the supernatant was aspirated and replaced with another 6mL of KMEM with 0.2% BSA. A Teflon pestle attached to the side rotor at a speed of 2000rpm was used for homogenization on ice over 8 slow passes. The lysate was transferred to a chilled 50mL conical vial and centrifuged (500 x g, 10 min, 4°C). The supernatant was poured into another chilled 50mL conical vial and centrifuged (10,000 x g, 10 min, 4°C), after which the supernatant was discarded and the pellet resuspended in 1mL of KMEM buffer with 0.2% BSA. The resuspended pellet was transferred into a chilled 1.7mL microcentrifuge tube and centrifuged (7,000 x g, 10 min, 4°C). The supernatant was aspirated, 1mL of KMEM buffer (without BSA) was added,

the pellet resuspended and the lysate centrifuged (7,000 × g, 10 min, 4°C). The last centrifugation was repeated with the speed changed (3,500 × g, 10 min, 4°C). Following aspiration of the supernatant, the pellet was resuspended in 200µL of SET buffer (250mM sucrose, 1mM EDTA, 10mM Tris-HCl, 2mM ATP, pH 7.4). The protein concentration was determined with a BCA protein assay (Sigma).

2.5.2 Mechanical Preparation from Gastrocnemius Muscle

Mitochondria were isolated as aforementioned with slight modifications to devoid the use of proteases. In this mechanical preparation, trimmed and weighed gastrocnemius muscles (~300mg) were minced 200x in the same 500µL of KMEM buffer but containing 0.5% BSA. The lysate was quantitatively transferred 3x using 500µL of KMEM buffer with 0.5% BSA each time into a 5mL polystyrene round-bottom tube and protease inhibitor cocktail was added (100x stock, Sigma, P8340). The sample was homogenized on ice for 5 s on setting 5 with a mini Ultra Turrax homogenizer then poured into a 10mL Duall tube. The polystyrene tube was rinsed with 3mL of KMEM buffer with 0.5% BSA and additional protease inhibitor cocktail was added. The lysate was homogenized on ice with a Teflon pestle attached to the bottom rotor at a speed of 2000rpm for 10 slow passes. Upon transfer to a chilled 50mL conical vial, the lysate was centrifuged (500 × g, 10 min, 4°C). The supernatant was poured through 2x gauze into another chilled 50mL conical vial and centrifuged (10,000 × g, 10 min, 4°C), after which the supernatant was discarded and the pellet resuspended in 1mL of KMEM buffer with

0.5% BSA. At this point, the isolation procedure continued exactly as previously described in the protease preparation from gastrocnemius muscle.

2.5.3 Mechanical Preparation from Liver

The liver was removed under Nembutal anesthesia (0.1mg/g body weight). A portion of the large lobe (~300mg) was stored in 500 μ L of ice-cold SET buffer in a 1.7mL microcentrifuge tube, while the remaining tissue was snap-frozen in liquid N₂. The tissue was minced 20x and the lysate transferred to a 15mL homogenization vial with 9.5mL of SET buffer added. The lysate was homogenized on ice with a Teflon pestle attached to the bottom rotor at a speed of 2000rpm for 8 slow passes. The lysate was then poured into a pre-chilled 50mL conical vial and the homogenization vial was rinsed with an equal volume (10mL) of SET buffer with 0.5% BSA, which was added to the 50mL conical vial. The contents were centrifuged (500 \times g, 10 min, 4°C). The supernatant was poured through 2x gauze into another chilled 50mL conical vial and centrifuged (10,000 \times g, 10 min, 4°C) after which the supernatant was discarded. The pellet was washed in 5mL SET buffer with 0.5% BSA to remove excess fat by gently swirling then rinsed with 5mL SET buffer (no BSA). The pellet was resuspended in 1mL SET buffer with 0.5% BSA, transferred into a chilled 1.7mL microcentrifuge tube and centrifuged (7,000 \times g, 10 min, 4°C). The supernatant was aspirated, 1mL of SET buffer (without BSA) was added, the pellet resuspended and the lysate centrifuged (7,000 \times g, 10 min, 4°C). The final centrifugation was repeated as written but at 3,500 \times g, 10 min,

4°C. Following aspiration of the supernatant, the pellet was resuspended in 500µL of SET buffer (no BSA). The protein concentration was determined with a BCA protein assay (Sigma).

2.6 Mouse Embryonic Fibroblasts (MEFs)

2.6.1 Isolation and Culture

The protocol was adapted from the Joseph Nevins lab (Duke University). On embryonic day 13, the pregnant mouse was sacrificed by CO₂ asphyxiation. The embryos were removed and placed in PBS supplemented with penicillin and streptomycin (PBS/P-S). Under the tissue culture hood, each embryo was dissected from its placenta and amniotic sac, washed in PBS/P-S and placed individually into 60mm culture dishes containing 4mL of PBS/P-S. The rostral portion of each embryo's head and any hematopoietic tissue was removed and the embryo minced before adding 1mL of 0.05% Trypsin-EDTA (Gibco 25300-054) for 30 min at 37°C. The trypsinization was neutralized in 4mL of DMEM with 15% heat-inactivated fetal bovine serum (DMEM/HIFBS) by vigorous repeated pipetting against the bottom of the dish. The tissue was then transferred to a T75 flask and supplemented with 15mL of DMEM/HIFBS, which was allowed to grow to over-confluency (≥ 48h) in an incubator (37°C, 5% CO₂). Each T75 flask was split into two T175 flasks and grown to confluency in 50mL of DMEM/HIFBs under the previously described conditions. MEFs were

collected in cell freezing media (65% DMEM, 25% FBS and 10% DMSO) at a density of 3×10^6 cells per vial for storage in liquid nitrogen.

2.7 Substrate Oxidation

2.7.1 Isolated Mitochondria

2.7.1.1 Pyruvate and Palmitate Oxidation

Isolated mitochondria were resuspended to $0.5\mu\text{g}/\mu\text{L}$ in SET buffer. Substrate oxidation rates were determined by measuring the production of $[^{14}\text{C}]\text{-CO}_2$ from either $0.625\mu\text{Ci}/\text{mL}$ $[2\text{-}^{14}\text{C}]\text{-pyruvate}$ (1mM with 0.15% BSA) or $0.625\mu\text{Ci}/\text{mL}$ $[1\text{-}^{14}\text{C}]\text{-palmitate}$ (100 μM bound to 0.15% BSA). 40 μL of isolated mitochondria were placed in the bottom of a polystyrene disposable culture tube (SIGMA, Z376787) to which 160 μL of incubation buffer were added (Kim et al., 2002). The incubation buffer (pH 7.4) was modified to 62.5mM sucrose, 12.5mM potassium phosphate, 100mM potassium chloride, 1.25mM magnesium chloride, 1.25mM carnitine, 0.13mM malic acid, 1.25mM DTT, 0.0625mM NAD^+ , 2mM ATP, 10mM Tris-HCl and 0.0625mM CoA. A trap tube containing 200 μL of 1N NaOH was placed in the culture tube, which was then sealed with a Suba-Seal septum (Sigma Z124567) and placed in a 37°C shaking water bath for 30 min. The reaction was terminated by adding 100 μL of 70% perchloric acid with a syringe and placed on a rotary shaker for 60 min to trap the $^{14}\text{CO}_2$ produced during the incubation. Radioactivity of CO_2 was determined by adding the 200 μL of NaOH to a scintillation

vial along with 4mL of Uniscint BD (National Diagnostics) for liquid scintillation counting.

2.7.1.2 Leucine Oxidation

Oxidation or activity rates were determined by measuring the production of [¹⁴C]-CO₂ from 2.5μCi/mL [U-¹⁴C]-leucine (100μM). The general protocol used was described above with the following exceptions. The isolated mitochondria were resuspended to 0.8μg/μL in SET buffer. The incubation buffer (pH 7.8) consisted of 62.5mM sucrose, 12.5mM potassium phosphate, 100mM potassium chloride, 1.25mM magnesium chloride, 2.5mM carnitine, 0.25mM malic acid, 1.25mM DTT, 2mM NAD⁺, 2mM ATP, 10mM Tris-HCl, 0.5mM CoA, 0.1mM pyroxidal phosphate, 0.4mM thiamine pyrophosphate (TPP), and 0.5mM α-ketoglutarate. To the final volume of incubation buffer was added appropriate volumes of lipoyl dehydrogenase (5U/mL) and BCAA transaminase (BCAT), where 1U converts 1.0μmol of leucine per minute to 2-ketoisocaproate at 37°C in the presence of α-ketoglutarate and pyroxidal phosphate. The incubation buffer was kept in a shaking water bath at 37°C for at least 3 h before use to allow for the conversion of the radiolabeled leucine to its labeled intermediate, 2-ketoisocaproate. All other aspects of the procedure were unchanged from that previously reported.

2.7.2 Whole Muscle

[1-¹⁴C]-palmitate oxidation and [U-¹⁴C]-leucine oxidation in intact soleus and EDL muscles were conducted as formerly described (Muoio et al., 1999; Muoio et al., 2012). Muscles were harvested under Nembutal anesthesia (0.1mg/g body weight) and incubated in pre-gassed low calcium KHB buffer supplemented with 5mM glucose, 0.5mM carnitine and 1% BSA. Upon completion of the harvest, the muscles were re-oxygenated for 20 min at 29°C, which was then increased to 37°C for a final 10 min. Muscles were transferred to parafilm-sealed wells containing 1mL of incubation buffer, which consisted of either 2μCi/mL [1-¹⁴C]-palmitate (500μM bound to 1% BSA) or 2μCi/mL [U-¹⁴C]-leucine (200μM with 1% BSA) ± 100nM insulin and 10mM glucose, and incubated in an environmental shaker for 2 h at 37°C and 200rpm. The incubation buffer (500μL) was transferred to a culture tube, a 200μL NaOH trap was added and the tube sealed with a Suba-Seal septum (Sigma Z124567). The reaction was acidified with 100μL of 70% perchloric acid and placed on a rotary shaker for 60 min to trap the ¹⁴CO₂ produced. Radioactivity of CO₂ was determined by adding the 200μL of NaOH to a scintillation vial along with 4mL of Uniscint BD (National Diagnostics) for liquid scintillation counting. The muscles were washed 3x in low calcium KHB buffer supplemented with 5mM glucose, 0.5mM carnitine and 1% BSA for 10 min intervals while on ice on an orbital shaker at 150rpm before being weighed for the normalization of oxidation rates to tissue mass.

A similar procedure was used for measuring [U-¹⁴C]-glucose oxidation in low calcium KHB buffer containing 5mM glucose, 0.5mM carnitine and 12.5mM HEPES ± 100nM insulin. Incubation media was also collected for the spectrophotometric assessment of lactate production via the reduction of NAD⁺ at 340nm, as already described.

2.7.3 MEFs

2.7.3.1 Palmitate Oxidation

MEFs were grown in 24-well plates in high glucose (25mM) DMEM (Invitrogen 11965) supplemented with 10% FBS, 1mM sodium pyruvate and 100µM carnitine. The oxidation buffer [low glucose (5.5mM) DMEM (Invitrogen 11885084) supplemented with 1mM carnitine, 1mM sodium pyruvate, 12.5mM HEPES, 0.5% BSA and 1µCi/mL [1-¹⁴C]-palmitate] (100µM) was made the day before the actual assay and gassed O/N in an incubator (37°C, 5% CO₂). For the assay, MEFs were rinsed 2x with PBS to remove residual media, 500µL of oxidation buffer was added per well and the plate incubated at 37°C for 3 h. After 3 h, 400µL of the oxidation media was transferred to a culture tube, in which a trap tube containing 200µL of 1N NaOH was placed. The tube was sealed with a Suba-Seal septum (Sigma Z124567) and placed in a 37°C shaking water bath for 30 min. The reaction was terminated by adding 100µL of 70% perchloric acid with a syringe and placed on a rotary shaker for 60 min to trap the ¹⁴CO₂ produced during the incubation. Radioactivity of CO₂ was determined by adding the 200µL of NaOH to a

scintillation vial along with 4mL of Uniscint BD (National Diagnostics) for liquid scintillation counting. Protein was quantified with a BCA assay (Sigma) after the MEFs were washed 2x in PBS, the plate freeze-fractured in liquid nitrogen and the cells lysed and collected in 300 μ L of 0.5% SDS.

2.7.3.2 Leucine Oxidation

All aspects of the protocol are the same as the palmitate oxidation with the exception of the oxidation buffer, which consisted of 117mM NaCl, 4.7mM KCl, 1.25mM MgSO₄, 0.3mM CaCl₂, 25mM sodium bicarbonate, 12.5mM HEPES, 5.5mM glucose, 1mM carnitine and 1 μ Ci/mL [U-¹⁴C]-leucine (100 μ M).

2.8 Mitochondrial Content / Mass

Total DNA was extracted from mixed gastrocnemius muscle using phenol/chloroform (25:4) followed by ethanol precipitation as previously described (Guo et al., 2009). The ratio of mitochondrial DNA to nuclear DNA was measured using real-time quantitative PCR by calculating the ratio of the fold change from the $\Delta\Delta$ Ct of a mitochondrial encoded gene (COX1) and a nuclear encoded gene (β -actin).

2.9 Respirometry / Electron Transport Chain (ETC) Function

2.9.1 Isolated Mitochondrial Oxygen Consumption

Mitochondria were resuspended at 0.5mg/ml in MiR05 respiration media (Boushel et al., 2007) and 12.5 μ g of mitochondrial protein was added in triplicate to media containing 10mM pyruvate + 5mM malate in the absence or presence of 1 μ M

FCCP or 10mM succinate + 1mg/mL rotenone in the absence or presence of 1 μ M FCCP in wells of a BD Oxygen Biosensor plate (BD Biosciences, MA) in a final volume of 0.2ml. Wells were overlaid with mineral oil and fluorescence was measured at 485ex/630em at 25°C over 2 hours. State 3 respiration was determined in the presence of 100mM ADP. State 3 rates of respiration were calculated during the first 30 minutes of the assay and were followed by state 4 rates after depletion of ADP. Well fluorescence was normalized to those of the blank plate as described in technical bulletin #448 and change in fluorescence was converted to oxygen consumption using the Stern-Volmer equation as described in technical bulletin #443.

2.9.2 Permeabilized Muscle Fiber Bundles (PmFB)

2.9.2.1 Preparation of the PmFB

The technique is partially adapted from previous methods (Kuznetsov et al., 1996; Tonkonogi et al., 2003) and has been described previously (Anderson et al., 2007; Perry et al., 2011). Small portions of muscle were dissected and placed in ice-cold *buffer X*, containing (in mM) 50 MES, 7.23 K₂EGTA, 2.77 CaK₂EGTA, 20 imidazole, 0.5 DTT, 20 taurine, 5.7 ATP, 14.3 PCr, and 6.56 MgCl₂·6 H₂O (pH 7.1, 290 mOsm). The muscle was trimmed of connective tissue and fat. Small muscle bundles (~2-7mm, 1.0-2.5mg wet weight) of red gastrocnemius were prepared from each mouse. Each bundle was gently separated along their longitudinal axis with a pair of needle-tipped forceps under magnification (MX6 Stereoscope, Leica Microsystems, Inc., Wetzlar, DE). Bundles were

then treated with 40µg/ml saponin in ice-cold *buffer X*, and incubated on a rotor for 30 min at 4°C. Saponin is a cholesterol-specific detergent that selectively permeabilizes the sarcolemmal membranes while keeping mitochondrial membranes, which contain trace cholesterol, completely intact (Kuznetsov et al., 2008; Veksler et al., 1987). Following permeabilization the permeabilized muscle fiber bundles (PmFB) were placed in *buffer Z* containing (in mM) 105 K-MES, 30 KCl, 1 EGTA, 10 KH₂PO₄, and 5 MgCl₂-6 H₂O with 0.5 mg/ml BSA (pH 7.4, 290 mOsm). PmFB remained in *buffer Z* on a rotator at 4°C until analysis (< 30 min).

2.9.2.2 Mitochondrial Respiration in PmFB

High-resolution oxygen consumption measurements were conducted in 2mL of *buffer Z* using the OROBOROS Oxygraph-2k (OROBOROS INSTRUMENTS, Corp., Innsbruck, AT) with stirring at 750rpm. *Buffer Z* contained 20mM creatine hydrate to saturate creatine kinase, which facilitates mitochondrial ADP transport (Anderson et al., 2007; Perry et al., 2011; Saks et al., 1991; Saks et al., 1994; Saks et al., 1995; Walsh et al., 2001). Respiratory kinetics was assessed via electron entry into complex I (NADH), complex II and/or ETF (FADH₂) in State III conditions (5mM ADP) using the following substrate titration protocols: complex I, glutamate or pyruvate (with 2mM Malate); complex II, succinate (with 10µM Rotenone); combined I, II and ETF, palmitoyl-carnitine (with 2mM Malate). ADP-stimulated respiratory kinetics was assessed via ADP titrations supported by 5mM Pyruvate and 2mM Malate. Each titration was performed

in a separate PmFB. Substrates were titrated in step-wise increments. All experiments were conducted at 37°C and beginning with ~350µM [O₂] to ensure completion of the protocols before oxygraph chamber [O₂] reached 150µM. 25µM Blebbistatin (myosin ATPase inhibitor) was used to avoid potential confounding effects of spontaneous PmFB contraction on respiratory kinetics and maintain PmFB integrity for obtaining accurate dry weights following the experiments (Perry et al., 2011). At the conclusion of each experiment, PmFBs were washed in double-distilled H₂O to remove salts, frozen at -20°C, and dried via lyophilization (Labconco Corp., Kansas City, MO). Polarographic oxygen measurements were acquired in 2-second intervals, with the rate of respiration derived from 40 data points, and expressed as pmol/second/mg dry weight. Dry and wet bundle weights were consistently between 0.15 - 0.3mg. Cytochrome *c* was added to test for mitochondrial membrane integrity, with all experiments demonstrating <10% increase in respiration.

2.9.2.3 H₂O₂ Emission in PmFB

Mitochondrial H₂O₂ emission was measured in *buffer Z* at 30°C during state 4 respiration (10µg/mL oligomycin) by monitoring oxidation of Amplex Red with a SPEX Fluoromax 3 (HORIBA Jobin Yvon) spectrofluorometer as previously described (Anderson et al., 2009). Prior to measurements, fiber bundles were depleted of all endogenous adenine nucleotides with a brief incubation in 10mM pyrophosphate and to inhibit contraction of the fibers during the assay. At the conclusion of each experiment,

PmFBs were washed in double-distilled H₂O to remove salts, frozen at -20°C, and dried via lyophilization (Labconco Corp., Kansas City, MO). Mitochondrial H₂O₂ emission is expressed as pmol/min/mg dry weight.

2.10 Targeted Metabolic Profiling

Mixed gastrocnemius, liver and plasma samples were profiled by the Sarah W. Stedman Nutrition and Metabolism Center Metabolomics Core Facilities at Duke University. Acylcarnitine measurements were obtained using flow injection tandem mass spectrometry and sample preparation methods as previously described (An et al., 2004; Haqq et al., 2005; Koves et al., 2008; Millington et al., 1990). Data were acquired with a Micromass Quattro Micro TM systems equipped with a model 2777 autosampler, a model 1525 HPLC solvent delivery system and a data system controlled by MassLynx 4.0 operating system (Waters, Millford, MA). Organic acid measurements were acquired with a Trace Ultra GC coupled to a Trace DSQ MS operating under Excalibur 1.4 (Thermo Fisher Scientific, Austin TX). AcylCoAs were derived to their acylCoA esters and separated on a phenylhexyl column by high-performance liquid chromatography (Beckman System Gold 126).

2.11 Enzyme Activity Assays

2.11.1 Citrate Synthase

Citrate synthase is the rate-limiting enzyme of the TCA cycle that catalyzes the conversion of acetyl-CoA and oxaloacetate into citrate and CoASH. The formation of

citrate cannot be measured directly, but the reduction of DTNB over time by CoASH can be measured spectrophotometrically at 412nm and is proportional to citrate synthase activity (Srere, 1969). The following reagents were needed: 100mM Tris (pH 8.3), 30mM acetyl-CoA, 10mM DTNB, 1.05mM oxaloacetate and citrate synthase activity buffer (0.1mM DTNB and 0.45mM acetyl-CoA). Mitochondria samples were prepared with proteases, freeze-fractured 3x and sonicated. To each well was added 10 μ L of homogenate (or serial dilutions of homogenate) and 190 μ L of citrate synthase reaction buffer. The plate was read kinetically on the SpectroMax spectrophotometer (Molecular Devices, Silicon Valley, CA) for 2 min to obtain baseline readings. To start the reaction, 10 μ L of 1.05mM oxaloacetate (50 μ M final concentration) was quickly added to each well before kinetically reading the plate for an additional 7 min. The difference in slopes between the final reading and the baseline represented the citrate synthase activity. The data was normalized to the molar extinction coefficient for DTNB (13.6mM⁻¹ • cm⁻¹) and protein content using the following equation: specific activity = $(r_A / l * \epsilon_B * V_B) \times (V_{\text{well}} / V_{\text{sample}} * \rho)$, where r_A is the rate in OD/min, l is the path length in cm, ϵ_B is the molar extinction coefficient for DTNB in mM⁻¹ • cm⁻¹, V_B is the stoichiometric number of DTNB, V_{well} is the volume in the well in μ L, V_{sample} is the volume of the sample in μ L and ρ is the protein concentration in mg/mL. Therefore, the final units for citrate synthase specific activity were expressed as μ mol/min/mg mitochondrial protein.

2.11.2 Short-Chain Hydroxyacyl-CoA Dehydrogenase (SCHAD)

SCHAD is the chain-length-specific form of the third enzyme in mitochondrial β -oxidation, which catalyzes the conversion of β -hydroxyacyl-CoA and NAD^+ to β -ketoacyl-CoA and NADH. The enzyme was assayed in a 96-well plate employing the reverse direction by measuring the decrease in absorbance at 340nm due to the dehydrogenation of NADH using a modified protocol (Binstock and Schulz, 1981; Hale et al., 1997). Mitochondrial samples are prepared with proteases the day of the assay, freeze-fractured 3x and sonicated. To each well was added 10 μ L of homogenate (or serial dilutions of homogenate) and 190 μ L of SCHAD assay buffer (100mM potassium phosphate, 0.1mM EDTA, 0.1mM NADH and 0.3mg/mL of essential fatty acid free BSA, pH 6.5). The plate was read kinetically at 340nm at 30°C for 2 min on the SpectroMax spectrophotometer (Molecular Devices, Silicon Valley, CA) for a baseline reading. The reaction was started with the addition of 10 μ L of 1.05mM C_4 (acetoacetyl-CoA) to a final concentration of 50 μ M. The plate was read kinetically for an additional 5 min to obtain a final reading, which consisted of the slope only during the linear range. The difference in slopes between the final reading and the baseline represented SCHAD activity. The data was normalized to the molar extinction coefficient for NADH (6.22mM⁻¹ • cm⁻¹) and protein content using the previously described specific activity equation.

2.11.3 β -Hydroxybutyrate Dehydrogenase (BDH1)

BDH1 is the enzyme that catalyzes the conversion of β -hydroxybutyrate and NAD^+ to acetoacetate and NADH in the oxidation of ketones. This enzyme activity assay was modified from previously described methods (Grinblat et al., 1986; Lehninger et al., 1960; Lippolis et al., 1988) and measured the reduction of NAD^+ at 37°C over 15 min. Mitochondria were isolated the day of the assay with proteases, freeze-fractured 3x, thoroughly sonicated and resuspended to $1\mu\text{g}/\mu\text{L}$ in SET buffer. Sonication was performed in 10 s bursts over 1 min on ice using a 60 Sonic Dismembrator (Fisher-Scientific) at a speed of 9kc. Each sample was assayed on a SpectroMax spectrophotometer (Molecular Devices, Silicon Valley, CA) in a cuvette by adding $200\mu\text{L}$ of $1\mu\text{g}/\mu\text{L}$ mitochondria to $722\mu\text{L}$ of BDH1 activity buffer (50mM Tris-HCl, 2mM NAD^+ , 20mM sodium hydroxybutyrate, 1mM KCN, $0.4\mu\text{g}/\text{mL}$ rotenone and $0.4\text{mg}/\text{mL}$ BSA). Initial readings were obtained at 37°C over 2 to 3 min at 340nm, until a flat baseline was reached. The reaction was started with the addition of $50\mu\text{L}$ of 400mM 3-hydroxybutyrate (final concentration $20\mu\text{M}$) and read over an additional 15 min. The slope of the reaction was determined over the linear range and used to calculate BDH1 activity using the previously described specific activity equation.

2.11.4 Branched-Chain Ketoacid Dehydrogenase (BCKAD)

BCKAD activity rates were determined by measuring the production of $[^{14}\text{C}]\text{-CO}_2$ from $1.25\mu\text{Ci}/\text{mL}$ $[1\text{-}^{14}\text{C}]\text{-leucine}$ ($100\mu\text{M}$) to target just the BCKAD enzymatic reaction,

which involves the conversion of the intermediate 2-ketoisocaproic acid to isovaleryl-CoA. Otherwise, the protocol was unchanged from that described for leucine oxidation in isolated mitochondria.

2.11.5 Isocitrate Dehydrogenase (ICD2 & ICD3)

Isocitrate dehydrogenase is the enzyme that catalyzes the oxidative decarboxylation of isocitrate to form α -ketoglutarate and CO₂. ICD3 is the NAD⁺-dependent isoform that functions as part of the TCA cycle, while ICD2 functions outside of the TCA cycle and uses NADP⁺ as a cofactor instead of NAD⁺. The assays were modified from previously described methods (Reisch and Elpeleg, 2007; Yarian et al., 2006) and measured the reduction of either NAD⁺ or NADP⁺ over time at 30°C. Mitochondria were prepared the day of the assay using proteases, resuspended to 1 μ g/ μ L in SET buffer, freeze-fractured 3x and sonicated. The ICD enzyme activity assay buffer (70mM Tris-HCl, pH 7.2, 2mM NAD⁺ or NADP⁺, 2mM ADP, 8mM MgCl₂, 1mM MnCl₂ and 5 μ L/mL of Antimycin A [5% in EtOH]) was prepared from stock solutions, 675 μ L added to a microcentrifuge tube and warmed in a 37°C water bath. The warmed buffer was transferred to a cuvette and blanked on a SpectroMax spectrophotometer (Molecular Devices, Silicon Valley, CA) at 30°C, 340nm to establish a reference reading. To the cuvette were added 150 μ g of mitochondria and a baseline reading was obtained for 5 min or until flattened. To initiate the reaction a mixture of 10mM citrate and 1.5mM Ds-isocitrate was added with readings monitored for another 7 min. The slope

of the reaction was determined over the linear range and used to calculate the specific activity of ICD2 or ICD3 as previously described.

2.11.6 Succinate Dehydrogenase (SDHA)

SDHA provides the binding site for the oxidation of succinate to fumarate in the TCA cycle using FAD⁺ as a co-factor, while the remaining subunits are involved the reduction of ubiquinone to ubiquinol, as part of the ETC. Unlike other TCA cycle enzymes, the key components, including FAD⁺, cannot be measured directly. Therefore, SDHA was measured spectrophotometrically at 600nm based upon the reduction of an artificial electron acceptor, 2,6-dichlorophenolindophenol (DCIP), by phenazine methosulfate (PMS). This assay was modified from those previously described (Reisch and Elpeleg, 2007; Yarian et al., 2006). Mitochondria were prepared the day of the assay using proteases, resuspended to 1 μ g/ μ L in SET buffer, freeze-fractured 3x and sonicated. To activate the enzyme, 100mM potassium phosphate buffer (pH 7.4) was preincubated with 20mM succinate and 5-10 μ g of mitochondria for 5 min at 37°C. The warmed buffer was transferred to a cuvette and blanked on a SpectroMax spectrophotometer (Molecular Devices, Silicon Valley, CA) at 30°C, 600nm to establish a reference reading. A baseline reading was taken after the addition of 2mM KCN for 2 min or until the slope flattened. To initiate the reaction, 200 μ M DCIP and 1.6mM PMS were added to the cuvette and the reading continued for another 5 min. The slope of the reaction was determined over the linear range and used to calculate the specific activity of SDHA,

which was normalized to the molar extinction coefficient for DCIP ($21\text{mM}^{-1} \cdot \text{cm}^{-1}$) and protein content.

2.11.7 Pyruvate Dehydrogenase (PDH)

PDH activity rates were determined by measuring the production of [^{14}C]- CO_2 from $0.625\mu\text{Ci/mL}$ [^{14}C]-pyruvate (1mM with 0.15% BSA) to target just the PDH reaction, which involves the oxidative decarboxylation of pyruvate to acetyl-CoA. Otherwise, the protocol was unchanged from that described for pyruvate oxidation in isolated mitochondria.

2.11.8 Aconitase

Aconitase catalyzes the isomerization of citrate to isocitrate. Its activity was measured by the Szweda lab, as previously described (Nulton-Persson and Szweda, 2001). Mitochondria were isolated using a mechanical preparation, resuspended to $1.5\mu\text{g}/\mu\text{L}$ in KMEM and shipped on dry ice O/N to the Szweda lab. Mitochondria were diluted to $0.05\mu\text{g}/\mu\text{L}$ in 25.0mM potassium phosphate buffer (pH 7.25) with 0.5mM EDTA and 0.01% Triton X-100 and sonicated. Aconitase activity was assayed as the rate of NADP^+ reduction (340nm , $\epsilon = 6.2\text{mM}^{-1} \cdot \text{cm}^{-1}$) by isocitrate dehydrogenase upon the addition of 5.0mM sodium citrate, 0.6mM MgCl_2 , 0.2mM NADP^+ , and 1.0 Unit/mL isocitrate dehydrogenase to the mitochondria.

2.11.9 α -Ketoglutarate Dehydrogenase (α -KGD)

α -KGD catalyzes the decarboxylation of α -ketoglutarate with the reduction of NAD⁺ to form the end product, succinyl-CoA. α -KGD activity was assayed by the Szweda lab, as previously described (Applegate et al., 2008). The same concentrated mitochondria used for the evaluation of aconitase activity were used here. Briefly, the mitochondria were diluted to 0.05mg/mL in 25mM MOPS with 0.05% Triton X-100 (pH 7.4). α -KGD activity was measured spectrophotometrically following the reduction of NAD⁺ (340nm, $\epsilon = 6.2\text{mM}^{-1} \cdot \text{cm}^{-1}$) upon the addition of 5.0mM MgCl₂, 2.5mM α -ketoglutarate, 0.1mM CoASH, 40.0 μ M rotenone, 0.2mM thiamine pyrophosphate and 1.0mM NAD⁺. Where indicated, deglutathionylation of α -KGD was accomplished by the addition of glutaredoxin (1.0 U/mL, CalBiochem) and GSH (0.5mM) prior to analysis of activity.

2.12 Analysis of mRNA Expression

Total RNA was isolated from mixed gastrocnemius using the total RNA isolation kit (Qiagen, Valencia, CA). RNA quality and quantity were determined with a NanoDrop 8000 (Thermo Scientific). cDNA was synthesized from 1 μ g RNA using the IScript cDNA synthesis kit (Bio-Rad, Hercules, CA) in a 20 μ L reaction volume and diluted 5-fold for subsequent RT-PCR. mRNA abundance was assayed by real-time quantitative PCR using a Prism 7000 with TaqMan real-time master mix and pre-designed/pre-validated FAM-labeled Assays-on-Demand (Applied Biosystems, Foster

City, CA). Data was normalized using values from a duplexed reaction with a VIC-labeled 18S endogenous control (Applied Biosystems).

2.13 Protein Expression

Gastrocnemius muscle and liver lysates were prepared in a homogenization buffer containing 20mM HEPES, 2mM EGTA, 50mM NaF, 100mM KCl, 0.2mM EDTA, 50mM β -glycerphosphate, 5.6mM CHAPS, 1:100 Triton X-100, Protease Inhibitor Cocktail (SIGMA), Phosphatase Inhibitor Cocktails 2 and 3 (SIGMA) and 0.0001 μ g/ μ L microcystin. Protein concentrations were determined using a BCA Assay (SIGMA) and separated on Criterion gels (Bio-Rad, Hercules, CA). Blots were blocked with 0.45% fish gelatin for 1 h then exposed to primary antibody to detect citrate synthase (Alpha Diagnostics International, San Antonio, TX), OXPHOS complexes (Mitosciences), BDH1, ICD3 (Abcam, Cambridge, UK), BCKAD E1 α (generously provided by Dr. Chris Lynch) and TXNIP (generously provided by Dr. Roger Davis). MemCode (Pierce, Rockford, IL) protein staining served as a loading control for each blot with band intensity being quantified using ImageQuant software (Amersham Biosciences). Proteins were visualized with secondary antibodies labeled with IRDye infrared dyes using an Odyssey CLx Infrared Imaging System and Image Studio software (LI-COR Biosciences, Lincoln, NE).

2.14 GSH/GSSG Assay

This protocol was adapted and optimized for tissue and cells from the Biotech® GSH/GSSG-412 assay kit for whole blood (OxisResearch, Portland, OR). The following reagents are provided in the kit: Assay buffer, GSSG buffer, Enzyme (glutathione reductase), Chromogen (DTNB), GSH standards (0.00, 0.005, 0.0125, 0.025, 0.075 and 0.150 μ mol) and NADPH (resuspended in assay buffer). Metaphosphoric acid (5%w/v) and 25mM M2VP (pH 2.8) were prepared in dH₂O (Sigma-Aldrich). M2VP is a reagent that scavenges GSH, but does not interfere with the enzymatic assay, thus allowing only for the measurement of GSSG.

2.14.1.1 Muscle Tissue

For each animal, two 2.0mL microcentrifuge tubes containing ~10-15mg of powdered gastrocnemius muscle were kept in liquid N₂. For the GSH sample, 5% metaphosphoric acid (1:20 dilution) was added to the tube, with a 3mm glass bead, vortexed and placed on ice. For the GSSG sample, 5% metaphosphoric acid (1:20 dilution) and the 25mM stock of M2VP (to a final concentration of 2.5mM or 1:21 dilution) was added immediately before adding the 3mm glass bead and vortexing. To prepare the blank, 25 μ L of 5% metaphosphoric acid was added to 175 μ L of GSSG buffer (1:8 dilution). All samples were then homogenized 2x for 2 min at 30Hz using the TissueLyser II (Qiagen) and returned to ice. All samples were centrifuged (14,000 \times g, 5 min, 4°C), supernatant removed and stored on ice. Adding 9 μ L of sample extract to

189 μ L of Assay buffer further diluted the GSH samples (a 1:22 dilution so the final dilution is 1/440), while adding 50 μ L of sample extract to 150 μ L of GSSG buffer diluted the GSSG samples another 1:4 (1:84 final dilution).

The assay employs DTNB, which reacts with GSH to form a spectrophotometrically detectable product at 412nm, while GSSG can be determined by the reduction of GSSG to GSH. The reaction rate is proportional to the GSH and GSSG concentrations. To each well on a 96-well plate was added 50 μ L of standards, blank or samples, followed by 50 μ L of chromogen (DTNB) and 50 μ L of enzyme (glutathione reductase). The plate was mixed and incubated at room temperature for 5 min. The assay was started with the addition of 50 μ L of NADPH to each well. The basic kinetics protocol of the SpectroMax spectrophotometer (Molecular Devices, Silicon Valley, CA) was used to record the change of absorbance every 10 s at 412nm for 3 min and determine the slope.

The concentrations of total GSH and GSSG in the samples were determined from their respective calibration curves. The GSH curve consisted of the 0.00, 1.50 and 3.00 μ M GSH data points, while the GSSG curve consisted of the 0.00, 0.10, 0.25, 0.50, 1.50 and 3.00 μ M data points. Total GSH (GSH_t) and GSSG were expressed as nmol GSH/g muscle tissue using the following equation: GSH_t or GSSG = [(net rate–intercept/slope) x dilution factor]. For total GSH, the final dilution factor is 440. To calculate GSH as μ mol, multiply the answer by 50 (because you used 50 μ L of standard per well) and

divide by 1,000,000 to get the proper units. Divide by g of tissue to obtain $\mu\text{mol GSH/g}$ tissue. Multiply by 1000 to obtain final units of nmol GSH/g tissue . The dilution factor for GSSG accounts for the conversion of GSH to GSSG (84-fold dilution divided by 2 GSH molecules). Therefore, the GSSG dilution factor is 42. Lastly, the GSH/GSSG ratio was calculated using following equation: $\text{ratio} = (\text{GSH}_t - 2\text{GSSG})/\text{GSSG}$.

2.14.1.2 MEFs

For each treatment condition, three wells of a 6-well plate were used to measure the concentrations of GSH, GSSG and protein, respectively. GSH sample wells were washed 2x in PBS and cells lysed and collected in 200 μL of 5% metaphosphoric acid by scraping with a plastic spatula. Cells in the GSSG sample wells were lysed and collected in 200 μL of 5% metaphosphoric acid with 20 μL of 25mM M2VP. All samples were sonicated, incubated on ice for 5 min and centrifuged (14,000 $\times g$, 5 min, 4°C). The supernatant from the GSH samples were further diluted (1:20) by adding 10 μL of extract to 190 μL of Assay buffer, while the GSSG samples were diluted (1:4) by adding 50 μL of extract to 150 μL of GSSG buffer. The blank was prepared from 50 μL of 5% metaphosphoric acid and 150 μL of GSSG buffer. The cells in the protein sample wells were washed 2x in PBS, lysed and collected in 2x SDS. After three repeated freeze-thaw cycles and sonication, the samples were centrifuged (14,000 $\times g$, 5 min, room temperature) and the extract used for protein quantification using a BCA assay (Sigma-Aldrich).

All remaining aspects of the assay were conducted as previously described. GSH and GSSG were expressed as $\mu\text{mol GSH/g protein}$ using the following equation: $\text{GSH or GSSG} = [(\text{net rate-intercept})/\text{slope}] \times \text{dilution factor}$, where the GSH dilution factor was 20 and the GSSG dilution factor was 2. The GSH/GSSG ratio calculation was unchanged.

2.15 NADH and NADPH

NADH and NADPH concentrations were measured spectrofluorometrically as previously described with excitation and emission wavelengths of 340 and 460nm, respectively (Nulton-Persson and Szweda, 2001).

2.16 Statistical Analysis

Data are expressed as means \pm SEM. Results were analyzed by *Student's* t-test unless otherwise indicated in the figure legends. A *p* value less than or equal to 0.05 was considered statistically significant.

3. Targeted Metabolomics Connects TXNIP to Adaptive Fuel Selection and Regulation of Specific Mitochondrial Oxidoreductase Enzymes in Skeletal Muscle

3.1 Introduction

Thioredoxin-interacting protein (TXNIP), also known as vitamin D₃ up-regulated protein 1 (VDUP-1) (Chen and DeLuca, 1994) and thioredoxin-binding protein 2 (TBP-2) (Nishiyama et al., 1999), is a ubiquitously expressed 46-kDa protein that binds to the catalytic center of thioredoxin (TXN), an antioxidant protein that regulates the reversible oxidation/reduction of protein thiols/disulfides (Bodnar et al., 2002; Nordberg and Arner, 2001). Thus, TXNIP serves as a negative regulator of TXN activity and sensitizes the cell to oxidative stress (Nishiyama et al., 1999). Structurally, TXNIP belongs to the α -arrestin super family of proteins that are characterized by a two-lobe, immunoglobulin-like β -strand sandwich motif (Alvarez, 2008). Recent findings suggest that at least some biological functions of TXNIP are mediated via the arrestin domain rather than its redox sensitive cysteine residues (Spindel et al., 2012).

Evidence that TXNIP plays a critical role in metabolic regulation first came to light when the hyperlipidemic phenotype of the HcB-19/Dem (HcB-19) mouse strain was linked to a nonsense mutation in the *txnip* gene, resulting in complete loss of the protein. In addition to hypertriglyceridemia, hypercholesterolemia and increased secretion of triglyceride-rich lipoproteins (Bodnar et al., 2002), HcB-19 mice have abnormally high

levels of free fatty acids and ketones during food restriction, suggesting perturbations in either the production or clearance of these fuels (Bodnar et al., 2002; Donnelly et al., 2004; Hui et al., 2004; Sheth et al., 2005). Many of the same metabolic features were recapitulated in three additional mouse models with targeted disruptions in the *txnip* gene (Chutkow et al., 2010; Chutkow et al., 2008; Hui et al., 2008; Oka et al., 2006a). As compared to the HcB-19 strain, the genetically engineered mouse lines develop a more severe phenotype that encompasses liver steatosis, gastrointestinal bleeding and poor survivability during prolonged (≥ 48 h) fasting (Oka et al., 2006a).

In addition to regulating lipid metabolism, strong evidence has established a central role for TXNIP in cellular glucose homeostasis. For example, numerous studies in cultured cells have shown that overexpression of TXNIP lowers glucose uptake, whereas silencing of the gene imparts the opposite effect. Likewise, each of the foregoing mouse models of TXNIP deficiency is characterized by fasting-induced hypoglycemia, improved glucose tolerance, enhanced insulin sensitivity and increased glucose transport into peripheral tissues (Chutkow et al., 2010; Chutkow et al., 2008; Hui et al., 2008; Oka et al., 2006a). Notably, this insulin sensitive phenotype is maintained even when TXNIP null animals are fed a high fat diet (Chutkow et al., 2010; Hui et al., 2008) or bred into the obese, *ob/ob* background (Yoshihara et al., 2010), raising interest in this protein as a potential antidiabetic drug target.

The molecular mechanisms underlying the profound metabolic consequences of TXNIP deficiency appear to be highly complex and tissue dependent. Previous studies have implicated perturbations in pancreatic insulin secretion (Hui et al., 2004), hepatic glucose output (Chutkow et al., 2008), Akt signaling (Hui et al., 2008), GLUT1 trafficking (Wu et al., 2013), NLRP3 inflammasome activation (Zhou et al., 2010) and oxidative stress (Schulze et al., 2004). There is growing suspicion that at least some of these outcomes are secondary to mitochondrial dysfunction and impaired oxidative metabolism. For example, reduced gluconeogenesis in liver of the TBP2^{-/-} mice was linked to diminished fatty acid flux through the TCA cycle (Bodnar et al., 2002; Donnelly et al., 2004; Oka et al., 2006b; Sheth et al., 2005). Additionally, oxidation rates of [¹⁴C]-labeled glucose, fatty acids and ketones are lower in isolated skeletal muscles from TXNIP knockout (TKO) mice compared to their littermate controls (Hui et al., 2008); and pyruvate oxidation is disrupted in heart mitochondria from TKO mice (Yoshioka et al., 2012). Most notably, in both cell culture and animal models, deletion of TXNIP results in robust increases in lactate production, a strong biomarker of oxidative insufficiency (Bodnar et al., 2002; Chutkow et al., 2008; Hui et al., 2008; Parikh et al., 2007; Sheth et al., 2005; Yoshioka et al., 2012).

Collectively, the foregoing findings point to potential respiratory deficits in multiple tissues of TKO mice, fueling widespread speculation surrounding a critical role for this protein in regulating mitochondrial function. Importantly however, rigorous

experimental evidence to support this presumption is sparse. The purpose of the present study was to further delineate the connection between TXNIP and oxidative metabolism in skeletal muscle and liver. To this end, we employed targeted metabolomics and comprehensive bioenergetic analyses to evaluate oxidative metabolism and respiratory kinetics in mouse models of total body and skeletal muscle-specific *txnip* deficiency. In aggregate, our results show that TXNIP is not required for normal functioning of the electron transport chain (ETC), but is essential for maintaining skeletal muscle protein expression of specific mitochondrial dehydrogenase enzymes that permit switching from glucose to alternative fuels. These findings shed new insight into the physiological function of TXNIP and the metabolic turmoil caused by its deficiency.

3.2 Results

3.2.1 TXNIP Deficiency Disrupts Whole Body Energy Metabolism

Previous studies examining the metabolic consequences of whole body *txnip* deficiency were performed in the context of prolonged food deprivation (18-36 h) (Bodnar et al., 2002; Chen et al., 2008b; Hui et al., 2008; Oka et al., 2006a; Sheth et al., 2005). To avoid the complexities of a starvation response, herein we examined metabolic regulation during a 5-6 h fast. In the morning after overnight *ad libitum* feeding and throughout 6 h of food withdrawal, *txnip* knockout (TKO) mice had lower blood glucose levels and higher blood lactate (Fig. 3-1A). In line with earlier reports, when challenged

with an intraperitoneal injection of glucose, TKO mice exhibited exquisite glucose tolerance (Fig. 3-1B) despite increased body weight (Fig. 3-1C) and higher circulating levels of lipid-derived fuels such as triglycerides (TAGs), NEFAs and ketones (Fig. 3-1D). Because TXNIP is expressed abundantly in skeletal muscle (Fig. 3-1E), the principal contributor to circulating lactate, we proceeded to examine muscle glucose metabolism *ex-vivo*. In isolated soleus muscles from TXNIP KO compared to WT mice lactate production was increased in both the basal and insulin-stimulated states, whereas glycogen synthesis was elevated only in the latter condition (Fig. 3-1F-G). Using the Lox-P/Cre strategy described in Material and Methods, we then generated mice lacking *txnip* specifically in skeletal muscle (TXNIP^{SKM^{-/-}}), but retaining expression in heart (Fig. 3-1H). The metabolic phenotype of these mice was remarkably similar to the TKO line (Fig. 3-1I-L), suggesting derangements in skeletal muscle energy metabolism contribute substantially to the phenotype of the TKO model. In sum, these findings are consistent with the idea that genetic ablation of TXNIP promotes glucose uptake and glycolytic metabolism in muscle.

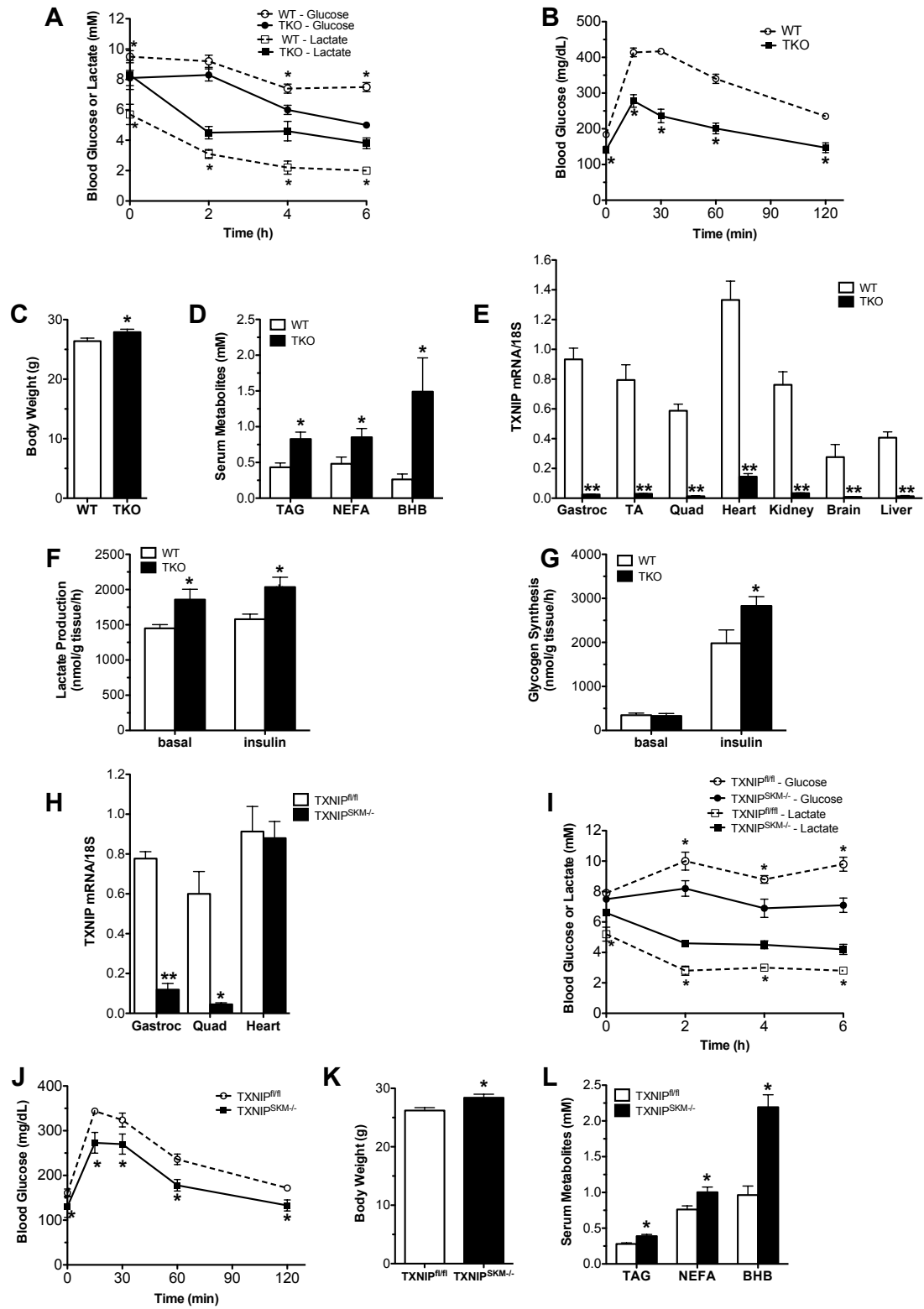


Figure 3-1: TXNIP Deficiency Alters Whole Body Energy Metabolism

TKO mice and WT littermates were fed a standard chow diet and metabolic parameters were measured at 18-22 weeks unless otherwise noted. (A) Blood glucose and lactate levels were measured 0-6 h following food withdrawal (n = 6). (B) Glucose tolerance tests were performed at 12 weeks of age using 1.75g/kg glucose administered 6 h after food withdrawal (n = 12). (C) Body weight at 22 weeks. (D) Plasma triglycerides (TAG), non-esterified fatty acids (NEFA) and β -hydroxybutyrate (BHB) were measured 5 h after food withdrawal at 9-12 weeks of age (n = 6-8). (E) TXNIP mRNA tissue distribution was measured by real-time quantitative PCR and normalized to 18S as an endogenous control gene (n = 5). (F) Lactate production and (G) rates of [14 C] glucose incorporation into glycogen were measured in isolated soleus muscles incubated 1 h \pm 100 nM insulin. (H) TXNIP mRNA expression in skeletal muscle and heart from TXNIP^{SKM-/-} and TXNIP^{fl/fl} mice (n = 3). Metabolic parameters of TXNIP^{SKM-/-} mice and TXNIP^{fl/fl} littermate controls measured at 12-14 weeks of age. (I) Blood glucose and lactate levels (n = 5). (J) Glucose tolerance tests (n = 6). (K) Body weight at sacrifice. (L) Plasma metabolites (n = 9). Data are means \pm SEM and results were analyzed by Student's t-test (*p \leq 0.05).

3.2.2 TXNIP Deficiency Compromises Exercise Tolerance

The higher glycolytic rates in TKO mice could be due to oxidative deficits, as previously suggested (Hui et al., 2008). Surprisingly however, when whole body energy metabolism was monitored by indirect calorimetry during a 72 h period we were unable to detect differences between genotypes in the respiratory exchange ratio (RER), heat production and oxygen consumption (data not shown). Physical activity and food consumption were also similar between groups. To further explore the connection between TXNIP and oxidative capacity in the context of increased energetic demand we challenged the mice with two distinct exercise tests. During a graded, high intensity regimen, peak VO₂ obtained by the TKO mice was 13% lower than that measured in their WT counterparts (Fig. 3-2A) whereas RER was elevated throughout the test, indicative of a substrate shift toward carbohydrate oxidation (Fig. 3-2B). Because fatty

acid oxidation becomes an essential source of energy during prolonged exercise, we next subjected the animals to a graded, mid-intensity endurance run using an open-air treadmill. As anticipated, exercise endurance was diminished in the TKO mice relative to the WT controls, evidenced by reduced time (78.0 ± 2.19 min vs. 84.8 ± 1.28 min) and distance (1774 ± 81.8 m vs. 2035 ± 52.3 m) to exhaustion (Fig. 3-2C-D). Circulating levels of β -hydroxybutyrate measured immediately after exercise were elevated in the TKO mice, consistent with impaired ketone uptake and/or catabolism (Fig. 3-2E). Importantly, TXNIP^{SKM^{-/-}} mice exhibited a similar exercise intolerant phenotype during both treadmill tests (Fig. 3-2F-J), again implicating muscle as a major site of metabolic dysregulation in the TKO mice. Although these results clearly point to a role for TXNIP in regulating muscle substrate selection, both loss-of-function models maintained considerable oxidative reserve, arguing against a severe defect in mitochondrial respiratory function.

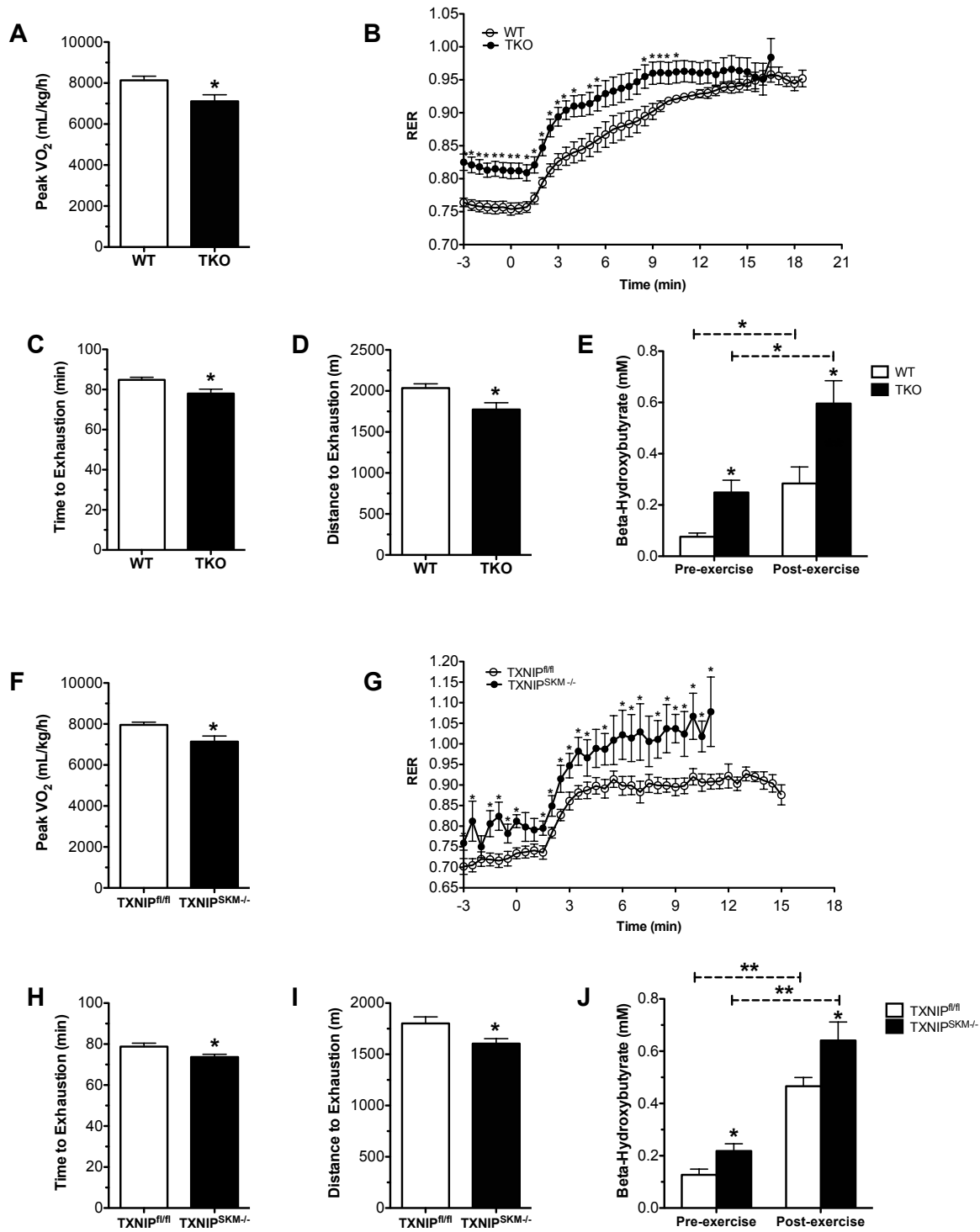


Figure 3-2: TXNIP Deficiency Decreases Exercise Tolerance

TKO mice and WT littermates were subjected to two different treadmill exercises at 12-15 weeks of age. Indirect calorimetry was used to measure (A) peak VO_2 and (B) the respiratory exchange ratio (RER) (VCO_2/VO_2) as a function workload during a graded, high intensity regimen. Exercise endurance was evaluated using an open-air treadmill and a mid-intensity regimen. Performance was assessed by measuring (C) time (min) and (D) distance (meters) to exhaustion. (E) Plasma β -hydroxybutyrate was measured prior to and immediately after endurance exercise. Data are expressed as means \pm SEM from 7-8 animals per group. The same tests were administered to TXNIP^{SKM^{-/-}} mice and TXNIP^{fl/fl} littermate controls at 22-24 weeks of age. (F) Peak VO_2 . (G) RER. (H) Time and (I) distance to exhaustion. (J) Plasma β -hydroxybutyrate concentrations. Data are expressed as means \pm SEM from 5-7 animals per group and results were analyzed by Student's t-test (* $p \leq 0.05$ and ** $p \leq 0.001$). Panels B and G were evaluated using a one-factor ANOVA and post hoc analysis to determine differences between groups.

3.2.3 TXNIP Deficiency Diminishes Substrate Oxidation in Muscle but Not Liver Mitochondria

We next sought to pinpoint the specific sites of oxidative dysfunction in the TXNIP null condition. Because TXNIP has been implicated in regulating energy metabolism in both skeletal muscle and liver, TKO mice were used to permit direct comparisons between these two tissues. Measurement of substrate oxidation in isolated soleus and EDL muscles revealed marked genotype-dependent deficits in glucose, fatty acid and amino acid catabolism (Fig. 3-3A-C). Notably, whereas TXNIP deficiency lowered glucose and fatty acid oxidation 25-30% in both soleus and EDL, oxidation rates of the branched chain amino acid (BCAA), leucine, were diminished 68% in soleus and 87% in EDL, as compared to WT muscles. Experiments in isolated mitochondria from TKO gastrocnemius muscles produced similar results, again showing moderate declines in pyruvate and palmitate oxidation (Fig. 3-3D-E) and a much more striking 75% deficit in leucine oxidation (Fig. 3-3F). By contrast, oxidation rates of all three substrates were

normal in liver mitochondria harvested from TKO compared to WT mice (Fig. 3-3G-I). Thus metabolic insufficiencies measured at the whole body level appeared to be due in large part to remodeling of the muscle oxidative machinery.

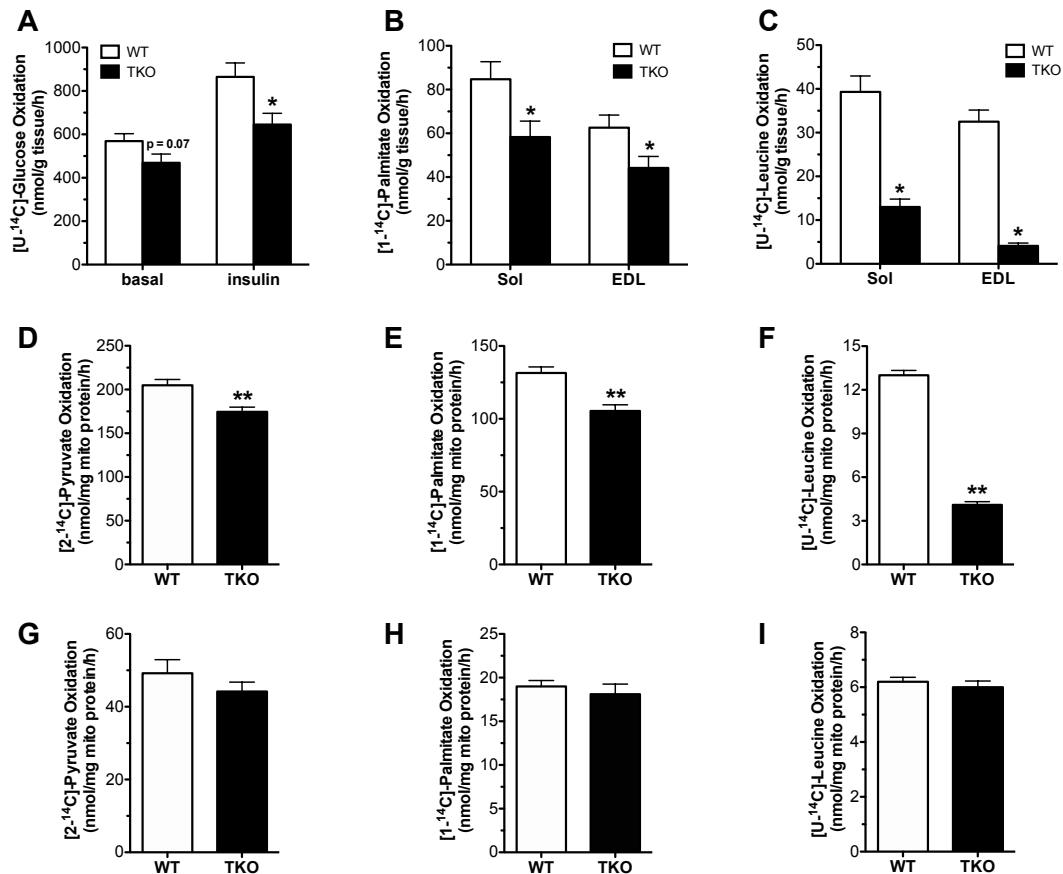


Figure 3-3: Mitochondrial Substrate Oxidation in Skeletal Muscle and Liver

Substrate oxidation assays were performed in tissues and mitochondria from TKO mice and WT littermates harvested 5-6 h after food withdrawal. (A) Oxidation of [U-¹⁴C]glucose to CO₂ was measured in isolated soleus muscles during a 2 h incubation in modified KHB buffer containing 5mM glucose ± 100nM insulin. (B) Oxidation of 500μM [1-¹⁴C]palmitate or (C) 200μM [U-¹⁴C]leucine to CO₂ was measured in isolated soleus and extensor digitorum longus (EDL) muscles during a 2 h incubation in modified KHB (n = 6). Isolated mitochondria from gastrocnemius muscles were used to measure substrate oxidation to CO₂ in the presence of (D) 1mM [2-¹⁴C]-pyruvate, (E) 100μM [1-¹⁴C]palmitate or (F) 100μM [U-¹⁴C]leucine for 30 min (n = 11-12). Isolated mitochondria from liver was used measure substrate oxidation to CO₂ in the presence of (G)

1mM [2-¹⁴C]-pyruvate, (H) 100μM [1-¹⁴C]palmitate or (I) 100μM [U-¹⁴C]leucine for 30 min (n = 6-12). Data are expressed as means ± SEM and results were analyzed using a one-factor ANOVA and post hoc analysis to determine differences between groups.

3.2.4 TXNIP Deficiency Does Not Affect Mitochondrial Content or Respiratory Function

We questioned whether the foregoing deficits in oxidative metabolism were related to changes in mitochondrial mass and/or respiratory function. Contrary to this possibility, muscle quantities of mitochondrial DNA (Fig. 3-4A), citrate synthase protein content (Fig. 3-4B) and enzyme activity (Fig. 3-4C), as well as protein abundance of several constituents of the electron transport chain (ETC) (Fig. 3-4D-E), were similar between genotypes. Comprehensive evaluation of respiratory function using isolated mitochondria and permeabilized fiber bundles also proved unremarkable. Thus, oxygen consumption measured under state 3, state 4 and uncoupled conditions in the presence of complex I-linked (glutamate/malate) or complex II-linked (succinate) substrates was similar in mitochondria isolated from gastrocnemius muscles of TKO and WT mice (Fig. 3-4F-G). Likewise, more rigorous assessment of respiratory kinetics using permeabilized fiber bundles in combination with a high resolution respirometry system revealed only modest abnormalities in ETC function (Fig. 3-4H). ADP-stimulated V_{max} in the presence of saturating glutamate-malate concentrations was 20% lower in the TKO mice, implying a minor deficit in maximal rates of ATP synthesis at Complex V. When substrate kinetics were analyzed at more physiological, submaximal

concentrations, we identified a subtle shift towards increased sensitivity (lower K_m) to glutamate, suggesting enhanced use of this fuel to provide NADH to Complex I (Fig. 3-4I). These findings argue against a major impingement at the level of the ETC.

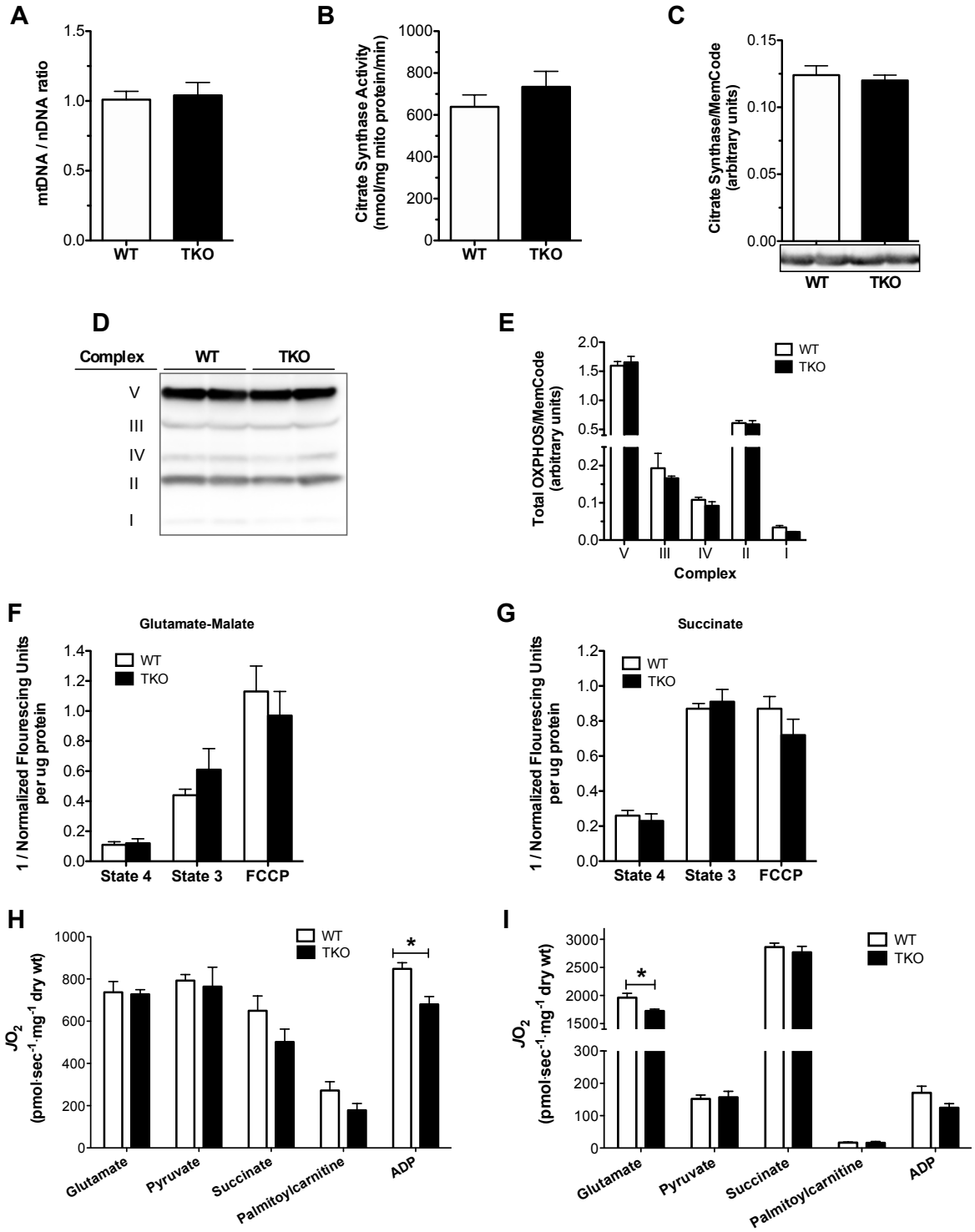


Figure 3-4: Mitochondrial Content and Respiratory Function in Skeletal Muscle

Gastrocnemius muscles from TKO mice and WT littermate controls were used to assess mitochondrial content and function. (A) Abundance of the COX1 gene encoded by mitochondrial DNA (mtDNA) relative to the β -actin gene encoded by nuclear (nDNA) performed by qRT-PCR. (B) Citrate synthase activity. (C) Citrate synthase protein expression and representative Western blot. (D) Western blot of complexes I-V of the electron transport chain (ETC) and (E) quantified results normalized to MemCode staining to control for loading. Oxygen consumption rates were measured in isolated mitochondria under state 3 and state 4 conditions or in response to chemical uncoupling (FCCP) in the presence of (F) glutamate/malate or (G) succinate. Respiratory function in situ was measured using permeabilized fiber bundles under (H) state 3 respiration conditions in the presence of maximal substrate concentrations, or (I) a range of low submaximal to maximal concentrations to determine substrate sensitivity (K_m). Data are expressed as means \pm SEM from 5-6 animals per group and results were analyzed by Student's t-test (* $p \leq 0.05$).

3.2.5 TXNIP Deficiency Disrupts Redox Balance Without Affecting Mitochondrial ROS Emission

Because TXNIP is best known for its role in redox regulation, we sought to determine whether the unique form of mitochondrial dysfunction in muscles from the TKO mice might be related to changes in redox balance. To this end, we measured a series of metabolites that report on shifts in cellular energy charge and oxidative stress. Interestingly, despite high rates of glycolysis and lactate production, muscle concentrations of NADH (Fig. 3-5A) were unchanged in the TKO mice. By contrast, levels of NADPH, which can also arise from glucose metabolism via the pentose-phosphate-shunt, were elevated 2.5-fold in the TKO mice (Fig. 3-5B), resulting in a striking decrease in the NADH/NADPH ratio (Fig. 3-5C). Conversely, TXNIP deficiency resulted in a 25% decline in muscle concentrations of reduced glutathione (GSH) and increased levels (33%) of the oxidized form, GSSG (Fig. 3-5D-F). Considering that GSH

participates in antioxidant defense, we questioned whether the low levels of this metabolite in TKO muscles were related to increased mitochondrial production of reactive oxygen species (ROS). On the contrary, when assayed in permeabilized fiber bundles, rates of succinate-supported mitochondrial H₂O₂ emission trended lower in the TKO group (Fig. 3-5G). Thus, the metabolic defects in TKO muscles did not appear to result from mitochondrial-derived oxidative stress.

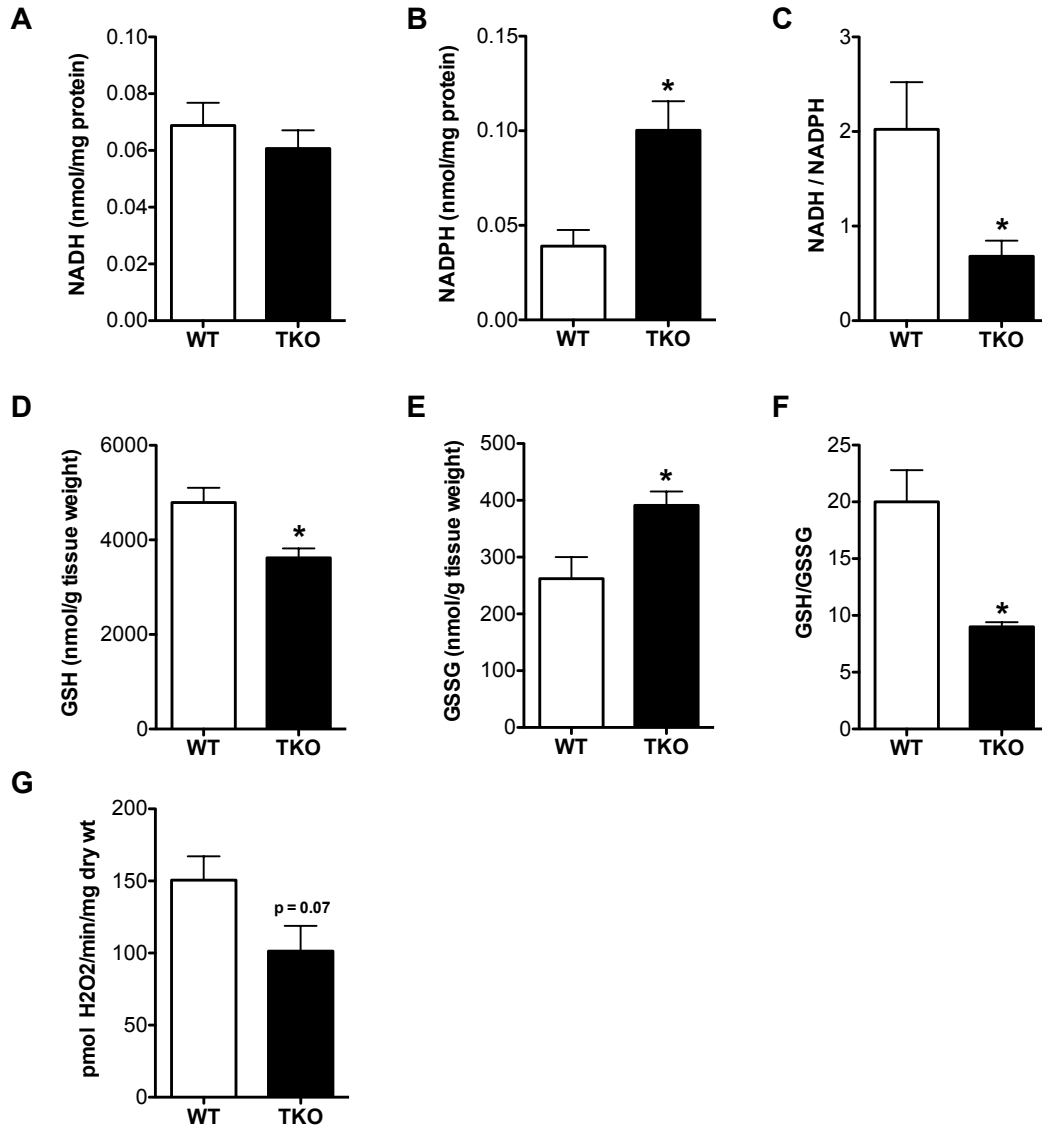


Figure 3-5: Redox Imbalance In TXNIP Deficient Skeletal Muscles

Skeletal muscles from TKO mice and WT littermate controls were harvested 5 h after food withdrawal and immediately flash frozen in liquid N₂ for subsequent assessment of redox metabolites. Gastrocnemius muscles were used to measure (A) NADH, (B) NADPH and (C) the NADH/NADPH ratio. Quadriceps muscles were used to measure (D) Reduced glutathione (GSH), (E) Oxidized glutathione (GSSG) and (F) the GSH/GSSG ratio. (G) Mitochondrial potential for producing reactive oxygen species was assessed in permeabilized fiber bundles by measuring succinate-supported H₂O₂ emission rates under state 4 conditions. Data are expressed as means ± SEM from 5-6 animals per group and results were analyzed by Student's t-test (*p ≤ 0.05).

3.2.6 Targeted Metabolomics Revealed Several Muscle-Specific Roadblocks in Mitochondrial Carbon Flux

To gain further insight into the oxidative lesions arising from TXNIP deficiency we used a targeted metabolomics approach to capture a snapshot of intermediary metabolism *in vivo*. Because mitochondrial degradation of carbon fuels results in the production of multiple acyl-CoA intermediates, we expected muscle quantities of these molecules to change in association with TXNIP expression. A survey of acyl-CoAs in gastrocnemius muscle from TKO compared to WT mice revealed a 35% reduction in acetyl-CoA (Fig. 3-6A), the universal end product of carbohydrate, fat and protein catabolism. Additionally, the leucine-derived metabolite, isovaleryl-CoA, was 65% lower in the TKO mice (Fig. 3-6A), and a similar trend was evident for several even chain, fatty acid-derived species (Fig. 3-6A). By virtue of the mitochondrial carnitine acyltransferase enzymes, the foregoing acyl-CoA intermediates give rise to their corresponding acylcarnitine conjugates, which also report on substrate flux at specific mitochondrial enzymes. Whereas muscle levels of acetyl-CoA-derived acetylcarnitine (C2) were unaffected by genotype (Fig. 3-6B), most odd chain/amino acid-derived acylcarnitines, as well as several medium and long chain/fatty acid-derived species, were reduced in accord with TXNIP deficiency (Fig. 3-6B). Long chain acylcarnitines are produced by the carnitine palmitoyltransferase enzymes (CPT1 and CPT2), which reside in the outer and inner mitochondrial membranes, respectively, and catalyze the initial steps in β -oxidation. Although a reduction in total long chain acylcarnitines (Fig. 3-6B)

is consistent with diminished CPT1 activity, tissue concentrations of malonyl-CoA, a potent glucose-derived inhibitor of CPT-1 (McGarry et al., 1978), were similar between genotypes (Fig. 3-6A). Therefore, reduced lipid catabolism in the TKO mice does not appear to result from malonyl-CoA-mediated inhibition of fat oxidation.

In contrast to many other even chain species, levels of 3-hydroxybutyrylcarnitine (C4-OH) were robustly elevated in the muscle of TKO mice (Fig. 3-6B). Because the C4OH metabolite can arise from the ketone intermediate, 3-hydroxybutyryl-CoA (Soeters et al., 2012), this finding is consistent with a severe bottleneck in ketolysis. Muscle concentrations of several glucose-derived organic acids and amino acids (including glycine, alanine and lactate) were elevated in the TXNIP null condition, whereas intermediates directly involved in anaplerotic entry of carbons into tricarboxylic acid (TCA) cycle (such as aspartate, glutamate, α -ketoglutarate and fumarate) were diminished (Fig. 3-6C-D). These results are consistent with perturbations in glycolysis and TCA cycle flux and might reflect increased trafficking through the malate/aspartate and glutamate/aspartate shuttles. Although muscle concentrations of the BCAAs (valine, leucine, isoleucine) were similar between groups (Fig. 3-6D), circulating levels of these metabolites were elevated in the TKO mice (Fig. 3-6E), consistent with a defect in BCAA catabolism. Whereas the metabolite signature in skeletal muscle was clearly distinguishable between genotypes, the only differentially abundant metabolites in TKO liver were the lower levels of long chain acylcarnitines

(Fig. 3-7A-C), which again occurred independent of changes in malonyl-CoA (not shown). In aggregate, these results add further evidence that TXNIP plays a key role in maintaining oxidative metabolism at sites upstream of the ETC.

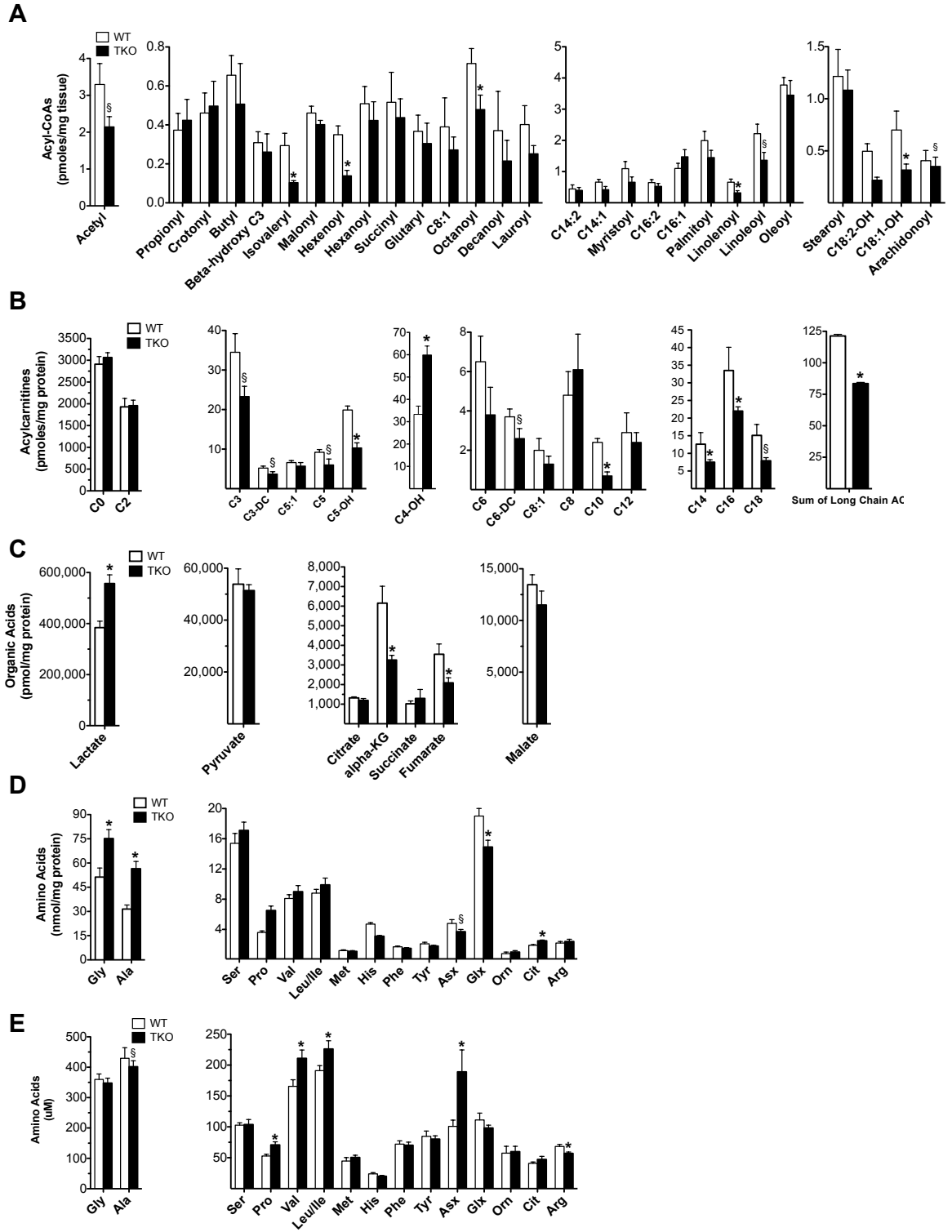


Figure 3-6: Targeted Metabolic Profiling of Skeletal Muscle and Serum

Gastrocnemius muscles and serum from TKO mice and WT littermate controls were harvested 5-6 h following food withdrawal at 18 weeks of age. Tissues were immediately flash frozen in liquid N₂ and subsequently processed for mass spectrometry-based measurement of (A) acyl-CoAs, (B) acylcarnitines, (C) organic acids, (D) amino acids and (E) serum amino acids. Data are expressed as means ± SEM from 5-7 animals per group. Results were analyzed by Student's t-test (*p ≤ 0.05 and §p ≤ 0.10).

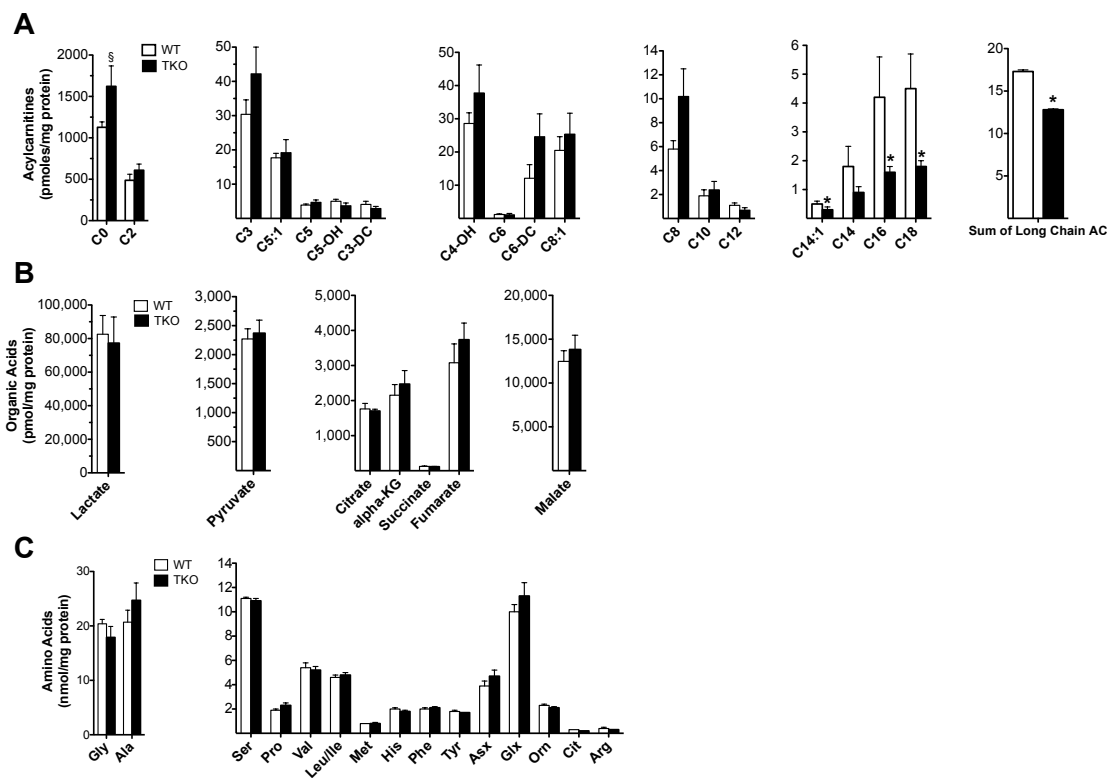


Figure 3-7: Targeted Metabolic Profiling of Liver

Liver from TKO mice and WT littermate controls were harvested 5-6 h following food withdrawal at 18 weeks of age. Specimens were immediately flash frozen in liquid N₂ and subsequently processed for mass spectrometry-based measurement of (A) acylcarnitines and (B) organic acids and (C) amino acids. Data are means ± SEM from 6 animals per group and results were analyzed by Student's t-test (*p ≤ 0.05 and §p ≤ 0.10).

3.2.7 TXNIP Deficiency Results in Muscle-Specific Deficits in Multiple Dehydrogenase Enzymes

The foregoing static metabolic profiles, taken together with the flux analyses presented in (Fig. 3-6A-E), pointed us toward several specific mitochondrial oxidoreductase enzymes responsible for degrading BCAAs, ketones and fatty acids, including branched-chain ketoacid dehydrogenase (BCKAD), β -hydroxybutyrate dehydrogenase (BDH1) and short-chain hydroxyacyl-CoA dehydrogenase (SCHAD). As predicted, the activities of these three enzymes were diminished 65%, 47% and 15%, respectively in mitochondria from TKO compared to WT muscles (Table 1). Likewise, activity of the NAD-dependent TCA cycle enzyme, isocitrate dehydrogenase (ICD3), was 27% lower in muscles from TKO compared to WT mice (Table 1). It is noteworthy however that the impact of TXNIP deficiency on mitochondrial dehydrogenase enzymes was not universal, as the activities of succinate dehydrogenase (SDHA), pyruvate dehydrogenase (PDH) and the NADPH-dependent isoform of isocitrate dehydrogenase (ICD2), were similar between genotypes (Table 1).

Table 1: Mitochondrial Dehydrogenase Activity

Enzyme	Activity (nmol/mg protein/h)		Percent Change
	WT	TKO	
BCKAD	66.7 (±1.42)	23.7 (±0.73)**	↓ 65%
BDH1	47.9 (±5.34)	24.8 (±2.52)**	↓ 47%
SCHAD	902 (±39.9)	770 (±40.5)*	↓ 15%
ICD3	129.3 (±9.55)	94.8 (±7.02)**	↓ 27%
SDHA	889 (±47.7)	817 (±25.4)	=
PDH	1229 (±28.0)	1240 (±29.6)	=
ICD2	215 (±9.1)	204 (±12.1)	=

Data are means ± SEM (n = 5 or 6 per group).

Results are analyzed by *Student's t-test* (* $p \leq 0.05$ and ** $p \leq 0.001$).

The = and ↓ indicate percent change in the TKO relative the WT control.

We proceeded to determine whether the decline in the aforementioned enzyme activities was related to changes in gene and/or protein expression. Whereas mRNA expression of these enzymes was similar between TKO and WT mice (Fig. 3-8A), Western blot analyses revealed marked deficits at the level of protein expression, as quantities of the BCKAD E1 α subunit, BDH1 and ICD3 were decreased 77%, 65% and

ICD3 22%, respectively (Fig. 3-8B). These changes in protein abundance were remarkably similar in muscles from TXNIP^{SKM^{-/-}} mice (Fig. 3-8C) and mirrored the degree to which oxidation rates of each respective substrate were diminished in the TXNIP null condition. By contrast, expression levels of the same three proteins were unchanged in liver of TKO mice as compared to their control littermates (Fig. 3-8D). Lastly, because TXNIP appeared to be essential for maximum oxidation of BCAA and ketones, we questioned whether TXNIP is transcriptionally upregulated in response to physiological stresses known to increase muscle reliance on alternative fuels. Indeed, overnight fasting, genetic diabetes and prolonged exercise increased TXNIP mRNA levels in rodent skeletal muscles. In sum, these findings establish a tissue-specific role for TXNIP in preserving mitochondrial capacity to switch substrates during glucose deprivation.

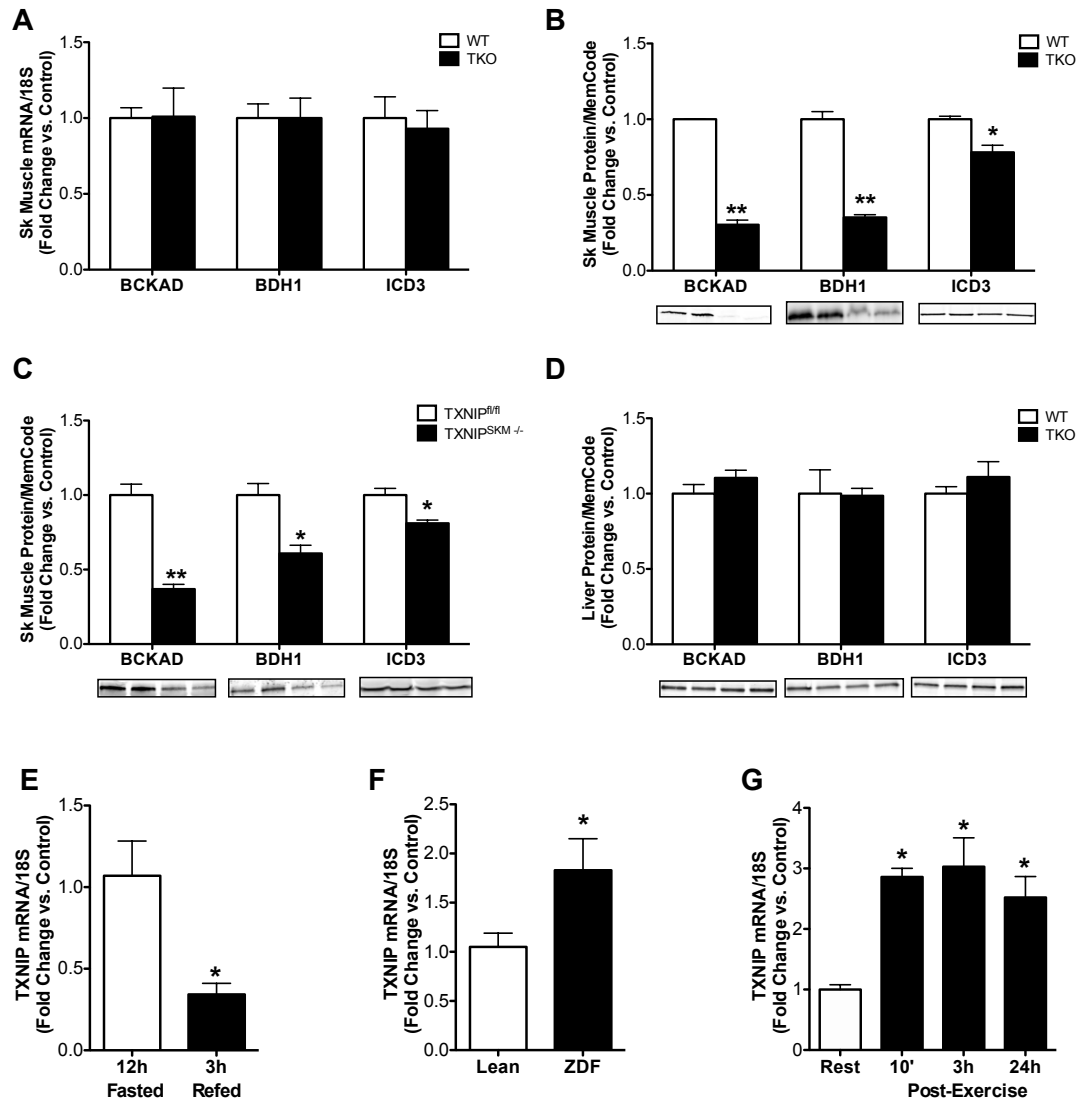


Figure 3-8: Expression of Mitochondrial Dehydrogenase Enzymes in Skeletal Muscle and Liver

Tissues were harvested 5-6 h following food withdrawal at 18-22 weeks of age. Skeletal muscles from TKO mice and littermate controls were used for qRT-PCR analysis of mRNAs encoding (A) *bckad*, *bdh1* and *icd3* normalized to 18S, and Western blot analysis of the (B) BCKAD E1 α , BDH1 and ICD3 proteins normalized to Memcode staining. Expression of the same proteins was measured in (C) gastrocnemius muscles from TXNIP^{SKM-/-} mice and TXNIP^{fl/fl} controls and (D) liver from TKO and WT controls. qRT-PCR analysis of mRNA encoding *Txnip* normalized to 18S was measured in skeletal muscles from (E) 12 h fasted and 3 h refed C57BL/6J mice, (F) Zucker Diabetic Fatty (ZDF) rats and lean controls (G) C57BL/6J mice at rest and 10 min, 3 h or 24 h after

a 90 min graded treadmill exercise. Data are means \pm SEM (n = 5 per group) and results were analyzed by Student's t-test (*p \leq 0.05 and **p \leq 0.001).

3.3 Discussion

TXNIP is a multifaceted molecule that sits at the crossroad of redox sensing, oxidative stress and metabolic control (Bodnar et al., 2002; Chutkow et al., 2010; Chutkow et al., 2008; Donnelly et al., 2004; Hui et al., 2008; Hui et al., 2004; Muoio, 2007; Oka et al., 2006b; Parikh et al., 2007; Sheth et al., 2005). Despite numerous reports showing that TXNIP deficiency causes profound derangements in energy metabolism, the molecular mechanisms underlying these consequences remain murky. Previous reports have suggested that loss of TXNIP leads to redox-mediated respiratory dysfunction that in turn gives rise to aerobic glycolysis, also known as the Warburg effect (Chutkow et al., 2008; Hui et al., 2008; Hui et al., 2004; Oka et al., 2006a; Sheth et al., 2005). Herein, we explored the connection between TXNIP and mitochondrial performance in skeletal muscle and liver, two principal organs responsible for whole body glucose and lipid homeostasis. We report several new and enlightening observations that add to our current physiological understanding this protein. First, TXNIP deficiency in skeletal muscle resulted in diminished oxidation of all major substrates, leading to reduced exercise tolerance. Second, the oxidative insufficiencies in TXNIP null muscles were not due to reductions in mitochondrial mass, impaired ETC function or increased mitochondrial ROS production; but instead were attributed to

decreased protein abundance of specific mitochondrial dehydrogenase enzymes, particularly those required for ketone and amino acid degradation. Lastly, the consequences of TXNIP deficiency were tissue-dependent, as the marked metabolic deficits evident in muscle mitochondria of TKO mice were absent in liver.

An important distinction between the current study and many previous investigations is that our analyses of the TKO mice were not preceded by a prolonged fast, which tends to expose and exacerbate defects in hepatocyte function. Herein, metabolic derangements in the TXNIP null mice were clearly evident in the fed state as well as during short-term food restriction. However, despite marked changes in circulating levels of several metabolic fuels, whole body energy expenditure and substrate selection were unchanged. This observation aligns with an earlier report (Chutkow et al., 2010) and fits with the finding that TXNIP deficiency did not affect substrate oxidation rates in isolated mitochondria from liver, an organ that contributes substantially to resting RER. By contrast, when animals were confronted with an exercise challenge, the genotype-dependent differences in muscle fuel selection were revealed. The higher RER in the TKO mice undergoing exercise agreed with the lower rates of fatty acid and amino acid oxidation measured in isolated muscles and isolated mitochondria. Although exercise tolerance was diminished in both TKO and TXNIP^{SKM-/-} mice, these animals were still capable of reaching and maintaining relatively high workloads during an acute treadmill test. This outcome is inconsistent with severe

respiratory defects. Indeed, subsequent experiments showed that mitochondrial content and ETC function were essentially normal in TXNIP null skeletal muscles. However, our analysis of respiratory kinetics did show subtle shifts in substrate sensitivity to glutamate, which enters the TCA cycle downstream of isocitrate dehydrogenase after its conversion to α -KG by glutamate dehydrogenase or aspartate aminotransferase. Thus, the lower K_m of glutamate could reflect enhanced flux through one or both of these enzymes.

Also noteworthy, despite high rates of glycolysis in the TXNIP null muscles, NADH levels were unchanged. This result adds further support to the notion that ETC function is not a limiting factor in the TKO mice, and raises the possibility that enhanced transfer of glucose-derived NADH to complex I via the malate/aspartate shuttle (Fig. 9) might compensate for deficiencies in fatty acid and amino acid catabolism during exercise. Additionally, this finding conflicts with the idea that NADH accumulation in TKO muscles might lead to inactivation of PTEN, a redox-sensitive phosphatidylinositol 3-phosphatase that lowers cellular levels of (3,4,5)-trisphosphate, thereby dampening Akt phosphorylation and insulin signaling (Hui et al., 2008). Because high NADH levels have been shown block TXN/NADP(H)-dependent activation of PTEN, investigators suggested that a rise in the cellular NADH/NADPH ratio, secondary to respiratory dysfunction, might be responsible for constitutive oxidation and inactivation PTEN, thus amplifying Akt phosphorylation. Although the latter outcomes were clearly apparent in

TKO muscles (Hui et al., 2008), NADH and NADPH were not measured. Herein, TXNIP deficiency did not affect NADH levels but instead caused a twofold rise in NADPH, possibly resulting from increased glucose transport (Mailloux and Harper, 2010) and subsequent metabolism in the pentose phosphate pathway (Stanton, 2012; Wamelink et al., 2008). NADPH provides reducing power for regenerating GSH and TXN. Surprisingly however, elevated NADPH levels in the TKO muscles were accompanied by lower GSH concentrations. Although the reason for this disconnect is uncertain, we suspect that substrate driven pressure on membrane associated NADPH oxidase (NOX), which generates superoxide, might give rise to non-mitochondrial H₂O₂ production, thereby increasing demands on the GSH oxidant scavenging system. Interestingly, NOX-derived ROS has been shown to target and inactivate PTEN as a part of a feed forward mechanism that boosts insulin action (Seo et al., 2005).

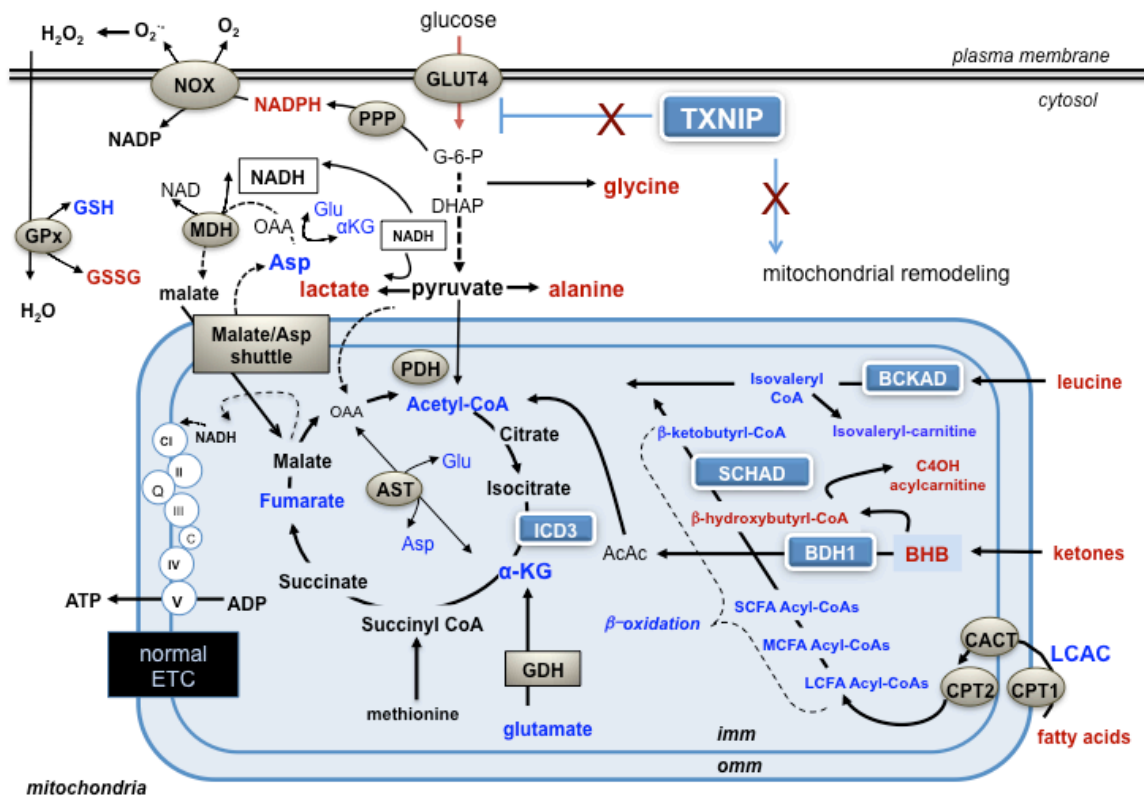


Figure 3-9: TXNIP Deficiency Disrupts Mitochondrial Fuel Selection

During periods of carbohydrate deprivation, upregulation of TXNIP serves to limit glucose transport into skeletal muscle and promote mitochondrial oxidation of alternative fuels. TXNIP deficiency enhances glucose uptake and flux through both glycolysis and the PPP. Despite this shift to glycolytic metabolism, respiratory function of the ETC remains intact, thereby permitting transfer of glucose-derived NADH to complex I via the malate/aspartate shuttle. Diminished protein expression and activities of specific mitochondrial dehydrogenase enzymes lowers capacity for fatty acid, amino acid and ketone catabolism, thus disrupting adaptive mitochondrial fuel switching in response to starvation and exercise. Key: Metabolites affected by TXNIP deficiency are indicated in red (increased) and blue (decreased). Abbreviations: AcAc (acetoacetate), α -KG (α -ketoglutarate dehydrogenase), AST (aspartate aminotransferase), BCKAD (branched-chain ketoacid dehydrogenase), BHB (β -hydroxybutyrate), BDH1 (β -hydroxybutyrate dehydrogenase), CACT (carnitine acylcarnitine translocase), CPT1 & CPT2 (carnitine palmitoyltransferase 1 and 2), DHAP (dihydroxyacetone phosphate), ETC (electron transport chain), G-6-P (glucose-6-phosphate), GDH (glutamate dehydrogenase), GPx (glutathione peroxidase), GSH (reduce glutathione), GSSG (oxidized glutathione) ICD3 (NAD⁺-dependent isocitrate dehydrogenase), LCAC (long chain acylcarnitine) and LCFA-CoA (long-chain fatty acid acyl-CoA), MDH (malate dehydrogenase), NOX (NADPH oxidase), PDH (pyruvate dehydrogenase), PPP (pentose phosphate pathway) and SCHAD (3-hydroxyacyl-CoA dehydrogenase).

To our knowledge, this investigation was the first to apply comprehensive metabolic profiling tools to the TXNIP null models. When the targeted metabolomics analyses were combined with results of the foregoing substrate oxidation and respiratory function assays, a clearer picture of TXNIP deficiency began to take shape (Fig. 3-9). First, the tissue-specific role of this protein in regulating mitochondrial metabolism was further underscored, as the only commonality between the muscle and liver was the long chain acylcarnitine profile. In both tissues, the decline in long chain acylcarnitines suggested a decrease in either CPT1 activity or substrate delivery. Because neither CPT1 protein abundance nor malonyl-CoA levels were affected by genotype, we suspect that loss of TXNIP impedes fatty acid transport into tissues via a yet unknown mechanism. Second, the reduction in skeletal muscle acetyl-CoA levels was consistent with catabolic defects upstream of the ETC, and both the acyl-CoA and acylcarnitine profiles pointed to major defects in the pathways of amino acid and ketone degradation. Most notably, muscle content of isovaleryl-CoA (C5) as well as each of the odd-chain acylcarnitines, were robustly decreased in the TKO group; whereas circulating BCAA levels were elevated. Considering that isovaleryl-CoA is produced by BCKAD, and because this metabolic profile resembles BCKAD deficiency in humans and mice (Chuang, 2001), attention was drawn to this complex. Also quite striking in the TKO mice was the marked rise in intramuscular levels of β -hydroxybutyrylcarnitine. This metabolite derives from 3-hydroxyacyl-CoA, a product of ketone metabolism and a

substrate of the SCHAD enzyme (Koeberl et al., 2003; Rinaldo et al., 2008). Additionally, the decline in muscle levels of α -KG suggested a potential impingement in TCA cycle flux at the ICD3 step. Collectively, these signatures led us to discover that TXNIP deficiency in muscle results in a near complete loss of both the BCKAD E1A subunit and BDH1 protein, with more modest declines in protein abundance of SCHAD and ICD3. These findings help to explain the elevated circulating levels of ketones, fatty acids and amino acids in the TXNIP deficient models as well as their intolerance to prolonged fasting (Oka et al., 2006a) and endurance exercise.

The mechanism(s) by which TXNIP protects specific oxidoreductase enzymes remains unknown, although our data point to regulation at the level of protein synthesis and/or stability. TXNIP can form intermolecular disulfide bonds with reduced thioredoxin as well as other proteins containing a CXXC motif. Importantly, emerging evidence suggests that TXNIP is present and functionally active in the mitochondrial matrix (Nishiyama et al., 2001; Saxena et al., 2010; Zhou et al., 2011). For instance, recent experiments in HEK293 cells used immunoprecipitation techniques to demonstrate a physical association between recombinant TXNIP and a HA-tagged variant of the E1 α subunit of PDH (Yoshioka et al., 2012). This interaction, which presumably favors enzyme activity, was offered as a possible explanation for the low rates of pyruvate oxidation measured in mitochondria from TKO hearts (Yoshioka et al., 2012). Moreover, in INS1 cells, recombinant TXNIP was shown to translocate to the mitochondria in

response to oxidative stress, which in turn activated the apoptosis signaling protein ASK1 by disrupting its interaction with mitochondrial localized TXN2 (Saxena et al., 2010). Additionally, TNX has been shown to bind directly to various 2-oxoacid dehydrogenase complexes, which appears to modulate enzyme activity *in vitro* (Bunik et al., 1999; Bunik, 2003). Thus, the absence of TXNIP might alter interactions between TXN2 and other redox-sensitive mitochondrial proteins. Also intriguing, albeit purely speculative, is the prospect that TXNIP might function as an mRNA binding protein, thereby altering transcript stability and/or translation. This prediction stems from an *in silico* analysis using the RNAPred webserver (Kumar et al., 2011), which identified TXNIP as a strong candidate for an mRNA binding protein.

Lastly, we consider the physiological relevance of our findings in the settings of feast and famine. Transcriptional induction of TXNIP is typically viewed as a negative feedback response to excessive glucose exposure, mediated via the activation of carbohydrate-responsive transcription factors, ChREBP and MondoA (Stoltzman et al., 2008). Our finding that skeletal muscle mRNA expression of TXNIP is upregulated in the context of glucose depleted conditions such as fasting, diabetes and prolonged exercise, supports evidence that this protein can be regulated by nutrient signals other than glycolytic intermediates (Parikh et al., 2007; Rani et al., 2010; Shaked et al., 2009; Wang et al., 2006). Prominent among these is insulin, as TXNIP was identified as one of the most potently suppressed skeletal muscle mRNAs in healthy human individuals

subjected to a hyperinsulinemic-euglycemic clamp (Parikh et al., 2007). Taken together, these results imply that insulin-mediated suppression of TXNIP in the refeed state serves not only to disinhibit glucose uptake, but also to restrict ketone and BCAA oxidation and to promote net protein synthesis. Conversely, during periods of prolonged food restriction, skeletal muscles are reprogrammed to switch energy currency from glucose to fatty acids, ketones and amino acids. This is a fundamental survival mechanism that preserves glucose for the brain. We therefore surmise and show (Fig. 3-10) that fasting-induced upregulation of TXNIP functions to facilitate systemic glucose sparing and to encourage muscle use of alternative fuels.

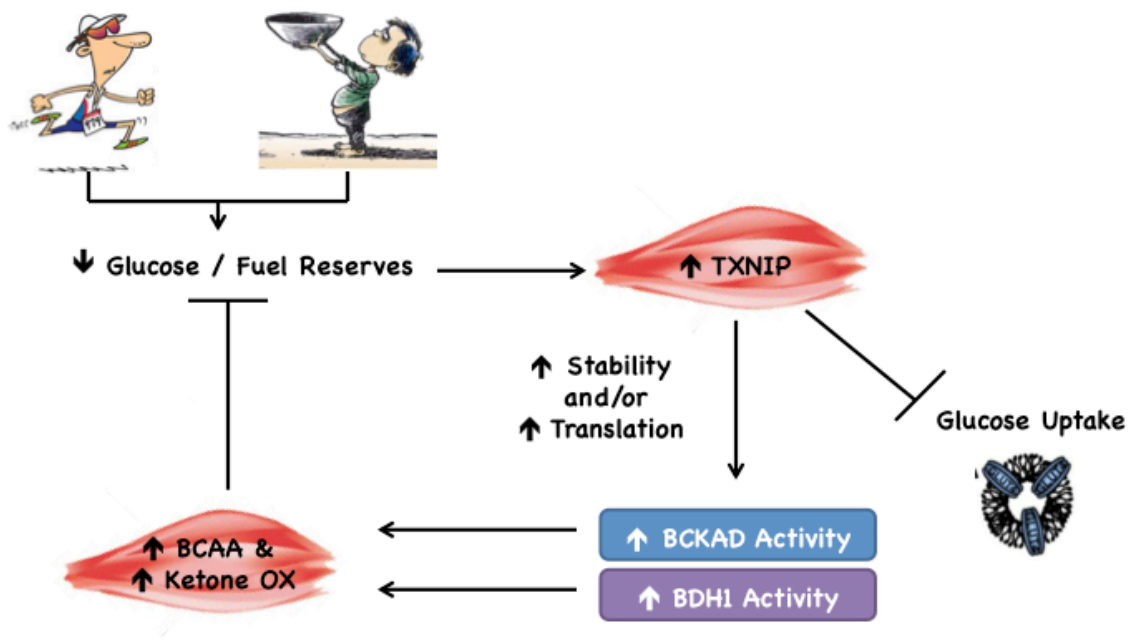


Figure 3-10: TXNIP Preserves Skeletal Muscle Mitochondrial Capacity to Switch Substrates During Glucose Deprivation.

Under conditions of decreased glucose reserves in skeletal muscle, such as exercise and fasting, TXNIP would be upregulated leading to inhibition of glucose uptake and increased enzymatic activity of BCKAD and BDH1 through a mechanism of increased protein stability and/or promotion of translation. Increased enzymatic activity of BCKAD and BDH1 causes increased BCAA and ketone oxidation in skeletal muscle, thus preventing the use of limited glucose stores, which can then be utilized by other tissues, such as the brain.

Whereas this mechanism would favor survival during times of famine, elevated TXNIP expression in nutrient replete muscles of obese and diabetic individuals might contribute to both glucose intolerance and nutrient-induced mitochondrial stress (Chen et al., 2008b; Chen et al., 2008c; Chutkow et al., 2010; Muoio, 2007; Yoshihara et al., 2010). Thus, in sum, this work identifies a novel role for TXNIP in coordinating fuel selection

in response to nutrient availability and furthers implicates this protein as a potential antidiabetic drug target.

4. TXNIP Deficiency Compromises Skeletal Muscle Redox Balance Leading to Glutathionylation and Reduced Activity of α -Ketoglutarate Dehydrogenase

4.1 Introduction

Reactive oxygen species (ROS) are important intracellular signaling transducers under physiological conditions before becoming potentially damaging in excessive quantities, thus causing oxidative stress (Nordberg and Arner, 2001). The TXN and GSH redox-mediated networks monitor and control the cellular redox state. Therefore, intracellular redox homeostasis is often determined by the concentration of GSH or the GSH/GSSG ratio. A decrease in either of these indicates a shift toward an oxidative intracellular environment. Since some of the functions of TXNIP, such as its interaction with TXN, are redox-mediated, we speculated whether there was a role for redox imbalance in facilitating the mitochondrial phenotype of the TXNIP KO mice, which we tested *in vitro* with MEFs and rat myocytes and *in vivo* with TKO mice.

One of the potential regulatory mechanisms employed under oxidative conditions is protein S-glutathionylation. It is a posttranslational mechanism, which involves the binding of GSH to protein thiols. The roles of protein S-glutathionylation involve cellular signaling and redox regulation of protein functions, storage of GSH and protection from the irreversible oxidation of protein thiols (Dalle-Donne et al., 2008). As

with protein phosphorylation, it is a reversible mechanism of protein regulation but linked to the redox status of the cell.

In our previous work, we concluded that TXNIP plays a key role in defending oxidative metabolism by maintaining protein synthesis and/or stability of mitochondrial oxidoreductase enzymes that permit muscle use of alternative fuels during glucose deprivation. We further questioned whether additional regulatory mechanisms could contribute to reduced oxidative metabolism in the absence of TXNIP, particularly since several enzymes involved in catabolic pathways and the TCA cycle have been shown to be redox-sensitive protein targets, possibly regulated by the TXN and GSH redox-mediated circuits or targets of protein S-glutathionylation (Bunik, 2003; Hurd et al., 2005). In aggregate, our results suggest that increased glucose uptake in TXNIP deficient muscles promotes non-mitochondrial ROS production, causing a cellular shift in redox balance, decreased GSH/GSSG and S-glutathionylation of α -ketoglutarate dehydrogenase (α -KGD).

4.2 Results

4.2.1 TXNIP Deficiency Disrupts Redox Balance in Skeletal Muscle

Because TXNIP is best known for its role in redox regulation, we sought to determine if the unique mitochondrial dysfunction seen in skeletal muscle from the TKO mice might be related to changes in redox balance. These results were shown in our

previous work, but are repeated here for convenience and emphasis. To this end, we measured a series of metabolites that report on shifts in cellular energy charge and oxidative stress. Interestingly, despite high rates of glycolysis and lactate production, muscle concentrations of NADH (Fig. 4-1A) were unchanged in the TKO mice. By contrast, levels of NADPH, which can also arise from glucose metabolism via the pentose-phosphate-shunt, were elevated 2.5-fold in the TKO mice (Fig. 4-1B), resulting in a striking decrease in the NADH/NADPH ratio (Fig. 4-1C). Conversely, TXNIP deficiency resulted in a 25% decline in muscle concentrations of reduced glutathione (GSH) and increased levels (33%) of the oxidized form, GSSG (Fig. 4-1D-F). Considering that GSH participates in antioxidant defense, we questioned whether the low levels of this metabolite in TKO muscles were related to increased mitochondrial production of reactive oxygen species (ROS). On the contrary, when assayed in permeabilized fiber bundles, rates of succinate-supported mitochondrial H₂O₂ emission trended lower in the TKO group (Fig. 4-1G). Thus, the metabolic defects in TKO muscles did not appear to result from mitochondrial-derived oxidative stress.

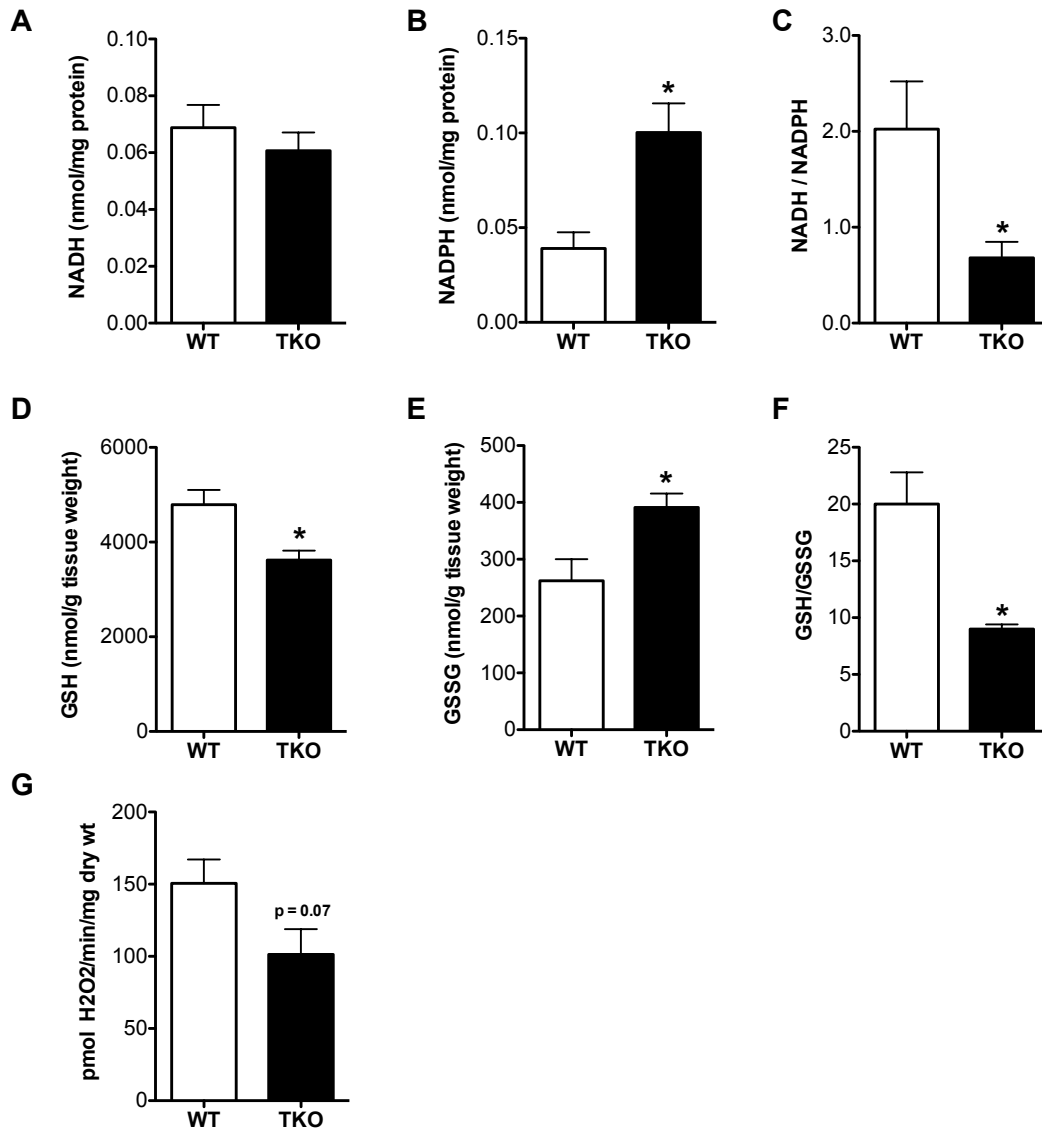


Figure 4-1: Redox Imbalance in TXNIP Deficient Skeletal Muscle

Skeletal muscles from TKO mice and WT littermate controls were harvested 5 h after food withdrawal and immediately flash frozen in liquid N₂ for subsequent assessment of redox metabolites. Gastrocnemius muscles were used to measure (A) NADH, (B) NADPH and (C) the NADH/NADPH ratio. Quadriceps muscles were used to measure (D) Reduced glutathione (GSH), (E) Oxidized glutathione (GSSG) and (F) the GSH/GSSG ratio. (G) Mitochondrial potential for producing reactive oxygen species was assessed in permeabilized fiber bundles by measuring succinate-supported H₂O₂ emission rates under state 4 conditions. Data are expressed as means ± SEM from 5-6 animals per group and results were analyzed by Student's t-test (*p ≤ 0.05).

4.2.2 Pharmacologically Depleting GSH and Increasing H₂O₂ in L6 Cells Diminishes Fat and Leucine Oxidation

Next we wanted to know if redox imbalance could contribute to the disrupted oxidative metabolism observed in TXNIP deficient skeletal muscle. To answer this question, we first pharmacologically depleted GSH in differentiated rat skeletal muscle myocytes (L6 cells) using buthione sulfoximine (BSO), an inhibitor of the synthesis of GSH, which was applied for 24 h (Fig. 4-2). Others in our lab have revealed that treating L6 cells with 100 μ M of BSO for 24 h results in increased ROS production as measured by dichlorofluorescein diacetate (DCFDA) staining and imaging with confocal microscopy (data not shown).

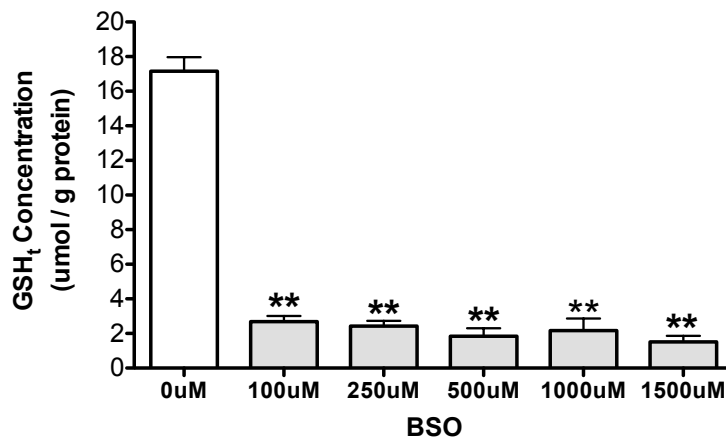


Figure 4-2: Decrease in GSH Concentration after 24 h Treatment with BSO

The GSH concentration in L6 myotubes was decreased >84% even with a low dose of buthione sulfoximine (BSO), an inhibitor of GSH synthesis, without affecting cell viability. Data are the

means \pm SEM of 3 individual experiments where each treatment condition was run in triplicate and analyzed by Student's t-test (** $p \leq 0.001$).

To replicate the oxidative stress condition, we also treated the cells with and without BSO in the presence or absence of H_2O_2 and measured palmitate and leucine oxidation (Fig. 4-3A-B). Results showed that just depleting GSH with $100\mu M$ BSO for 24 h had no effect on either palmitate or leucine oxidation in L6 cells. Also treating cells with just $100\mu M$ of H_2O_2 for 3 h did not significantly affect the oxidation of palmitate or leucine. However, treating the cells with $100\mu M$ BSO for 24 h and $100\mu M$ H_2O_2 for the last 3 h, significantly decreased palmitate and leucine oxidation by 53% and 24%, respectively. While we were not able to exactly replicate the oxidative phenotype of the TXNIP deficient skeletal muscle, this data suggest that decreased concentrations of GSH with associated increases in H_2O_2 , can contribute to the phenotype. However, this redox imbalance does not appear to be the driving force behind the phenotype.

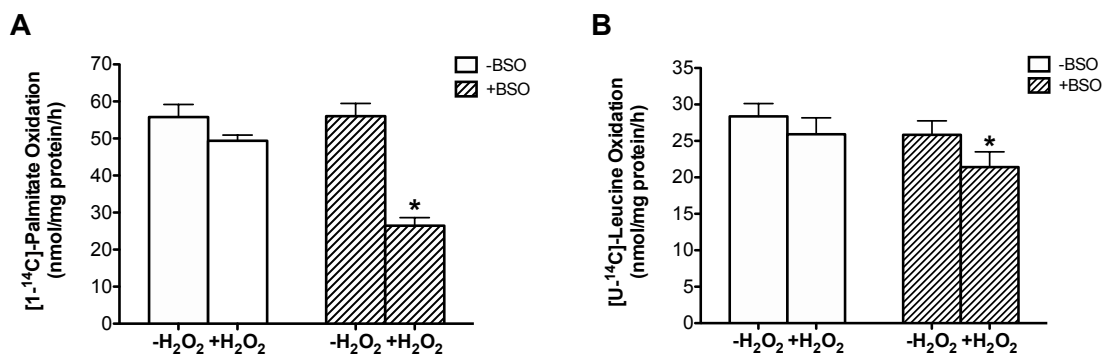


Figure 4-3: Depletion of GSH and Addition of H₂O₂ Diminishes Substrate Oxidation in L6 Cells

Depletion of GSH with 100 μ M BSO for 24 h or just the addition of 100 μ M H₂O₂ for 3 h does not inhibit (A) palmitate or (B) leucine oxidation in L6 rat myotubes. However, depletion of GSH with 100 μ M BSO for 24 h and the addition of 100 μ M H₂O₂ for the last 3 h, significantly decreases both palmitate and leucine oxidation. Data are the means \pm SEM of 3 individual experiments where each treatment condition was run in triplicate. Results were analyzed using a one-factor ANOVA and post hoc analysis to determine differences between groups. A *p* value of 0.05 was considered statistically significant.

4.2.3 N-acetylcysteine (NAC) Partially Rescues Oxidative Failure in TXNIP Deficient MEFs

If in the absence of TXNIP oxidative stress or imbalance plays any regulatory role, we surmised that treatment with the antioxidant N-acetylcysteine (NAC) should not only restore balance to the GSH/GSSG ratio, but also partially rescue mitochondrial substrate oxidation by improving TCA cycle flux. To test this hypothesis *in vitro*, we used mouse embryonic fibroblasts (MEFs) derived from TKO and WT control mice. GSH itself is too polar to cross the plasma membrane, so we employed NAC, a GSH precursor used to increase GSH concentration *in vivo* and *in vitro* (Choy et al., 2010; Sadowska et al., 2007; Traber et al., 1992). We were able to restore GSH concentrations

in the TKO to WT levels following 24 h treatment with 0.5mM NAC (Fig. 4-3A). Additional time and/or concentration of NAC did not result in higher GSH concentrations in either genotype (data not shown). The NAC treatment resulted in an exceedingly modest rescue of both palmitate (Fig. 4-3B) and leucine (Fig. 4-3C) oxidation in the TKO MEFs. This again suggests that oxidative stress is not the principle cause of oxidative failure in the TKO mice.

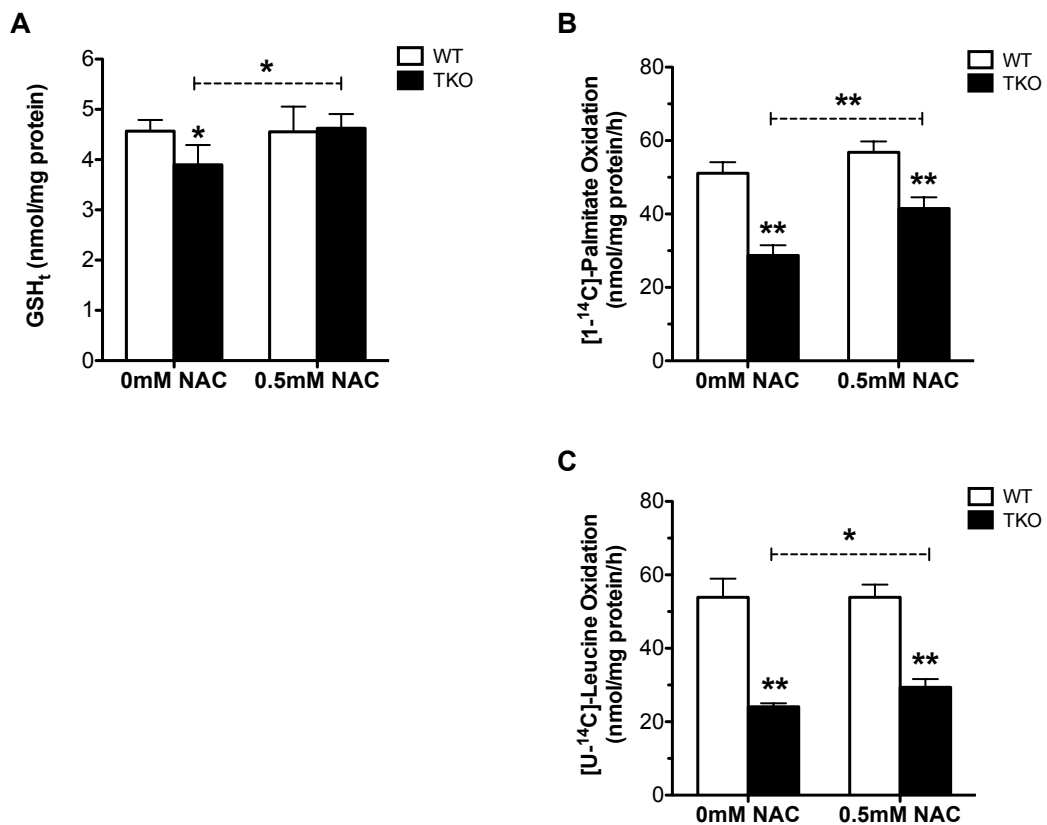


Figure 4-4: NAC Partially Rescues Oxidative Failure in TXNIP Deficient MEFs

MEFs were isolated from TKO and WT mice as described in Material and Methods. Cells were grown in 24-well plates. At ~90% confluency, they were treated with 0.5mM NAC or the vehicle control for 24 h. The cells were then measured for (A) GSH, (B) palmitate or (C) leucine oxidation as described. Data are means \pm SEM (3 experiments with quadruplicate samples per treatment condition per experiment). Results were analyzed by Student's t-test (* $p \leq 0.05$ and ** $p \leq 0.001$).

4.2.4 Rescue of Substrate Oxidation with NAC *in vivo* is Inconclusive

Despite only a partial rescue of substrate oxidation *in vitro*, we designed a pilot study to replicate the experiment *in vivo* with TKO mice to determine if the experimental environment was a factor. The drinking water of the TKO mice was supplemented with 20mM NAC or vehicle control for 9 weeks prior to assessment of total GSH and substrate oxidation in both isolated mitochondria and whole muscle (Fig. 4-5A-D). Total skeletal muscle GSH concentrations with and without NAC were not significantly different and actually trended lower in the +NAC condition (Fig. 4-5A). An elevation in the GSH concentration would have been expected if the NAC dosage and/or route of administration had been completely successful. Palmitate oxidation was able to be partially, although insignificantly ($p = 0.10$), rescued only in EDL (Fig. 4-5C). This was not observed in either the soleus (Fig. 4-5C) or isolated mitochondria (Fig. 4-5B). Leucine oxidation was also not rescued by NAC in the soleus or EDL and actually trended lower with both muscles under this condition. In total, the rescue of substrate oxidation with NAC is inconclusive with further study warranted.

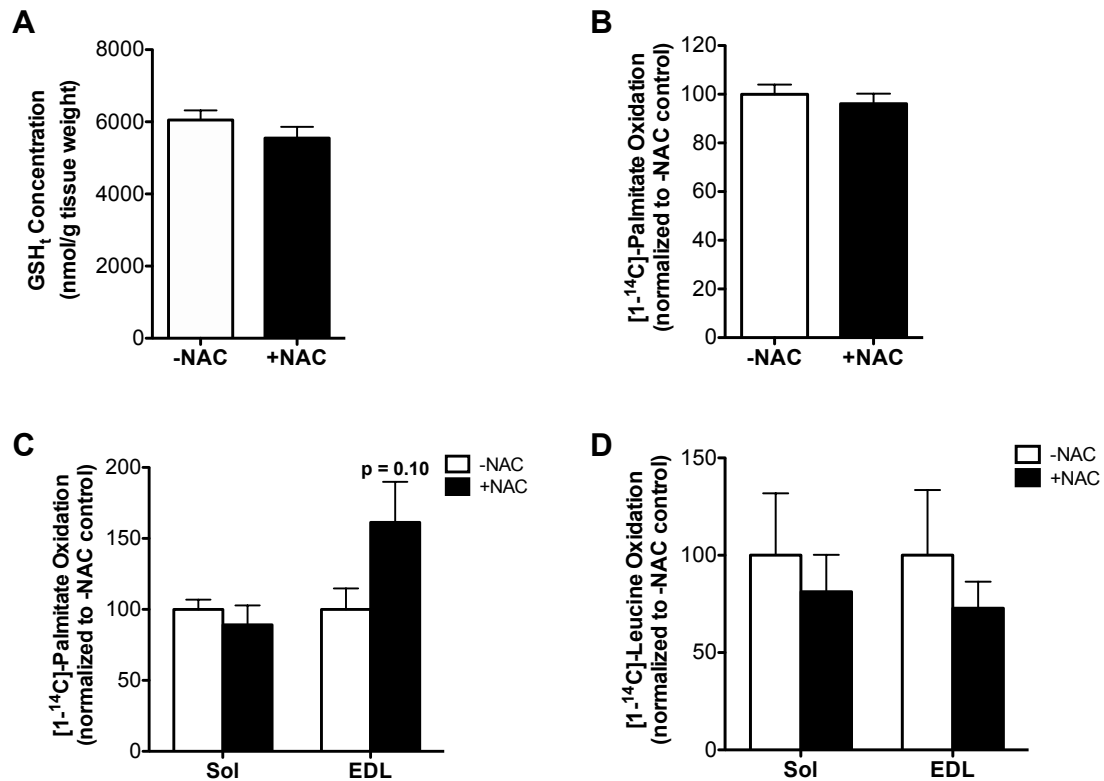


Figure 4-5: NAC Supplementation Has Mixed Results on Substrate Oxidation *in vivo*

Muscles were removed from TKO mice after a 5 h food pull. Mice had been supplemented with of 20mM NAC or vehicle control in the drinking water for 9 weeks prior to harvest. One gastrocnemius muscle was immediately flash frozen in liquid N₂ until assessed for (D) total GSH as described in Material and Methods. Mitochondria from the second gastrocnemius muscle were isolated via a protease preparation and (B) palmitate oxidation was evaluated. Whole isolated muscles (soleus and EDL) were measured for (C) palmitate and (D) leucine oxidation. Data are means \pm SEM (n = 5 per group, 2 male and 3 female) and results were analyzed by Student's t-test (*p \leq 0.05).

4.2.5 TXNIP Deficiency Reduces the Activities of TCA Cycle Enzymes in Skeletal Muscle

Although redox imbalance does not appear to be the principle cause of oxidative failure in the TXNIP deficient mice, it does seem to play a regulatory role requiring

further investigation. Since increased levels of NADPH may originate from cataplerosis of TCA cycle intermediates through pyruvate cycling, particularly if TCA cycle flux is compromised, and lower GSH might disrupt TCA enzyme balance, we sought to measure the activities of two TCA cycle enzymes known to redox regulated (Applegate et al., 2008; Eaton et al., 2002; Hurd et al., 2005; Nulton-Persson et al., 2003). We discovered that the activities of aconitase and α -ketoglutarate dehydrogenase (α -KGD) were reduced by 22% and 17%, respectively, in the absence of TXNIP (Fig. 4-6A-B). Interestingly, both of these enzymes have been shown to be susceptible to S-glutathionylation (Applegate et al., 2008; Eaton et al., 2002; Hurd et al., 2005; Nulton-Persson et al., 2003)

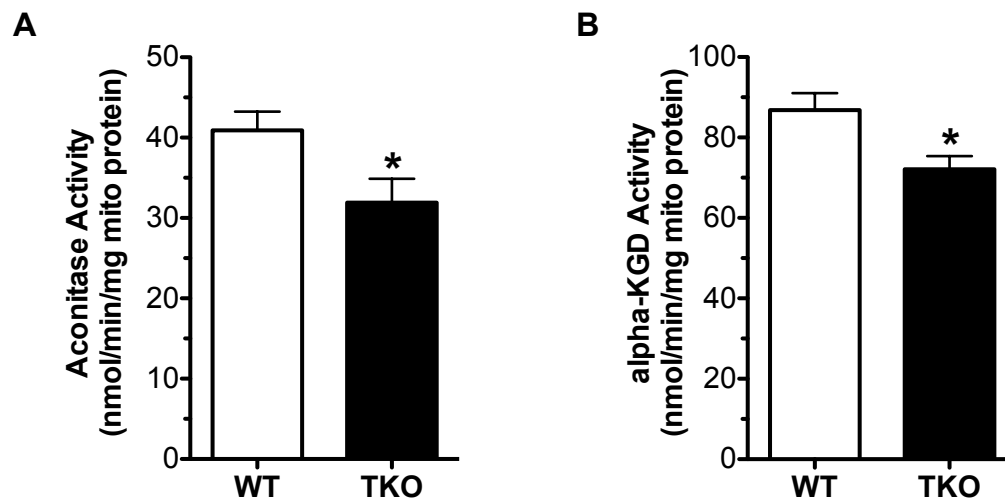


Figure 4-6: TXNIP Deficiency Disrupts Two TCA Cycle Enzymes Susceptible to Redox Regulation in Skeletal Muscle

Skeletal muscle was harvested from TKO and WT controls after a 5 h food withdrawal. Mitochondria were isolated using a protease preparation as described in Material and Methods.

Spectrophotometric analyses were used to measure the activities of: (A) aconitase and (B) α -KGD. Data are means \pm SEM (n = 5 per group) and results were analyzed by Student's t-test (*p \leq 0.05 and **p \leq 0.001).

4.2.6 The Reduced Activity of α -Ketoglutarate Dehydrogenase is Secondary to Glutathionylation

A post-translational mechanism used under conditions of oxidative stress to protect proteins and reduced GSH is reversible S-glutathionylation. S-glutathionylated proteins are protected from irreversible damage from oxidation, but while bound to GSH, their functioning is also compromised. Therefore, we wondered if this were the situation with aconitase and α -KGD. We reported in chapter 3 that the decreased protein expression of other mitochondrial enzymes directly correlated with their decrease in activity. However, this did not appear to be the circumstance with aconitase and α -KGD as there were no changes between the TKO and WT controls at the level of protein expression (data not shown). We found that the regulation of the activity of α -KGD was due to reversible S-glutathionylation, as its activity could be completely restored in the presence of glutaredoxin and GSH (Fig. 4-7). This implies that TXNIP deficiency affects the glutathionylation state and thus regulation of this enzyme. Unfortunately, we have yet to examine aconitase.

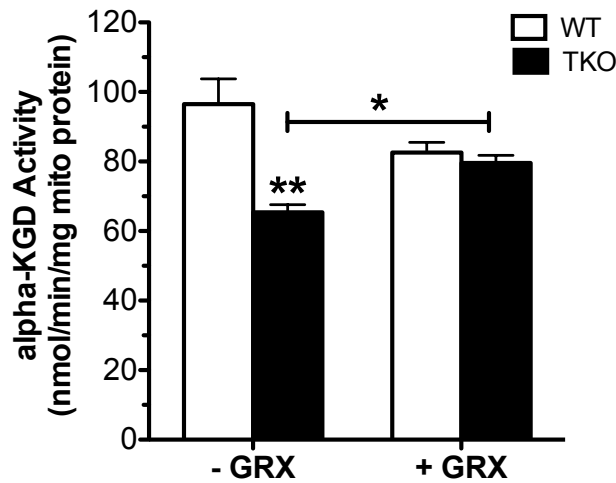


Figure 4-7: Reversing S-glutathionylation Completely Rescues the Activity of α -ketoglutarate dehydrogenase

Skeletal muscle was harvested from TKO and WT controls after a 5 h food withdrawal. Mitochondria were isolated using a protease preparation as described in Material and Methods. Spectrophotometric analyses were used to measure the activity of α -KGD before and after reversing S-glutathionylation with glutaredoxin and GSH. Data are means \pm SEM (n = 5 per group) and results were analyzed by Student's t-test (*p \leq 0.05 and **p \leq 0.001).

4.3 Discussion

TXNIP is 46-kDa protein that we have shown to be critical in mitochondrial regulation by stabilizing and/or promoting the translation of specific mitochondrial dehydrogenases required for ketone and amino acid degradation. The mechanism of how this is accomplished remains unknown. However, regulation by TXNIP has been reported to be both redox-dependent, usually involving its binding to TXN, or redox-independent, usually involving its function as an α -arrestin protein. We discovered that

in the absence of TXNIP in skeletal muscle, not only is there global diminished substrate oxidation, but there is a redox imbalance resulting in a decrease in the GSH/GSSG ratio caused by ROS that is not derived from the mitochondria. Herein, we wanted to understand if this redox imbalance contributed any regulatory control to the diminished substrate oxidation measured in the TKO mice. Many important findings emerged that contribute to our physiological understanding of this protein.

First, replicating the redox imbalance measured in the skeletal muscle of the TXNIP deficient mice *in vitro* does diminish palmitate and leucine oxidation in L6 rat myotubes. Second, in MEFs derived from the TKO mice, we measured decreased palmitate and leucine oxidation. Third, correcting the redox imbalance *in vitro* with the antioxidant NAC resulted in the partial rescue of palmitate and leucine oxidation in TKO MEFs but not in TKO mice. Fourth, we discovered that the functioning of two key enzymes of the TCA cycle, which would contribute to catabolism of substrates, were significantly impaired in the TKO skeletal muscle mitochondria. Fifth, the cause for the reduced functioning of at least one of these enzymes is reversible S-glutathionylation.

To determine if the redox imbalance in the TKO mice was a driving cause in the metabolic phenotype, we attempted to replicate the phenotype in L6 rat myotubes by depleting GSH and slightly increasing H₂O₂ levels. Since we were able to achieve diminished palmitate and leucine oxidation under this condition, we then examined palmitate and leucine oxidation in MEF cells generated from the TKO and WT control

mice. In the absence of NAC, palmitate and leucine oxidation were lower in the TKO as compared with controls. Following 24 h treatment with NAC, we were able to partially rescue oxidation of both substrates. This partial rescue suggested that although redox imbalance does appear to be a contributory factor to the metabolic phenotype, it is not the driving force or key regulatory mechanism for the reduced oxidative catabolism.

Since our previous work demonstrated that the role of TXNIP is tissue-specific, with diminished oxidative catabolism in skeletal muscle, but not liver, we wondered if what we were seeing was an artifact. Since MEFs are generated from embryonic tissue, not skeletal muscle, we wondered if greater success would prevail *in vivo*. Unfortunately, the data are questionable at best, although promising in the EDL. Because this was a pilot study with multiple inherent problems, such as minimal animals to correct for statistical fluctuation, a mixed gender cohort, lack of WT animals for proper controls and no preliminary studies to determine the proper NAC dosage and route of administration, the results of NAC supplementation *in vivo* on rescue of substrate oxidation are inconclusive. Therefore, repetition of the experiment with proper controls is warranted.

Previously, we had shown that the activities of β -hydroxybutyrate (BDH) and branched-chain ketoacid dehydrogenase (BCKAD) in TKO skeletal muscle were diminished due to decreased protein expression that was unchanged at the mRNA level. A third enzyme with the same activity/expression pattern was NADP⁺-dependent

isocitrate dehydrogenase (ICD3), an enzyme of the TCA cycle that catalyzes the oxidative decarboxylation of isocitrate to α -ketoglutarate (α -KG) and CO₂. Since the TCA cycle is involved in the oxidation of acetate from all fuels, such as carbohydrates, protein and fats, any decrease in enzyme activity would disrupt flux and contribute to the impairment of the catabolism of these substrates. Further, many of the TCA cycle enzymes are known redox-sensitive targets. Therefore, we examined other TCA cycle enzymes and found a similar loss of activity of aconitase and α -KGD. As with ICD3, the loss of activity was not as dramatic as BDH1 and BCKAD, but was significantly decreased at 22 and 17%, respectively. Unlike BDH1, BCKAD and ICD3, there was no associated loss of protein expression, which pointed toward a different regulatory mechanism.

Both aconitase and α -KGD are redox-sensitive protein targets, which can undergo reversible S-glutathionylation (Applegate et al., 2008; Eaton et al., 2002; Hurd et al., 2005; Nulton-Persson et al., 2003). Using established methods, we were able to show that α -KGD was indeed glutathionylated (Nulton-Persson et al., 2003). Further, we were able to reverse the glutathionylation with glutaredoxin and GSH to fully rescue the activity of the enzyme. Although aconitase still requires experimental analysis, this data reveals that in the absence of TXNIP, the resulting oxidative environment results in the protection of key TCA cycle enzymes and GSH. This protection comes at a cost,

however, which is the diminished activity of the enzyme, subsequent reduced TCA cycle flux and decreased substrate oxidation.

Does this then imply that S-glutathionylation is not a modulating factor in the presence of TXNIP? When TXNIP is present, a reducing environment in the mitochondria should be favored, but the reversibility of glutathionylation should allow for it to occur should the redox imbalance emerge even under these conditions. Further, it has now been established that this post-translational mechanism can and does occur even under basal (reduced) physiological conditions (Dalle-Donne et al., 2008; Townsend, 2007).

5. Conclusions, Remaining Questions and Future Directions

TXNIP is an α -arrestin protein involved in redox sensing and metabolic control. Herein, we employed models of TXNIP deficiency to comprehensively understand the effects of TXNIP's absence on mitochondrial metabolism in both skeletal muscle and liver. Several key findings emerged. In chapter 3, we reported that TXNIP deficiency leads to compromised metabolism of all major substrates at rest and during exercise in skeletal muscle. Further, this reduced oxidative metabolism was not associated with diminished mitochondrial mass, critical defects in the ETC or production of mitochondrial ROS, but secondary to the reduced activities of a subset of mitochondrial

dehydrogenases involved in several catabolic pathways. We showed that the loss of activities of BCKAD, BDH1 and ICD3 were the result of decreased protein abundance without changes in mRNA expression and that this was tissue specific to skeletal muscle and not liver. Moreover, in the absence of TXNIP we found a cellular shift in redox balance in skeletal muscle as measured by a decrease in GSH and the GSH/GSSG ratio. In chapter 4, we were able to partially rescue the diminished oxidative metabolism of palmitate and leucine in MEFs derived from the TKO and WT mice using the antioxidant N-acetylcysteine (NAC). However, this partial rescue underscored the conclusion that redox imbalance was not the key regulatory mechanism in the diminished oxidative capacity of the TXNIP deficient skeletal muscle. Nevertheless, redox imbalance did contribute to the loss of activity of α -KGD and possibly aconitase, which we demonstrated in the case of α -KGD to be caused by glutathionylation. Taken together, we surmised the role of TXNIP in skeletal muscle was to maintain the synthesis and/or stability of select mitochondrial dehydrogenase enzymes that permit oxidation of alternative fuels when glucose is sparse. Nevertheless, several unanswered questions remain that should help to direct continued research regarding the functional role of this protein. These questions and suggested experimental approaches to yield answers are found in subsequent sections.

5.1 *How Does TXNIP Regulate the Mitochondrial Dehydrogenases?*

5.1.1 Does TXNIP and/or TXN Stabilize the Mitochondrial Dehydrogenases?

In chapter 3, we provided evidence that TXNIP plays a key role in defending oxidative metabolism by maintaining protein synthesis and/or stability of mitochondrial oxidoreductase enzymes. Therefore, the next logical step would be to determine TXNIP modulates the chemical or physical stability of BCKAD and BDH1. Chemical instability, such as loss of activity due to the formation of disulfide bonds in an oxidative environment, could be examined with redox Westerns. Briefly, the proteins are resolved by SDS-PAGE under reducing and non-reducing conditions followed by immunoblotting for target proteins (Hui et al., 2008). This method would identify if the target protein had been oxidized. Therefore, the mRNA levels would be unchanged, but the post-translational modification to the protein would have diminished its activity. Alternately to assess oxidation state, the proteins can undergo derivatization with thiol-reactive reagent, 4-acetamido-4'-maleimidylstilbene-2,2'-disulfonic acid (AMS) to increase its mass and the oxidized and AMS-derivatized proteins can be separated by non-reducing SDS-PAGE followed by immunoblotting (Hansen et al., 2006).

TXNIP may also play a role in altering the physical characteristics of proteins. Physical instability involves denaturation or unfolding of the protein. Ideally, an approach that does not involve cumbersome isolation and purification of proteins

would be advantageous. The first reported direct measurement of *in vivo* protein stability involved the use of amide hydrogen exchange detected by MALDI mass spectroscopy (SUPREX) (Ghaemmaghami and Oas, 2001). More recent methods can quantitatively measure the stability of even low abundant proteins in cell or tissue lysates by measuring the fraction of folded proteins with pulse of proteolysis followed by Western blotting (Kim et al., 2009; Park and Marqusee, 2005). Briefly, a mixture of folded and unfolded proteins is digested with protease for one minute intervals to completely digest the unfolded proteins while the stabilized folded proteins resist proteolysis. The intact proteins for each pulse interval are identified using Western blotting. A purified protein of interest is also subjected to the same digest for comparison. This method could be used to compare tissue lysate from the TKO and WT mice to determine the differences in select protein stability between the genotypes. If differential stability is identified, then further analysis as to the method of the stabilization is warranted and covered in the next section.

5.1.2 Is Stability Modulated through Direct Binding of TXNIP or TXN to the Mitochondrial Dehydrogenases?

In the introduction, the redox-dependent and redox-independent regulation of proteins and their downstream cascades by TXNIP was covered in depth. To review briefly, in redox-dependent regulation TXNIP responds to changes in the redox state by intracellular translocation and formation of intermolecular bonds with reduced TXN or other proteins with a CXXC motif, and subsequent initiation of downstream signaling

cascades. For example, under conditions of oxidative stress, TXNIP shuttles into the mitochondria where it competes with ASK-1 for binding to TXN2, thus allowing for the phosphorylation/activation of ASK1 and the initiation of the apoptotic cascade (Saxena et al., 2010). Similarly, chronic hyperglycemia or inflammasome activators can lead to oxidative stress, under which the NLR protein 3 (NLRP3) inflammasome binds to TXNIP following its release from TXN. Once bound to TXNIP, the NLRP inflammasome causes procaspase-1 cleavage and interleukin-1 β (IL-1 β) secretion, which is implicated in islet cell dysfunction and the pathogenesis of T2DM (Davis and Ting, 2010; Zhou et al., 2010). In redox-independent regulation, TXNIP binds to WW domains in proteins such as GLUT1 (Wu et al., 2013), Redd1 (Jin et al., 2011) and Mybbp1 (Yoshihara et al., 2010), to name a few. A newer theory also suggests that TXN enhances the stability and regulates the function of TXNIP by direct interaction with the Cys247 residue of TXNIP (Chutkow and Lee, 2011).

To determine if TXNIP promotes the stability and functioning of the mitochondrial dehydrogenases BCKAD and BDH1 through direct binding, immunoprecipitation techniques could be employed. Using similar techniques, a physical association between TXNIP and the PDH subunit E1 α in the heart was demonstrated and implicated as necessary for the regulation of PDHE1 α activity (Yoshioka et al., 2012). Since PDH and BCKAD share the E1 α subunit of their enzymatic complexes, this association is highly probable. However, these authors also reported a

decrease in the activity of PDH when TXNIP was deficient in the heart, which we did not observe in TKO skeletal muscle. However, this could be due to differential expression of lactate dehydrogenase (LDH) isoforms, which will be covered in a later section. Lastly, a yeast two-hybrid strategy could be implemented to identify novel binding partners of TXNIP. This technique was recently employed to show that TXNIP interacts with human ecdysoless (hEcd) to increase the stability of p53 at the protein level and through mediated transcription (Suh et al., 2013).

It is possible that TXNIP does not directly bind to BCKAD and BDH1 but that an interaction is mediated through TXN. This finding would warrant similar interaction experiments with TXN, which has been shown to regulate enzymatic activity through direct binding to the 2-oxoacid dehydrogenase complexes (Bunik et al., 1999; Bunik, 2003). This occurred under oxidative conditions and suggests that TXN stabilizes the mitochondrial dehydrogenases through direct binding and stabilization becomes dysregulated in the absence of TXNIP.

TXN has also been implicated in ubiquitination of proteins through its role as a redox-active cofactor of the 26S proteasome. This complex along with the proteasome subunit Rpn11 targets eEF1A1, a substrate-recruiting factor of the proteasome (Andersen et al., 2009). The authors reported that this was the first example of a direct connection between protein reduction and proteolysis. Hence, a highly speculative,

though plausible scenario is that in the absence of TXNIP, TXN, TXN associates with the 26S proteasome and targets BCKAD and BDH1 for degradation.

Obviously, the mechanism of BCKAD and BDH1 stability could involve enzymatic cascades, in which TXNIP and/or TXN indirectly regulate their activity through upstream activators. Hence, ruling out direct binding by either TXNIP or TXN is a critical first step.

5.1.3 Is Translation of the Mitochondrial Dehydrogenases Promoted through mRNA Binding of TXNIP?

If direct or indirect binding to promote stability of these dehydrogenases is not the answer, then one could examine post-transcriptional modification by TXNIP, which would involve mRNA binding to allow for efficient translation. Regulation by RNA binding proteins is not unprecedented as it is the basis for cellular iron homeostasis. In this regulatory system, iron regulatory proteins 1 and 2 bind to the iron responsive elements (IREs) located in either the 3'- or 5'-untranslated regions (UTRs) of various mRNA encoding proteins involved in iron uptake, storage, utilization, export and the TCA cycle (Anderson et al., 2012; Eisenstein, 2000; Hentze et al., 2004). Depending on the protein, binding to IREs either reduces translation rates or increases mRNA stability.

Thus far, thousands of RNA-binding proteins (RBPs) have been identified each with unique RNA-binding activity and protein-protein interaction characteristics (Glisovic et al., 2008). RBPs are identified by the presence of RNA binding domains (RBDs) or RNA recognition motifs, such as arginine-rich motifs, $\alpha\beta$ protein domains,

zinc-finger motifs, Pumilio/FBF (PUF) domains and Piwi/Argonaut/Zwille (PAZ) domains, and function in RNA metabolism at all stages including transcription, nuclear export, subcellular localization, stabilization, RNA editing, translation (as activators or repressors) and degradation (Chen and Varani, 2005).

Often RBPs involved in controlling mRNA stability bind to *cis*-elements that either activate or inhibit mRNA decay. The most commonly known is the adenylate uridylate-rich (AU-rich) element (ARE). Databases exist that compile known AU-rich element containing mRNAs (ARED) (Bakheet et al., 2006; Khabar et al., 2005) and those that predict mRNA binding proteins (RNApred) (Kumar et al., 2011). We conducted an *in silico* analysis that revealed thioredoxin (TXN), thioredoxin-like 2 (TXNL2) and thioredoxin reductase 1 (TXNRD1) as having AREs, while TXNIP was predicted to be a strong RBP candidate. We then wondered if the mRNAs of BCKAD and BDH1 contained known AREs, but neither was listed in the ARED database. However, the ARED with its 4000 computationally mapped ARE-mRNA has not been updated since 2006 and may not contain all ARE-mRNAs.

Nonetheless, BCKAD and BDH1 have shown to be regulated post-transcriptionally at the mRNA level. For example, investigators reported a 3-fold increase in the activity state of BCKAD in skeletal muscle of starved rats with a significant change in the protein expression of subunit E1 β and no change in the mRNA expression of the genes of any of the subunits (E $_2$, E1 α , E1 β) (Serdikoff and Adibi, 2001).

Although we did not examine this enzyme, the regulation of BCKAD kinase, which phosphorylates and inactivates BCKAD, seems to also be post-transcriptionally regulated in skeletal muscle under conditions of diabetes (Lombardo et al., 1999). The protein expression of BCKAD kinase is decreased while its gene expression remains unchanged. This contributes to the increased activity of BCKAD and could potentially involve TXNIP. Gene expression of BDH1 was shown to be transcriptionally and/or post-transcriptionally regulated through mRNA stability during various developmental and physiological stages (Bailly et al., 1991) or by insulin (Bailly et al., 1990). However, the effect of insulin on the mRNA of BDH1 was dependent upon the extent and length of the diabetic state of the animal. That is, in Wistar rats with prolonged diabetes, insulin increased the mRNA expression of BDH1, while in control rats; it decreased the mRNA expression of BDH1 (Bailly et al., 1990). This suggests the regulation of BDH1 is complex and may involve multiple control mechanisms, of which TXNIP could be one, particularly in the early stages of diabetes or pre-diabetes.

In chapter 3, we reported that skeletal muscle mRNA expression of TXNIP is upregulated in the context of glucose depleted conditions such as fasting, obesity, diabetes and prolonged exercise (Fig. 3-8E-G). We proposed that the physiological role of TXNIP in skeletal muscle under these conditions is to spare glucose and stimulate the use alternative fuel sources, such as BCAAs and ketones, by promoting the translation of BDH1 and BCKAD. In a preliminary follow-up study, with obese and lean control

Zucker Diabetic Fatty (ZDF) rats, we showed an upregulation of TXNIP in the obese state with significantly increased protein expression of TXNIP and BCKAD (data not shown). Unfortunately, the results of the BCKAD mRNA expression were inconclusive due to variability. However, repeating this experiment is recommended, since a lack of change in the mRNA of BCKAD between the lean and obese conditions would support the hypothesis of TXNIP stabilizing the mRNA of BCKAD and promoting its translation in the obese state.

Other experiments would be required to confirm TXNIP as an RBP. For instance, TXNIP could be overexpressed in a cell system, ultraviolet (UV) cross-linked to RNA and isolated (Glisovic et al., 2008). Recently, this method has been adapted using a tagged protein of interest and including an immunoprecipitation (IP) step following cross-linking (cross-linking and IP or CLIP) (Anko and Neugebauer, 2012). A yeast-three hybrid system has also been used to identify RBPs and their target RNAs (Seay et al., 2006). Should TXNIP prove to be an RBP, approaches such as RNA immunoprecipitation (RIP) followed by microarray analysis (RIP-chip) could be used to identify RNA targets (Anko and Neugebauer, 2012).

5.2 Imbalances in Cellular Energetic Metabolites and the Redox State

5.2.1 The State of the Reducing Equivalents

A surprise finding presented in chapter 3 was that NADH levels were unchanged in the TKO skeletal muscle despite high rates of glycolysis. Since ETC

function and protein complexes were also normal in the TKO, despite decrease flux through the TCA cycle, we surmised that the ETC was receiving glucose-derived NADH at complex I via the malate-aspartate shuttle (Fig. 3-9). However, this has yet to be shown experimentally.

The mechanism of the malate-aspartate shuttle (MAS) is described (Lodish, 2003) and shown (Fig. 5-1). In a reaction catalyzed by cytosolic malate dehydrogenase (cMDH), NADH reduces oxaloacetate (OAA) to malate, which enters the inner mitochondrial matrix through an antiporter/carrier system that simultaneously exports α -KG. Inside the mitochondria, malate is converted to OAA by mitochondrial malate dehydrogenase (mMDH), which forms the NADH able to be used by the ETC. Mitochondrial aspartate aminotransferase (mAST) transaminates OAA to aspartate by glutamate, which is simultaneously converted to α -KG. Another antiporter/carrier transports aspartate out of the mitochondria in exchange for glutamate. In the cytosol, aspartate is converted to OAA by cytosolic AST (cAST). The net result is that NADH is transported into the mitochondria, which can generate 3 ATP molecules for every NADH transported in from the cytosol. The NAD^+ in the cytosol can be reduced again via another round of glycolysis.

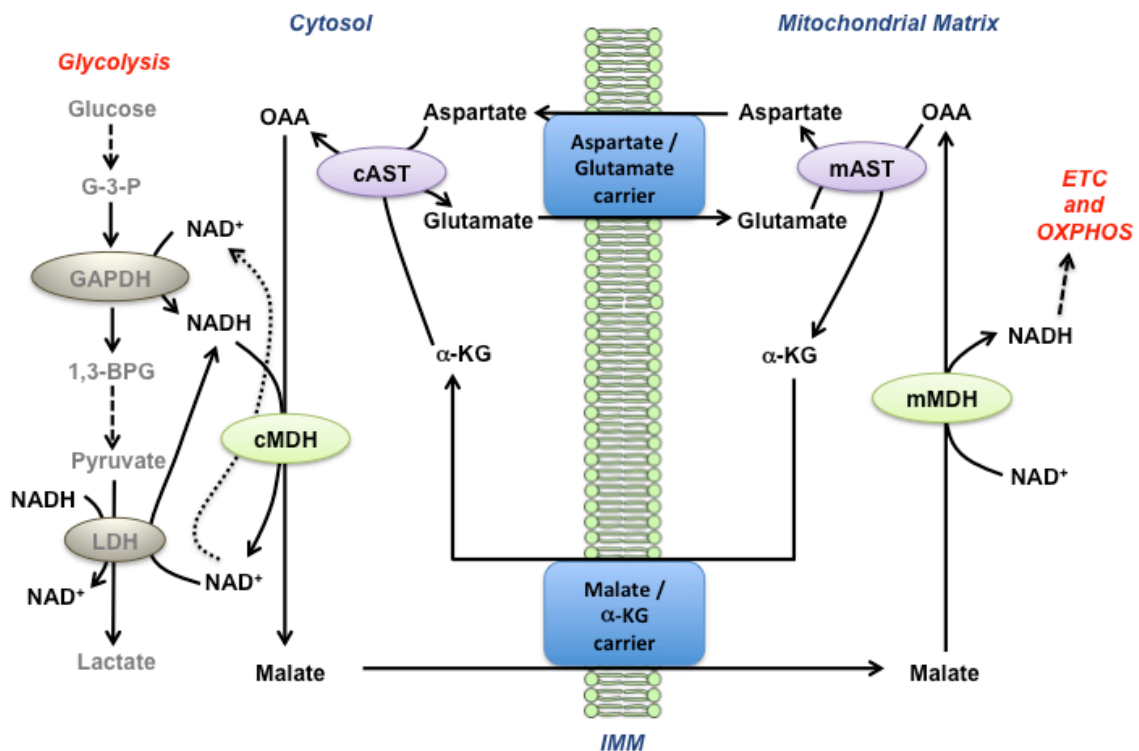


Figure 5-1: The Malate-Aspartate Shuttle

The malate-aspartate shuttle (MAS) is used for transferring reducing equivalents from the cytosol into the mitochondria. Electrons from glycolysis or oxidation of lactate to pyruvate are transferred from NADH as oxaloacetate (OAA) is converted to malate by cytosolic malate dehydrogenase (cMDH). Through the malate/ α -ketoglutarate (α -KG) carrier, malate is transported into the mitochondrial matrix in exchange for α -KG. The malate is then oxidized to OAA by mitochondrial malate dehydrogenase (mMDH) with the formation of NADH to be used by the ETC. OAA is then converted to aspartate by transamination with glutamate via mitochondrial aspartate aminotransferase (mAST). The aspartate leaves the mitochondria via the aspartate/glutamate carrier in exchange for glutamate. In the cytosol, aspartate is converted to OAA by transamination with α -KG catalyzed by cytosolic aspartate aminotransferase (cAST), which completes the cycle. Additional abbreviations: 1,3-BPG (1,3-biphosphoglycerate), G-3-P (glyceraldehyde-3-phosphate), GAPDH (glyceraldehyde phosphate dehydrogenase) and LDH (lactate dehydrogenase). Adapted from (McKenna et al., 2006).

One way to experimentally evaluate the functioning of the MAS is to measure and compare the activities of each of the enzymes of the shuttle between the TKO mice and WT controls. The enzymes have previously been shown to change in skeletal

muscle following various treatments, such as endurance training (Schantz et al., 1986). Mitochondria from skeletal muscle could be harvested as described in Materials and Methods with the cytosolic fraction assayed spectrophotometrically for cMDH and cAST activities and the isolated mitochondria assayed similarly for the mitochondrial versions of each enzymes (Goyary and Sharma, 2008). If no enzymatic activity differences are noted, one could also examine the antiporters because if the translocating capacity is rate limiting, the increase in enzyme activity will not increase the overall reaction rate of the shuttle (Schantz et al., 1986). Lastly, a more functional assessment of the activity of the MAS on bioenergetics would be to inhibit its functioning then examine both cytoplasmic NADH levels and respiratory function of the ETC with complex I-linked substrates as described in Chapter 3. This could either be done in permeabilized fibers or isolated mitochondria if the MAS is reconstituted following published methods (Abbrescia et al., 2012; Contreras and Satrustegui, 2009). Inhibition of the shuttle is achieved with aminooxyacetate, an inhibitor of AST (Barron et al., 1998). If respiratory function were diminished significantly in the TKO mice, it would suggest that NADH is being supplied by the shuttle, which would compensate for any diminished flux and lower production of reducing equivalents through the TCA cycle.

Another intriguing finding was that NADPH levels were increased 2.5-fold in the TKO mice as compared to the WT controls. In skeletal muscle, the sources of NADPH production are from the pentose phosphate pathway (PPP) (Lodish, 2003) and

possibly cataplerosis of TCA cycle intermediates through the pyruvate cycling pathway as observed in the β -cell (Ronnebaum et al., 2006). Given the high glucose uptake and increased glycolytic metabolism, increased flux of glucose-6-phosphate through the PPP should be examined (Mailloux and Harper, 2010). One could investigate the increased activities of the enzymes of the PPP or inhibit the PPP and measure NADPH, but the more functional assessment would be to measure ROS production as discussed in the next section.

5.2.2 What is the Source of ROS and Does It Contribute to the TKO Metabolic Phenotype?

TXNIP is best characterized as the endogenous inhibitor of TXN and inhibiting TXN sensitizes the cell to oxidative stress. One would hypothesize that in the absence of TXNIP a reduced environment would be expected, however, this was not the case in TKO skeletal muscle. In chapters 3 and 4, we reported an oxidative imbalance in the absence of TXNIP as measured by a 35% reduction in GSH and a 33% increase in GSSG. We also showed that succinate-supported H_2O_2 emission potential trended lower in the TKO mice. Therefore, we hypothesized that the source of ROS was most-likely non-mitochondrial emanating from increased NADPH oxidase (NOX) activity due to higher production of its substrate, NADPH.

NOX is an enzyme complex on the plasma membrane that generates superoxide (O_2^-) by transferring electrons from NADPH inside the cell and coupling this to molecular oxygen outside the cell. The O_2^- can re-enter the cell through anion channels

or as H₂O₂. H₂O₂ is rapidly generated outside the cell due to spontaneous and enzymatic dismutation, and is freely permeable through the cell membrane (Bedard and Krause, 2007). This influx of H₂O₂ reacts with glutathione peroxidase (GPx) converting it to H₂O by using reduced GSH and forming GSSG (Fig. 3-9).

Identifying the source of ROS and its downstream effects are a crucial next step in the understanding of mitochondrial functioning in the absence of TXNIP. For instance, would inhibition of NOX activity restore the GSH/GSSG balance and deter glucose uptake, but partially rescue glucose oxidation in TKO mice? First, NOX activity in skeletal muscle tissue or homogenate can be measured in an *in vitro* experiment using the lucigenin enhanced chemiluminescence method and superoxide dismutase (SOD)-inhibitable ferricytochrome *c* reduction assays as previously described (Li and Shah, 2002; Li et al., 1998; Sakellariou et al., 2013; Sohn et al., 2000; Wang et al., 2009). As a positive control, NOX activity can be inhibited in muscle with apocynin (Sakellariou et al., 2013; Wang et al., 2009). For the actual *in vivo* experiment, apocynin or a saline vehicle control can be administered daily to TKO and WT littermates via an intraperitoneal injection for a duration and dose predetermined from the literature. At sacrifice, outcome measures would include evaluation of NOX activity and GSH/GSSG in muscle homogenates and glucose uptake and glucose oxidation in isolated muscle.

5.2.3 How is the Insulin-Signaling Cascade Augmented in the TKO Skeletal Muscle?

In all mouse models in which TXNIP is disrupted, there is consistently improved glucose tolerance, insulin sensitivity and augmented glucose transport in some peripheral tissues (Chutkow et al., 2010; Chutkow et al., 2008; Hui et al., 2008; Oka et al., 2006a; Yoshihara et al., 2010). However, only two groups examined the effect of TXNIP deficiency on the insulin-signaling cascade. Hui et al. (2008) reported enhanced insulin signaling in skeletal muscle and heart, which they attributed to enhanced phosphorylation of Akt secondary to the accumulation of oxidized (inactive) PTEN. They proposed that the accretion of oxidized PTEN occurred because high NADH levels blocked the TXN/NADP(H)-dependent reduction of PTEN. Problematically, it appears this theory was formulated upon the work of others (Pelicano et al., 2006) and not experimentally evaluated, since our work shows that there was no measurable increase in NADH in the TKO animals. In a later work, Yoshihara et al. (2010) also reported increased phosphorylation of Akt in the skeletal muscle and heart of TBP-2^{-/-} and ob/ob•TBP-2^{-/-}. However, these authors also found enhanced IRS-1 expression in the skeletal muscle of both TBP-2^{-/-} and ob/ob•TBP-2^{-/-}, which is proximal to Akt in the insulin-signaling cascade. The molecular mechanism for how this occurs is under investigation. The authors also found several insulin signaling-related genes in skeletal muscle, such as *Igf1*, *Igf2bp2*, *Igf2bp4*, *Irs-1*, *Pik3r1*, *Pi3k3r5*, were also upregulated at the mRNA and protein expression levels.

I would propose that a thorough investigation of the proximal and distal arms of the insulin-signaling cascade is warranted. In the first paper (Hui et al., 2008) although the Western blots of oxidized and reduced PTEN in skeletal muscle were convincing, the Western blots of increased phosphorylation of Akt in the TKO mice were less so. Similarly in the second paper (Yoshihara et al., 2010) the increased phosphorylation of Akt in the TBP-2^{-/-} mice was less than resounding, visually appearing the same as the WT. To convince ourselves of this data we too performed a preliminary experiment in which we immunoblotted for phosphorylated Akt, total Akt and IRS-1 in standard chow fed WT and TKO skeletal muscle. We did observe an increase in IRS-1 expression in the TKO mice, but there was no difference between the genotypes in phosphorylation of Akt or total Akt. Therefore, due to inconsistencies, these experiments need to be repeated. Secondly, if expression levels are actually increased in any or all of these proteins, then a mechanism of action should be investigated, since the previously proposed high NADH levels inhibiting the TXN/NADP(H)-dependent reduction of PTEN is no longer sustainable.

In chapters 3 and 4, we reported a non-mitochondrial increase in ROS in the TKO mice. Interestingly, H₂O₂ (and other ROS) are known insulin mimetics, which may serve as second messengers in the insulin signaling cascade (Goldstein et al., 2005). The best characterized molecular targets are the protein-tyrosine phosphatases (PTPs), such as protein-tyrosine phosphatase 1B (PTP1B), protein serine/threonine phosphatase 2A

(PP2A), MAP kinase phosphatase; dual-specificity (serine/tyrosine) phosphatase (MKP-1), and PTEN (Goldstein et al., 2005). All of these molecules need to be in a reduced state to be active and serve as negative regulators of insulin action. However, all can be oxidized by ROS, thereby effectively blocking their enzyme activity and reversing their inhibitory effect on insulin signaling. Consequently, could the increase in ROS and not NADH contribute to the enhanced insulin signaling in TKO mice via the oxidation and inactivation of PTEN, convincingly shown in skeletal muscle (Hui et al., 2008), or other PTPs?

A variety of *in vitro* studies have demonstrated the regulatory links between PTP1B and the insulin receptor [reviewed in (Tonks, 2003)]. However, the most compelling evidence comes from *PTP1B* knockout studies in mice. As compared to WT mice, *PTP1B*^{-/-} mice were glucose and insulin tolerant, which was correlated with enhanced tyrosine phosphorylation of the insulin receptor in skeletal muscle and liver (Elchebly et al., 1999). Further, these mice were resistant to diet-induced obesity and maintained glucose and insulin tolerance. A second study confirmed the insulin sensitivity in skeletal muscle, but not adipose tissue, and reported increased basal metabolic rate in the *PTP1B*^{-/-} mice (Klaman et al., 2000). Other protein tyrosine phosphatases, such as PP2A (Guy et al., 1993) and PTEN (Lee et al., 2002; Leslie et al., 2003) involved in the regulation of insulin signaling have shown to be inhibited by ROS.

Insulin was shown over 30 years ago to stimulate the generation of H₂O₂ in adipocytes (May and de Haen, 1979) catalyzed by NADPH oxidase (NOX) (Mukherjee et al., 1978), which was discussed in the previous section as the probable cause for the oxidative redox imbalance in the TKO mice. In adipocytes and differentiated 3T3-L1 cells, NOX4 deletion constructs, which acted in a dominant negative fashion, decreased insulin-stimulated production of ROS that was coupled to the inhibition of the insulin receptor and IRS-1 phosphorylation (Mahadev et al., 2004). In parallel studies, siRNA knockdown of NOX4 decreased insulin-stimulated Akt phosphorylation, while NOX4 overexpression potentiated the transduction of insulin signaling via the oxidative inhibition of PTP1B catalytic activity (Mahadev et al., 2004). Similar results have been obtained in other cell types, such as murine osteoclasts (Yang et al., 2001) and mesangial cells (Gorin et al., 2003), and with other PTPs, such as PTEN (Seo et al., 2005). Further, glutathione peroxidase knockout mice (GPx^{-/-}) have increased insulin sensitivity attributed to PI3K/Akt signaling and glucose uptake in skeletal muscle (Loh et al., 2009). In MEFs isolated from GPx^{-/-} mice, the increased PI3K/Akt signaling was abrogated with the antioxidant N-acetylcysteine (NAC) or by inhibiting NOX. Lastly, in a condition similar to the TKO mice, high glucose conditions and increased glycolytic flux increased insulin-stimulated H₂O₂ production and enhanced the oxidative inhibition of total PTP and PTP1B activity (Wu et al., 2005).

In the previous section, I recommended examining the source of ROS and its downstream effects in the TKO mice employing inhibition of NOX with apocynin. Given the evidence presented herein, I would include investigating the proximal and distal arms of the insulin-signaling cascade in that study. In parallel, *in vitro* experiments with MEFs generated from the TKO mice and cultured myocytes overexpressing TXNIP would provide excellent models for the expanded study of glucose uptake, GLUT4 translocation, glucose oxidation and the insulin-signaling cascade with greater ability for manipulation.

5.2.4 Are Other Mitochondrial Proteins S-Glutathionylated?

In chapter 4, we questioned whether additional regulatory mechanisms could contribute to reduced oxidative metabolism in the absence of TXNIP, particularly since several enzymes involved in catabolic pathways and the TCA cycle have been shown to be redox-sensitive protein targets. We established decreased enzymatic activities of α -KGD and aconitase in TKO skeletal muscle and determined that the former was regulated by reversible S-glutathionylation. Due to the hypothesized non-mitochondrial ROS production and shift in redox balance in the TKO mice, I would recommend determining if other proteins involved in energy metabolism are also regulated by S-glutathionylation.

Several mitochondrial and glycolytic pathway proteins are regulated by S-glutathionylation, including aconitase (Han et al., 2005), complex I (NADH-ubiquinone

oxidoreductase) of the ETC (Taylor et al., 2003), ICD-3 (Kil and Park, 2005), α -KGD (Applegate et al., 2008; Nulton-Persson et al., 2003), several mitochondrial membrane proteins (Beer et al., 2004), PDH (Odin et al., 2001), pyruvate kinase, aldolase, PP2A (Fratelli et al., 2002), PTEN (Yu et al., 2005) and PTP1B (Townsend et al., 2006). Exploiting newer techniques such as redox proteomics using two-dimensional gel electrophoresis followed by MS analysis may help to uncover even more targets in the TKO mice (Dalle-Donne et al., 2009). Once targets have been identified, glutathionylation could be confirmed through activity assays as we performed for α -KGD, as well as, immunoprecipitation techniques with glutathionylation-protein complex antibodies (Dalle-Donne et al., 2008; Gao et al., 2009).

5.3 Why is PDH Activity Decreased in Heart but Not Skeletal Muscle in the Absence of TXNIP?

In chapter 3, we reported the results of our analysis of mitochondrial content and respiratory function in skeletal muscle mitochondria and permeabilized fibers (PmFB) between the TKO and WT control mice. A recent report from Dr. Richard Lee's lab also examined these parameters in heart from TXNIP null mice with contrasting results (Yoshioka et al., 2012). Since both skeletal muscle and heart are oxidative tissues with similar metabolic phenotypes in a model of TXNIP deficiency in mice (Hui et al., 2008), we questioned why the results would differ in skeletal muscle versus heart mitochondria.

We demonstrated that there were no differences in quantities of skeletal muscle mDNA, citrate synthase protein content and enzyme activity, as well as protein abundance of the OXPHOS complexes of the ETC (Fig. 3-4A-E). In the same way, Yoshioka et al. (2012) indicated there were no differences in the heart protein content of the OXPHOS complexes of the ETC. However, the ratio of TXNIP null heart mDNA to nuclear DNA was slightly, but significantly increased. They qualitatively assessed that there were no structural differences or evidence of autophagy in the heart mitochondria using transmission electron microscopy.

Yoshioka et al. (2012) noted mildly decreased state 3 respiration, but no change in state 4 or uncoupled conditions in mitochondria from TXNIP null hearts. In contrast, our data in skeletal muscle mitochondria, under state 3 (ADP-dependent), state 4 (ADP-independent) and uncoupled conditions in the presence of complex I-linked (glutamate-malate) and complex-II-linked (succinate) showed no measurable differences (Fig. 3-4F-G). Both groups assessed respiratory function in PmFB, which corroborated their respective results and actually showed a minor deficit in maximal ATP synthesis at Complex V in both skeletal muscle (Fig. 3-4H-I) and heart. As a whole, the disparities were not dramatically divergent between skeletal muscle and the heart, although it does point to a mild functional loss of ADP-stimulated respiration in heart mitochondria not seen in skeletal muscle. It is possible that these differences emerged as a result of strain

differences, discrete aspects of the gene targeting approaches, and variances in the isolation of mitochondria and the preparation of the PmFb.

Nevertheless, a dramatic distinction did emerge using the precursor substrate pyruvate. Whereas we did not observe reduced state 3 respiration, Yoshioka et al. (2012) reported a 35% reduction in state 3 rates with this substrate. Since pyruvate dehydrogenase (PDH) is the gatekeeper for the entry of pyruvate into the mitochondria, both quantity and activity were measured. We found no difference in the quantity of the total PDH complex or PDH E1 α (data not shown) nor did we discern a difference in the activity between the genotypes (Table 1). Although there was no difference in quantity of the total PDH complex in heart, there was a 54% decrease in activity in the TXNIP null hearts compared to the WT mice (Yoshioka et al., 2012). These findings could explain the disparity in respiration of pyruvate between skeletal muscle and heart mitochondria when TXNIP is deficient.

Our remaining question is, “Why heart and skeletal muscle display contrasting PDH activity and what role does TXNIP play in the control of mitochondrial pyruvate flux?” To address the dissimilarities in PDH activity, I would suggest examining lactate dehydrogenase (LDH) isoenzymes between skeletal muscle and heart. There are five isoenzymes composed of tetramers of two different subunits, M and H. LDH-5 (M₄) is composed of M subunits only and is the predominant form in skeletal muscle, whereas LDH-1 (H₄) is composed of H subunits only and is the predominant form in the heart

(Dawson et al., 1964). The other three isozymes are composed of various combinations of the two subunits: M₃H, M₂H₂ and MH₃. The two major isozymes M₄ and H₄ are synthesized by two different genes, *LdhA* and *LdhB*, respectively, and have different physiological functions (Quistorff and Grunnet, 2011). The H₄ isoenzyme is more susceptible to substrate inhibition by pyruvate, while the M₄ isoenzyme resists inhibition by pyruvate (Dawson et al., 1964). Therefore, the M₄ isoenzyme preferentially catalyzes the reduction of pyruvate to lactate, thus supplying the necessary NADH to uphold glycolytic flux, and conversely the H₄ isoenzyme catalyzes the oxidation of lactate to pyruvate, thus favoring an acceleration of the PDH pathway. The balance of these isozymes in TXNIP deficient muscle may play a critical role in pyruvate metabolism.

It is not surprising then that *LDHA* is upregulated, or *LDHB* is silenced, in cancers relying on aerobic glycolysis or the Warburg effect for growth (Brahimi-Horn et al., 2007; Brown et al., 2013; Fan et al., 2011; Shim et al., 1997; Summermatter et al., 2013). It is possible that *LDHA* may be upregulated in skeletal muscle, particularly in the glycolysis-driven TKO mice. Since the H₄ isozyme is predominant in the heart, decreased PDH activity in TXNIP null hearts could divert the glycolytically derived pyruvate away from transport into the mitochondria and toward lactate production. Physiologically, this would serve to protect the heart from hypoxia due to ischemia-reperfusion injury (Yoshioka et al., 2012) and contribute to the increased glycolytic flux observed in both heart and skeletal muscle in TKO mice (Hui et al., 2008). To test this

hypothesis I would measure PDH activity in both skeletal muscle and heart in the same model of TXNIP ablation. Also, LDH activity and isoenzyme patterns should be determined as previously described (Summermatter et al., 2013). If there is a difference in PDH activity and the LDH isozymes are shifted, one could knockdown LDH in the heart and see if PDH activity is rescued.

The second question to tackle is how TXNIP controls pyruvate flux in the mitochondria? To address this, Yoshioka et al. (2012) successfully immunoprecipitated TXNIP with PDH E1 α , thus implying a direct mechanism of action by TXNIP in the regulation of PDH activity. Since PDH and BCKAD share a similar enzyme complex structure, I would also implement immunoprecipitation experiments between TXNIP and BCKAD and BDH1 as discussed in detail in an earlier section.

5.4 What Effects Would a High Fat Diet Have on TKO Mice?

5.4.1 Muscle Insulin Resistance, Lipid Oversupply and Mitochondrial Stress

Skeletal muscle is a major insulin target tissue and impairments in muscle glucose disposal and insulin signaling are universally present in patients affected by type 2 diabetes mellitus (T2DM). One theory to explain the etiology of skeletal muscle insulin resistance proposes that increased systemic lipid delivery, coupled with reduced mitochondrial fat oxidation, leads to rising intracellular fatty acid metabolites, such as long-chain fatty acyl-CoAs (LCFA-CoAs), diacylglycerol (DAG) and ceramides. These cytosolic lipids are thought to activate serine/threonine kinases, such as the PKC family,

resulting in serine phosphorylation of the insulin receptor (IR) and insulin receptor substrate (IRS-1) signaling proteins, and thus inhibition of PI3K-Akt activity and GLUT4 translocation (Itani et al., 2002; Morino et al., 2006; Petersen and Shulman, 2002). However, other evidence suggests that mitochondrial dysfunction might occur as a late-stage consequence of overnutrition and/or insulin resistance rather than a cause (Muoio and Newgard, 2008). Moreover, data from our lab and others suggest that insulin resistance stems from excessive mitochondrial fat oxidation rather than the converse. For instance, we found that diet-induced and genetic forms of obesity in rodents are closely associated with elevated incomplete fat oxidation, which occurs when high rates of β -oxidation exceed TCA cycle flux (Koves et al., 2005; Koves et al., 2008). Most notably, we showed that malonyl-CoA decarboxylase knockout (*mcd*^{-/-}) mice are protected against high fat diet-induced glucose intolerance, despite high intramuscular levels of LCFA-CoAs (Koves et al., 2008). Malonyl-CoA is the endogenous inhibitor of carnitine palmitoyltransferase-1 (CPT-1), which allows for fatty acid import into the mitochondria. Malonyl-CoA decarboxylase degrades malonyl-CoA and promotes fat oxidation. Therefore, the *mcd*^{-/-} mouse is a genetic model of reduced β -oxidation. These findings suggest that limited β -oxidation may be advantageous under high fat conditions. Similarly, targeted deletion of AIF in mice, the primary physiological role of which is the maintenance of a fully functional ETC, have decreased mitochondrial OXPHOS but are protected from obesity and insulin resistance. We now add further

support to this theory since the TKO mouse has globally decreased substrate oxidation, yet maintains insulin sensitivity. This suggests that “mitochondrial dysfunction,” as classically defined, might not be a causative factor in insulin resistance, but rather a compensatory adaptation. Taken together, these reports show that reduced mitochondrial metabolism might promote insulin action. We reason that the converse is also true; that an excessive and/or inappropriate metabolic burden on muscle mitochondria generates a state of mitochondrial stress, causing a “signal” which may be redox in nature that diminishes insulin sensitivity. A comparison of the two models of lipid dysregulation and skeletal muscle insulin resistance is shown (Fig. 5-2A-B). Studying TXNIP under a nutrient burden, such as a high fat diet, could provide clues as to whether TXNIP is upregulated in response to that putative signal and preserves mitochondrial function, but at the expense of glucose uptake and insulin resistance.

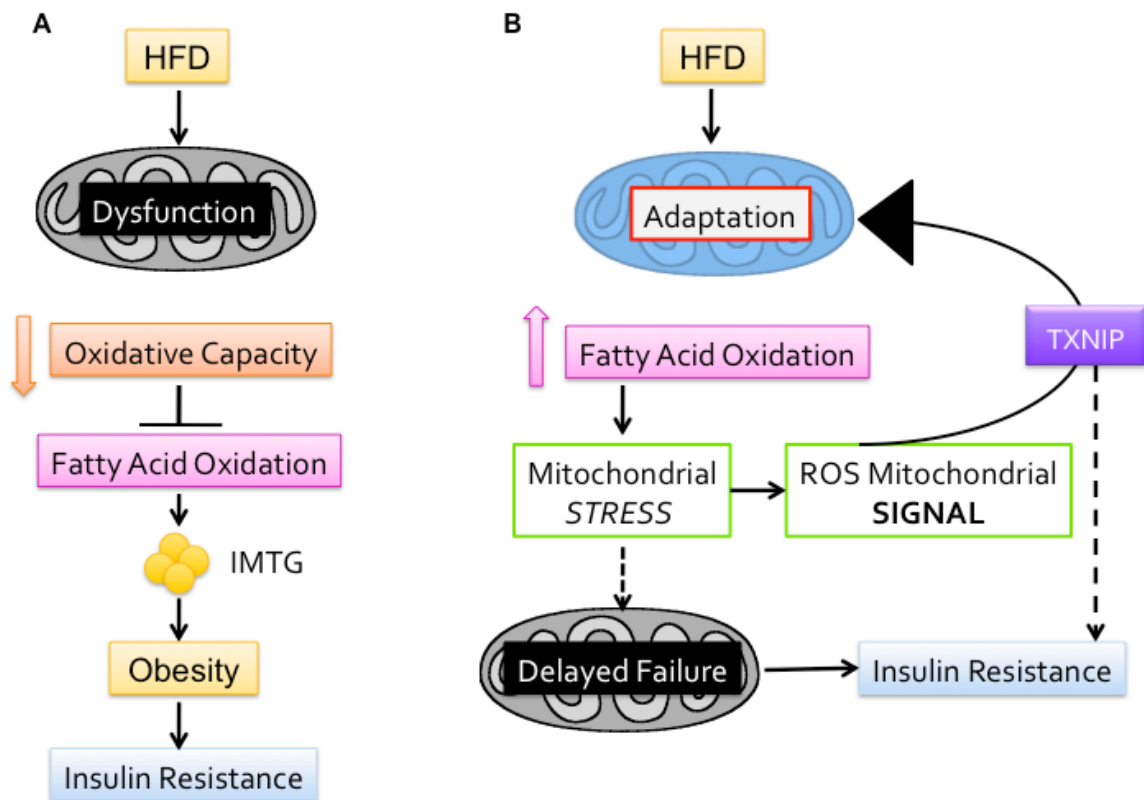


Figure 5-2: Models of Lipid Dysregulation and Skeletal Muscle Insulin Resistance

The lipotoxicity model presented in (A) suggests that a high fat diet causes mitochondrial dysfunction. Increased systemic lipid delivery results in reduced oxidative capacity and impaired fatty acid oxidation, which causes increased lipid metabolites (triacylglycerides, diacylglycerides and ceramides). These metabolites lead to obesity and insulin resistance. In the second model (B), mitochondrial failure is delayed. Fatty acids enter the mitochondria unimpeded and are oxidized. β -oxidation actually overwhelms TCA cycle flux, thus leading to a condition of “mitochondrial stress.” This causes a ROS derived signal leading to upregulation of TXNIP, which preserves mitochondrial function, thus delaying mitochondrial failure, but at the expense of insulin resistance. Therefore, TXNIP would serve as a molecular mediator connecting mitochondrial function, redox balance and insulin resistance.

5.4.2 TXNIP Expression Increases in Association with Fat, Incomplete Fat Oxidation and Decreases in Response to Pharmacological Inhibition of Fat Oxidation

TXNIP mRNA abundance increases over 2-fold in rat L6 myotubes when treated under high fat conditions for 24 h (Fig. 5-3A). In Wistar rats fed a standard chow diet, long- and medium-chain fatty acids increased during the transition from the fed to fasted state. By contrast, in rats fed a high fat diet acylcarnitines were persistently elevated, reflecting chronic availability and oxidation of lipid substrates (Koves et al., 2008). The accumulation of the acylcarnitines in the standard chow fasted and high fat diet conditions is suggestive of incomplete β -oxidation, supporting the idea that the development of skeletal muscle insulin resistance might stem from excessive β -oxidation and mitochondrial stress. Further, supporting TXNIP as a potential mitochondrial trigger under mitochondrial stress is the 60 – 100% mRNA upregulation of TXNIP in these same rats as compared to the standard chow fed control (Fig. 5.3B). We next examined the consequences of lipid surplus and inhibition of CPT-1 on TXNIP gene expression in cultured myocytes over time. Rat L6 myotubes were exposed to BSA alone or high fat conditions in the presence and absence of etomoxir (a potent inhibitor of CPT-1 and thus fat oxidation) (Fig. 5-3C). TXNIP gene expression was upregulated as early as 3 h after lipid exposure, and maximally by 48 h. Importantly, this upregulation was blocked by etomoxir, indicating that fat oxidation is necessary for this response.

Our lab has previously shown that etomoxir also prevents lipid-induced insulin resistance in cultured myocytes (Koves et al., 2008).

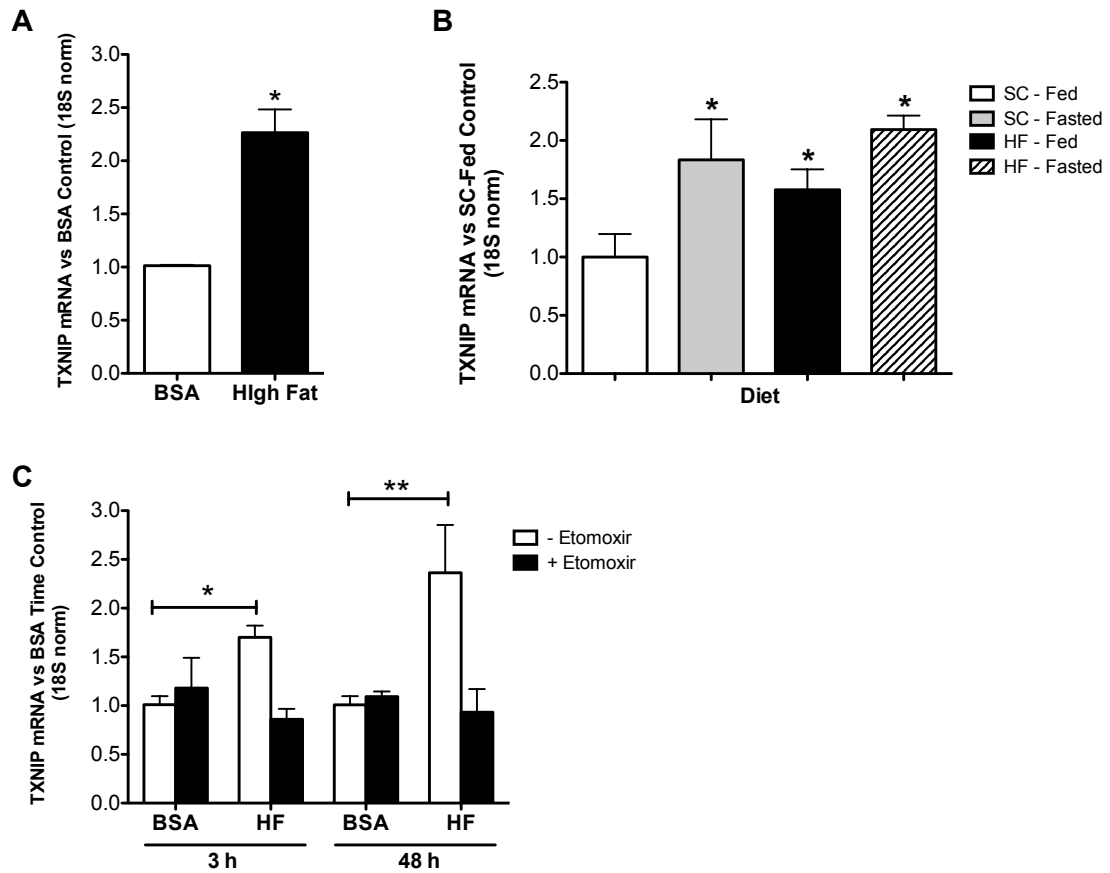


Figure 5-3: TXNIP Expression Increases in Association with Fat, Incomplete Fat Oxidation and Decreases in Response to Pharmacological Inhibition of Fat Oxidation

Real-time PCR analysis of mRNA encoding *TXNIP* normalized to 18S was conducted using the following: (A) Rat L6 myotubes were exposed to BSA alone (control) or complexed with an equimolar ratio of oleate to palmitate at a total concentration of 500 μ M. After 24 h, cell lysates were collected, RNA isolated and analyzed. (B) Wistar rats were fed either a standard chow or high fat diet for 12 weeks. Gastrocnemius muscle tissue was collected in the fed state or an overnight fast and immediately frozen in liquid N₂ and stored at -80°C. RNA was isolated from frozen, pulverized tissue and analyzed. (C) Rat L6 myotubes were exposed to a BSA control or oleate:palmitate (500 μ M) in the presence or absence of 0.1mM etomoxir from 3 to 48 h. Cell lysates were collected, RNA isolated and analyzed.

These findings support the hypothesis that obesity-related upregulation of *TXNIP* is secondary to excessive fat oxidation and that *TXNIP* might serve as the mechanistic link between incomplete fat oxidation and insulin resistance. This could be tested by evaluating regulation of *TXNIP* expression in *mcd*^{-/-} mice that have low rates of incomplete β -oxidation. If diet-induced upregulation of *TXNIP* requires fat oxidation, *TXNIP* expression levels should be lower in muscle of *mcd*^{-/-} mice as compared to WT controls. Positive findings would implicate *TXNIP* as a key link between excessive β -oxidation and insulin resistance.

5.4.3 Are TKO Mice More Susceptible to Diet-Induced Mitochondrial Dysfunction?

In chapter 3, we showed that TKO mice have reduced oxidative metabolism of several substrates, which was the result of marked deficits in skeletal muscle enzymes required for ketone and BCAA oxidation, as well as more modest reductions in enzymes of β -oxidation and the TCA cycle. Subjecting TKO and WT controls to 12 weeks of high fat feeding, should cause an even more severe form of mitochondrial dysfunction in TKO mice, particularly in the lipid catabolic pathway. If true, the identified enzymes of

β -oxidation and the TCA cycle previously with modest deficits should be exacerbated. Further, deficits in any of the other enzymes within this pathway that are regulated by TXNIP could be identified. This experiment allows for the testing of the hypothesis that obesity-related induction of TXNIP plays a role in delaying or attenuating mitochondrial failure.

One of the impairments that might be exacerbated under a high fat diet is the reduction in long-chain acylcarnitines observed in both the skeletal muscle and liver of TKO mice. This was a particularly confusing finding since this was the only deficit shared by the skeletal muscle and liver. We hypothesized that these data were the result of diminished CPT-1 activity, but the concentrations of malonyl-CoA, a potent inhibitor of CPT-1, were similar between genotypes. Therefore, since malonyl-CoA-mediated inhibition of fat oxidation or decreased protein abundance of CPT-1 does not appear to contribute to the reduced catabolism of fatty acids, I would consider examining fatty acid transport into cells.

Recommendations would be to begin with an evaluation of fatty acid translocase (CD36). CD36 is ubiquitously distributed membrane-associated fatty acid transporter (Glatz et al., 2010). *In vitro* studies show that it binds to long-chain but not short-chain fatty acids (Baillie et al., 1996). Mice with CD36 overexpression in muscle demonstrated enhanced fatty acid oxidation, reduced plasma triglycerides and fatty acids and increases in plasma glucose and insulin (Ibrahimi et al., 1999), an opposite phenotype

from the TKO mice. Therefore, I would first examine protein and mRNA expression of CD36 in TKO skeletal muscle and liver. One could also test if there is a reduction in the uptake of non-metabolizable fatty acid analogs, such as BMIPP and IPA, as previously described (Coburn et al., 2000).

5.4.4 Does Mitochondrial Dysfunction in TKO Mice Exacerbate or Protect Against Diet-Induced Defects in the Proximal Arm of the Insulin-Signaling Cascade?

In chapter 5.2.3, I discussed how only two groups examined the effect of TXNIP deficiency on the insulin-signaling cascade proteins. Both reported increases in Akt phosphorylation in the skeletal muscle of TXNIP deficient mice (Hui et al., 2008; Yoshihara et al., 2010), but the Western blots upon which these conclusions were based were less than convincing. Protein expression of IRS-1 was also examined in the skeletal muscle of TBP-2^{-/-} and ob/ob•TBP-2^{-/-} mice and although the Western blots suggesting greater phosphorylation of IRS-1 in the TXNIP deficient states as compared to their respective controls were slightly more convincing, there was no difference between the TXNIP null conditions. I also discussed how our preliminary data did not show any difference between the genotypes in phosphorylation of Akt or total Akt, but there was an increase in IRS-1 protein expression in the TKO mice. Since the proposed mechanism of action by Hui et al. (2008) has not been substantiated, no mechanism was proposed by Yoshihara et al. (2010) and there are striking inconsistencies in the data, I suggested a

systematic re-examination of the proximal and distal arms of the insulin-signaling pathway in the TKO mice on control and high fat diets.

The TKO mice would serve as an *in vivo* tool to explore the relationship between mitochondrial function and insulin action. Numerous studies have suggested that impaired mitochondrial oxidation of fat increases lipid molecules that oppose insulin signaling at the level of IR, IRS-1, PI3K and GLUT4 translocation (Itani et al., 2002; Morino et al., 2006; Petersen and Shulman, 2002). As shown in the *mcd^{-/-}* mice, despite a high lipid surplus, these mice are protected from glucose intolerance (Koves et al., 2008). Data provided in chapter 3 (Fig. 3-1), demonstrate that the TKO mice also have elevated blood lipids and impaired fat oxidation, yet remain insulin sensitive while on a standard chow diet. However, an important remaining question is whether or not these TKO mice accumulate intramuscular lipid molecules (TAG, DAG, acyl-CoAs) when fed a high fat diet (as would be predicted), and if so, does this result in impaired insulin-mediated activation or signaling molecules, such as serine rather than tyrosine phosphorylation. It has been reported that TXNIP null mice maintain insulin sensitivity after a 4-week high fat diet as measured by intraperitoneal insulin tolerance test (ITT) (Chutkow et al., 2010), but a thorough analysis of intramuscular lipid molecules (TAG, DAG, acyl-CoAs) was not provided. If the widely accepted “LC-CoA or lipotoxicity hypothesis” holds true, increased intramuscular lipid accumulation should result in serine phosphorylation and inactivation of IR, IRS-1 and PI3K. If on the other hand,

insulin activation of these molecules were not impaired, the results would argue against the lipotoxicity model while favoring a more direct connection between insulin resistance and excessive mitochondrial fat oxidation as predicted by the *mcd^{-/-}* model. In parallel, the question of whether TXNIP overexpression results in impaired glucose metabolism and insulin signaling under BSA control and high fat conditions could also be explored in cultured myocytes, where parameters of insulin insensitivity (glucose uptake, glucose oxidation and glycogen synthesis) and insulin signaling could be easily explored.

5.5 Summary

TXNIP is a fascinating, multifunctional protein with many avenues for continued study. Several suggestions were made here, but to prioritize I would begin with investigating how TXNIP stabilizes the mitochondrial dehydrogenases to determine a clear mechanism of action before moving on to the source of ROS and determining if the malate-aspartate shuttle is proving reducing equivalents to the ETC in the TKO mice. Answering these questions will provide greater understanding as to the role of TXNIP in mitochondrial function and insulin action and better design of pharmaceuticals using TXNIP as a potential antidiabetic drug target.

References

- Abbrescia, D.I., La Piana, G., and Lofrumento, N.E. (2012). Malate-aspartate shuttle and exogenous NADH/cytochrome c electron transport pathway as two independent cytosolic reducing equivalent transfer systems. *Arch Biochem Biophys* 518, 157-163.
- Advani, A., Gilbert, R.E., Thai, K., Gow, R.M., Langham, R.G., Cox, A.J., Connelly, K.A., Zhang, Y., Herzenberg, A.M., Christensen, P.K., *et al.* (2009). Expression, localization, and function of the thioredoxin system in diabetic nephropathy. *J Am Soc Nephrol* 20, 730-741.
- Ago, T., Liu, T., Zhai, P., Chen, W., Li, H., Molkenin, J.D., Vatner, S.F., and Sadoshima, J. (2008). A redox-dependent pathway for regulating class II HDACs and cardiac hypertrophy. *Cell* 133, 978-993.
- Ahsan, M.K., Okuyama, H., Hoshino, Y., Oka, S., Masutani, H., Yodoi, J., and Nakamura, H. (2009). Thioredoxin-binding protein-2 deficiency enhances methionine-choline deficient diet-induced hepatic steatosis but inhibits steatohepatitis in mice. *Antioxid Redox Signal* 11, 2573-2584.
- Alberti, K.G., Eckel, R.H., Grundy, S.M., Zimmet, P.Z., Cleeman, J.I., Donato, K.A., Fruchart, J.C., James, W.P., Loria, C.M., and Smith, S.C., Jr. (2009). Harmonizing the metabolic syndrome: a joint interim statement of the International Diabetes Federation Task Force on Epidemiology and Prevention; National Heart, Lung, and Blood Institute; American Heart Association; World Heart Federation; International Atherosclerosis Society; and International Association for the Study of Obesity. *Circulation* 120, 1640-1645.
- Alvarez, C.E. (2008). On the origins of arrestin and rhodopsin. *BMC Evol Biol* 8, 222.
- An, J., Muoio, D.M., Shiota, M., Fujimoto, Y., Cline, G.W., Shulman, G.I., Koves, T.R., Stevens, R., Millington, D., and Newgard, C.B. (2004). Hepatic expression of malonyl-CoA decarboxylase reverses muscle, liver and whole-animal insulin resistance. *Nat Med* 10, 268-274.
- Andersen, K.M., Madsen, L., Prag, S., Johnsen, A.H., Semple, C.A., Hendil, K.B., and Hartmann-Petersen, R. (2009). Thioredoxin Txn1/TRP32 is a redox-active cofactor of the 26 S proteasome. *J Biol Chem* 284, 15246-15254.

- Anderson, C.P., Shen, M., Eisenstein, R.S., and Leibold, E.A. (2012). Mammalian iron metabolism and its control by iron regulatory proteins. *Biochim Biophys Acta* 1823, 1468-1483.
- Anderson, E.J., Lustig, M.E., Boyle, K.E., Woodlief, T.L., Kane, D.A., Lin, C.T., Price, J.W., 3rd, Kang, L., Rabinovitch, P.S., Szeto, H.H., *et al.* (2009). Mitochondrial H₂O₂ emission and cellular redox state link excess fat intake to insulin resistance in both rodents and humans. *J Clin Invest* 119, 573-581.
- Anderson, E.J., Yamazaki, H., and Neuffer, P.D. (2007). Induction of endogenous uncoupling protein 3 suppresses mitochondrial oxidant emission during fatty acid-supported respiration. *J Biol Chem* 282, 31257-31266.
- Andres, A.M., Ratliff, E.P., Sachithanatham, S., and Hui, S.T. (2011). Diminished AMPK signaling response to fasting in thioredoxin-interacting protein knockout mice. *FEBS Lett* 585, 1223-1230.
- Anko, M.L., and Neugebauer, K.M. (2012). RNA-protein interactions in vivo: global gets specific. *Trends Biochem Sci* 37, 255-262.
- Applegate, M.A., Humphries, K.M., and Szweda, L.I. (2008). Reversible inhibition of alpha-ketoglutarate dehydrogenase by hydrogen peroxide: glutathionylation and protection of lipoic acid. *Biochemistry* 47, 473-478.
- Baillie, A.G., Coburn, C.T., and Abumrad, N.A. (1996). Reversible binding of long-chain fatty acids to purified FAT, the adipose CD36 homolog. *J Membr Biol* 153, 75-81.
- Bailly, A., Lone, Y.C., and Latruffe, N. (1990). Variations of specific mRNA and polypeptide contents of rat liver D-beta-hydroxybutyrate dehydrogenase during an experimental diabetes mellitus. *Biochimie* 72, 351-354.
- Bailly, A., Lone, Y.C., and Latruffe, N. (1991). Post-transcriptional analysis of rat mitochondrial D-3-hydroxybutyrate dehydrogenase control through development and physiological stages. *Biol Cell* 73, 121-129.
- Bakheet, T., Williams, B.R., and Khabar, K.S. (2006). ARED 3.0: the large and diverse AU-rich transcriptome. *Nucleic Acids Res* 34, D111-114.
- Barron, J.T., Gu, L., and Parrillo, J.E. (1998). Malate-aspartate shuttle, cytoplasmic NADH redox potential, and energetics in vascular smooth muscle. *J Mol Cell Cardiol* 30, 1571-1579.

- Bedard, K., and Krause, K.H. (2007). The NOX family of ROS-generating NADPH oxidases: physiology and pathophysiology. *Physiol Rev* 87, 245-313.
- Beer, S.M., Taylor, E.R., Brown, S.E., Dahm, C.C., Costa, N.J., Runswick, M.J., and Murphy, M.P. (2004). Glutaredoxin 2 catalyzes the reversible oxidation and glutathionylation of mitochondrial membrane thiol proteins: implications for mitochondrial redox regulation and antioxidant DEFENSE. *J Biol Chem* 279, 47939-47951.
- Billiet, L., Furman, C., Larigauderie, G., Copin, C., Page, S., Fruchart, J.C., Brand, K., and Rouis, M. (2008). Enhanced VDUP-1 gene expression by PPARgamma agonist induces apoptosis in human macrophage. *J Cell Physiol* 214, 183-191.
- Binstock, J.F., and Schulz, H. (1981). Fatty acid oxidation complex from *Escherichia coli*. *Methods in Enzymology* 71 Pt C, 403-411.
- Bodnar, J.S., Chatterjee, A., Castellani, L.W., Ross, D.A., Ohmen, J., Cavalcoli, J., Wu, C., Dains, K.M., Catanese, J., Chu, M., *et al.* (2002). Positional cloning of the combined hyperlipidemia gene *Hyplip1*. *Nat Genet* 30, 110-116.
- Boushel, R., Gnaiger, E., Schjerling, P., Skovbro, M., Kraunsoe, R., and Dela, F. (2007). Patients with type 2 diabetes have normal mitochondrial function in skeletal muscle. *Diabetologia* 50, 790-796.
- Brahimi-Horn, M.C., Chiche, J., and Pouyssegur, J. (2007). Hypoxia signalling controls metabolic demand. *Curr Opin Cell Biol* 19, 223-229.
- Brown, N.J., Higham, S.E., Perunovic, B., Arafa, M., Balasubramanian, S., and Rehman, I. (2013). Lactate dehydrogenase-B is silenced by promoter methylation in a high frequency of human breast cancers. *PLoS One* 8, e57697.
- Bunik, V., Raddatz, G., Lemaire, S., Meyer, Y., Jacquot, J.P., and Bisswanger, H. (1999). Interaction of thioredoxins with target proteins: role of particular structural elements and electrostatic properties of thioredoxins in their interplay with 2-oxoacid dehydrogenase complexes. *Protein Sci* 8, 65-74.
- Bunik, V.I. (2003). 2-Oxo acid dehydrogenase complexes in redox regulation. *Eur J Biochem* 270, 1036-1042.
- Butler, L.M., Zhou, X., Xu, W.S., Scher, H.I., Rifkind, R.A., Marks, P.A., and Richon, V.M. (2002). The histone deacetylase inhibitor SAHA arrests cancer cell growth, up-regulates

thioredoxin-binding protein-2, and down-regulates thioredoxin. *Proc Natl Acad Sci U S A* 99, 11700-11705.

Cha-Molstad, H., Saxena, G., Chen, J., and Shalev, A. (2009). Glucose-stimulated expression of Txnip is mediated by carbohydrate response element-binding protein, p300, and histone H4 acetylation in pancreatic beta cells. *J Biol Chem* 284, 16898-16905.

Chai, T.F., Hong, S.Y., He, H., Zheng, L., Hagen, T., Luo, Y., and Yu, F.X. (2012). A potential mechanism of metformin-mediated regulation of glucose homeostasis: inhibition of Thioredoxin-interacting protein (Txnip) gene expression. *Cell Signal* 24, 1700-1705.

Chen, C.L., Lin, C.F., Chang, W.T., Huang, W.C., Teng, C.F., and Lin, Y.S. (2008a). Ceramide induces p38 MAPK and JNK activation through a mechanism involving a thioredoxin-interacting protein-mediated pathway. *Blood* 111, 4365-4374.

Chen, J., Couto, F.M., Minn, A.H., and Shalev, A. (2006). Exenatide inhibits beta-cell apoptosis by decreasing thioredoxin-interacting protein. *Biochem Biophys Res Commun* 346, 1067-1074.

Chen, J., Hui, S.T., Couto, F.M., Mungrue, I.N., Davis, D.B., Attie, A.D., Lusic, A.J., Davis, R.A., and Shalev, A. (2008b). Thioredoxin-interacting protein deficiency induces Akt/Bcl-xL signaling and pancreatic beta-cell mass and protects against diabetes. *Faseb J* 22, 3581-3594.

Chen, J., Saxena, G., Mungrue, I.N., Lusic, A.J., and Shalev, A. (2008c). Thioredoxin-interacting protein: a critical link between glucose toxicity and beta-cell apoptosis. *Diabetes* 57, 938-944.

Chen, K.S., and DeLuca, H.F. (1994). Isolation and characterization of a novel cDNA from HL-60 cells treated with 1,25-dihydroxyvitamin D-3. *Biochim Biophys Acta* 1219, 26-32.

Chen, Y., and Varani, G. (2005). Protein families and RNA recognition. *Febs J* 272, 2088-2097.

Cheng, G.C., Schulze, P.C., Lee, R.T., Sylvan, J., Zetter, B.R., and Huang, H. (2004). Oxidative stress and thioredoxin-interacting protein promote intravasation of melanoma cells. *Exp Cell Res* 300, 297-307.

- Choy, K.H., Dean, O., Berk, M., Bush, A.I., and van den Buuse, M. (2010). Effects of N-acetyl-cysteine treatment on glutathione depletion and a short-term spatial memory deficit in 2-cyclohexene-1-one-treated rats. *Eur J Pharmacol* 649, 224-228.
- Chuang, D.T., Shih, V.E. (2001). Maple syrup urine disease (branched-chain ketoaciduria). In *The Metabolic & Molecular Bases of Inherited Disease*, C.R. Scriver, ed. (New York, McGraw-Hill), pp. 1971-2005.
- Chutkow, W.A., Birkenfeld, A.L., Brown, J.D., Lee, H.Y., Frederick, D.W., Yoshioka, J., Patwari, P., Kursawe, R., Cushman, S.W., Plutzky, J., *et al.* (2010). Deletion of the alpha-arrestin protein Txnip in mice promotes adiposity and adipogenesis while preserving insulin sensitivity. *Diabetes* 59, 1424-1434.
- Chutkow, W.A., and Lee, R.T. (2011). Thioredoxin regulates adipogenesis through thioredoxin-interacting protein (Txnip) protein stability. *J Biol Chem* 286, 29139-29145.
- Chutkow, W.A., Patwari, P., Yoshioka, J., and Lee, R.T. (2008). Thioredoxin-interacting protein (Txnip) is a critical regulator of hepatic glucose production. *J Biol Chem* 283, 2397-2406.
- Coburn, C.T., Knapp, F.F., Jr., Febbraio, M., Beets, A.L., Silverstein, R.L., and Abumrad, N.A. (2000). Defective uptake and utilization of long chain fatty acids in muscle and adipose tissues of CD36 knockout mice. *J Biol Chem* 275, 32523-32529.
- Contreras, L., and Satrustegui, J. (2009). Calcium signaling in brain mitochondria: interplay of malate aspartate NADH shuttle and calcium uniporter/mitochondrial dehydrogenase pathways. *J Biol Chem* 284, 7091-7099.
- Coon, H., Singh, N., Dunn, D., Eckfeldt, J.H., Province, M.A., Hopkins, P.N., Weiss, R., Hunt, S.C., and Leppert, M.F. (2004). TXNIP gene not associated with familial combined hyperlipidemia in the NHLBI Family Heart Study. *Atherosclerosis* 174, 357-362.
- Corbett, J.A. (2008). Thioredoxin-interacting protein is killing my beta-cells! *Diabetes* 57, 797-798.
- Dalle, S., Ravier, M.A., and Bertrand, G. (2011). Emerging roles for beta-arrestin-1 in the control of the pancreatic beta-cell function and mass: new therapeutic strategies and consequences for drug screening. *Cell Signal* 23, 522-528.
- Dalle-Donne, I., Milzani, A., Gagliano, N., Colombo, R., Giustarini, D., and Rossi, R. (2008). Molecular mechanisms and potential clinical significance of S-glutathionylation. *Antioxid Redox Signal* 10, 445-473.

- Dalle-Donne, I., Rossi, R., Colombo, G., Giustarini, D., and Milzani, A. (2009). Protein S-glutathionylation: a regulatory device from bacteria to humans. *Trends Biochem Sci* 34, 85-96.
- Dalton, T.P., Shertzer, H.G., and Puga, A. (1999). Regulation of gene expression by reactive oxygen. *Annu Rev Pharmacol Toxicol* 39, 67-101.
- Davis, B.K., and Ting, J.P. (2010). NLRP3 has a sweet tooth. *Nat Immunol* 11, 105-106.
- Dawson, D.M., Goodfriend, T.L., and Kaplan, N.O. (1964). Lactic Dehydrogenases: Functions of the Two Types Rates of Synthesis of the Two Major Forms Can Be Correlated with Metabolic Differentiation. *Science* 143, 929-933.
- Devi, T.S., Hosoya, K., Terasaki, T., and Singh, L.P. (2013). Critical role of TXNIP in oxidative stress, DNA damage and retinal pericyte apoptosis under high glucose: implications for diabetic retinopathy. *Exp Cell Res* 319, 1001-1012.
- DeWire, S.M., Ahn, S., Lefkowitz, R.J., and Shenoy, S.K. (2007). Beta-arrestins and cell signaling. *Annu Rev Physiol* 69, 483-510.
- Donnelly, K.L., Margosian, M.R., Sheth, S.S., Lusic, A.J., and Parks, E.J. (2004). Increased lipogenesis and fatty acid reesterification contribute to hepatic triacylglycerol stores in hyperlipidemic *Txnip*^{-/-} mice. *J Nutr* 134, 1475-1480.
- Draheim, K.M., Chen, H.B., Tao, Q., Moore, N., Roche, M., and Lyle, S. (2010). ARRDC3 suppresses breast cancer progression by negatively regulating integrin beta4. *Oncogene* 29, 5032-5047.
- Dutta, K.K., Nishinaka, Y., Masutani, H., Akatsuka, S., Aung, T.T., Shirase, T., Lee, W.H., Yamada, Y., Hiai, H., Yodoi, J., *et al.* (2005). Two distinct mechanisms for loss of thioredoxin-binding protein-2 in oxidative stress-induced renal carcinogenesis. *Lab Invest* 85, 798-807.
- Eaton, P., Byers, H.L., Leeds, N., Ward, M.A., and Shattock, M.J. (2002). Detection, quantitation, purification, and identification of cardiac proteins S-thiolated during ischemia and reperfusion. *J Biol Chem* 277, 9806-9811.
- Eisenstein, R.S. (2000). Iron regulatory proteins and the molecular control of mammalian iron metabolism. *Annu Rev Nutr* 20, 627-662.
- Elchebly, M., Payette, P., Michaliszyn, E., Cromlish, W., Collins, S., Loy, A.L., Normandin, D., Cheng, A., Himms-Hagen, J., Chan, C.C., *et al.* (1999). Increased insulin

sensitivity and obesity resistance in mice lacking the protein tyrosine phosphatase-1B gene. *Science* 283, 1544-1548.

Evans, J.L., Goldfine, I.D., Maddux, B.A., and Grodsky, G.M. (2002). Oxidative stress and stress-activated signaling pathways: a unifying hypothesis of type 2 diabetes. *Endocr Rev* 23, 599-622.

Fan, J., Hitosugi, T., Chung, T.W., Xie, J., Ge, Q., Gu, T.L., Polakiewicz, R.D., Chen, G.Z., Boggon, T.J., Lonial, S., *et al.* (2011). Tyrosine phosphorylation of lactate dehydrogenase A is important for NADH/NAD(+) redox homeostasis in cancer cells. *Mol Cell Biol* 31, 4938-4950.

Fratelli, M., Demol, H., Puype, M., Casagrande, S., Eberini, I., Salmons, M., Bonetto, V., Mengozzi, M., Duffieux, F., Miclet, E., *et al.* (2002). Identification by redox proteomics of glutathionylated proteins in oxidatively stressed human T lymphocytes. *Proc Natl Acad Sci U S A* 99, 3505-3510.

Gao, X.H., Bedhomme, M., Veyel, D., Zaffagnini, M., and Lemaire, S.D. (2009). Methods for analysis of protein glutathionylation and their application to photosynthetic organisms. *Mol Plant* 2, 218-235.

Ghaemmaghami, S., and Oas, T.G. (2001). Quantitative protein stability measurement in vivo. *Nat Struct Biol* 8, 879-882.

Glatz, J.F., Luiken, J.J., and Bonen, A. (2010). Membrane fatty acid transporters as regulators of lipid metabolism: implications for metabolic disease. *Physiol Rev* 90, 367-417.

Glisovic, T., Bachorik, J.L., Yong, J., and Dreyfuss, G. (2008). RNA-binding proteins and post-transcriptional gene regulation. *FEBS Lett* 582, 1977-1986.

Goldstein, B.J., Mahadev, K., and Wu, X. (2005). Redox paradox: insulin action is facilitated by insulin-stimulated reactive oxygen species with multiple potential signaling targets. *Diabetes* 54, 311-321.

Gorin, Y., Ricono, J.M., Kim, N.H., Bhandari, B., Choudhury, G.G., and Abboud, H.E. (2003). Nox4 mediates angiotensin II-induced activation of Akt/protein kinase B in mesangial cells. *Am J Physiol Renal Physiol* 285, F219-229.

Goyary, D., and Sharma, R. (2008). Late onset of dietary restriction reverses age-related decline of malate-aspartate shuttle enzymes in the liver and kidney of mice. *Biogerontology* 9, 11-18.

- Grinblat, L., Pacheco Bolanos, L.F., and Stoppani, A.O. (1986). Decreased rate of ketone-body oxidation and decreased activity of D-3-hydroxybutyrate dehydrogenase and succinyl-CoA:3-oxo-acid CoA-transferase in heart mitochondria of diabetic rats. *Biochem J* 240, 49-56.
- Guo, W., Jiang, L., Bhasin, S., Khan, S.M., and Swerdlow, R.H. (2009). DNA extraction procedures meaningfully influence qPCR-based mtDNA copy number determination. *Mitochondrion* 9, 261-265.
- Guy, G.R., Cairns, J., Ng, S.B., and Tan, Y.H. (1993). Inactivation of a redox-sensitive protein phosphatase during the early events of tumor necrosis factor/interleukin-1 signal transduction. *J Biol Chem* 268, 2141-2148.
- Hale, D.E., Cornell, J.E., and Bennett, M.J. (1997). Stability of long-chain and short-chain 3-hydroxyacyl-CoA dehydrogenase activity in postmortem liver. *Clin Chem* 43, 273-278.
- Han, D., Canali, R., Garcia, J., Aguilera, R., Gallaher, T.K., and Cadenas, E. (2005). Sites and mechanisms of aconitase inactivation by peroxynitrite: modulation by citrate and glutathione. *Biochemistry* 44, 11986-11996.
- Han, S.H., Jeon, J.H., Ju, H.R., Jung, U., Kim, K.Y., Yoo, H.S., Lee, Y.H., Song, K.S., Hwang, H.M., Na, Y.S., *et al.* (2003). VDUP1 upregulated by TGF-beta1 and 1,25-dihydroxyvitamin D3 inhibits tumor cell growth by blocking cell-cycle progression. *Oncogene* 22, 4035-4046.
- Hansen, J.M., Go, Y.M., and Jones, D.P. (2006). Nuclear and mitochondrial compartmentation of oxidative stress and redox signaling. *Annu Rev Pharmacol Toxicol* 46, 215-234.
- Haqq, A.M., Lien, L.F., Boan, J., Arlotto, M., Slentz, C.A., Muehlbauer, M.J., Rochon, J., Gallup, D., McMahon, R.L., Bain, J.R., *et al.* (2005). The Study of the Effects of Diet on Metabolism and Nutrition (STEDMAN) weight loss project: Rationale and design. *Contemp Clin Trials* 26, 616-625.
- Hentze, M.W., Muckenthaler, M.U., and Andrews, N.C. (2004). Balancing acts: molecular control of mammalian iron metabolism. *Cell* 117, 285-297.
- Hui, S.T., Andres, A.M., Miller, A.K., Spann, N.J., Potter, D.W., Post, N.M., Chen, A.Z., Sachithanatham, S., Jung, D.Y., Kim, J.K., *et al.* (2008). Txnip balances metabolic and growth signaling via PTEN disulfide reduction. *Proc Natl Acad Sci U S A* 105, 3921-3926.

- Hui, T.Y., Sheth, S.S., Diffley, J.M., Potter, D.W., Lusic, A.J., Attie, A.D., and Davis, R.A. (2004). Mice lacking thioredoxin-interacting protein provide evidence linking cellular redox state to appropriate response to nutritional signals. *J Biol Chem* 279, 24387-24393.
- Hurd, T.R., Costa, N.J., Dahm, C.C., Beer, S.M., Brown, S.E., Filipovska, A., and Murphy, M.P. (2005). Glutathionylation of mitochondrial proteins. *Antioxid Redox Signal* 7, 999-1010.
- Ibrahimi, A., Bonen, A., Blinn, W.D., Hajri, T., Li, X., Zhong, K., Cameron, R., and Abumrad, N.A. (1999). Muscle-specific overexpression of FAT/CD36 enhances fatty acid oxidation by contracting muscle, reduces plasma triglycerides and fatty acids, and increases plasma glucose and insulin. *J Biol Chem* 274, 26761-26766.
- Imamura, T., Huang, J., Dalle, S., Ugi, S., Usui, I., Luttrell, L.M., Miller, W.E., Lefkowitz, R.J., and Olefsky, J.M. (2001). beta -Arrestin-mediated recruitment of the Src family kinase Yes mediates endothelin-1-stimulated glucose transport. *J Biol Chem* 276, 43663-43667.
- Itani, S.I., Ruderman, N.B., Schmedier, F., and Boden, G. (2002). Lipid-induced insulin resistance in human muscle is associated with changes in diacylglycerol, protein kinase C, and IkappaB-alpha. *Diabetes* 51, 2005-2011.
- Jeon, J.H., Lee, K.N., Hwang, C.Y., Kwon, K.S., You, K.H., and Choi, I. (2005). Tumor suppressor VDUP1 increases p27(kip1) stability by inhibiting JAB1. *Cancer Res* 65, 4485-4489.
- Jin, H.O., Seo, S.K., Kim, Y.S., Woo, S.H., Lee, K.H., Yi, J.Y., Lee, S.J., Choe, T.B., Lee, J.H., An, S., *et al.* (2011). TXNIP potentiates Redd1-induced mTOR suppression through stabilization of Redd1. *Oncogene* 30, 3792-3801.
- Joguchi, A., Otsuka, I., Minagawa, S., Suzuki, T., Fujii, M., and Ayusawa, D. (2002). Overexpression of VDUP1 mRNA sensitizes HeLa cells to paraquat. *Biochem Biophys Res Commun* 293, 293-297.
- Jones, D.P. (2006). Disruption of mitochondrial redox circuitry in oxidative stress. *Chem Biol Interact* 163, 38-53.
- Jones, D.P. (2008). Radical-free biology of oxidative stress. *Am J Physiol Cell Physiol* 295, C849-868.

- Junn, E., Han, S.H., Im, J.Y., Yang, Y., Cho, E.W., Um, H.D., Kim, D.K., Lee, K.W., Han, P.L., Rhee, S.G., *et al.* (2000). Vitamin D3 up-regulated protein 1 mediates oxidative stress via suppressing the thioredoxin function. *J Immunol* 164, 6287-6295.
- Kaadige, M.R., Looper, R.E., Kamalanaadhan, S., and Ayer, D.E. (2009). Glutamine-dependent anapleurosis dictates glucose uptake and cell growth by regulating MondoA transcriptional activity. *Proc Natl Acad Sci U S A* 106, 14878-14883.
- Kelly, S.A., Nehrenberg, D.L., Hua, K., Garland, T., Jr., and Pomp, D. (2012). Functional genomic architecture of predisposition to voluntary exercise in mice: expression QTL in the brain. *Genetics* 191, 643-654.
- Kelly, S.A., Nehrenberg, D.L., Peirce, J.L., Hua, K., Steffy, B.M., Wiltshire, T., Pardo-Manuel de Villena, F., Garland, T., Jr., and Pomp, D. (2010). Genetic architecture of voluntary exercise in an advanced intercross line of mice. *Physiol Genomics* 42, 190-200.
- Khabar, K.S., Bakheet, T., and Williams, B.R. (2005). AU-rich transient response transcripts in the human genome: expressed sequence tag clustering and gene discovery approach. *Genomics* 85, 165-175.
- Kil, I.S., and Park, J.W. (2005). Regulation of mitochondrial NADP⁺-dependent isocitrate dehydrogenase activity by glutathionylation. *J Biol Chem* 280, 10846-10854.
- Kim, J.Y., Koves, T.R., Yu, G.S., Gulick, T., Cortright, R.N., Dohm, G.L., and Muoio, D.M. (2002). Evidence of a malonyl-CoA-insensitive carnitine palmitoyltransferase I activity in red skeletal muscle. *Am J Physiol Endocrinol Metab* 282, E1014-1022.
- Kim, K.Y., Shin, S.M., Kim, J.K., Paik, S.G., Yang, Y., and Choi, I. (2004). Heat shock factor regulates VDUP1 gene expression. *Biochem Biophys Res Commun* 315, 369-375.
- Kim, M.S., Song, J., and Park, C. (2009). Determining protein stability in cell lysates by pulse proteolysis and Western blotting. *Protein Sci* 18, 1051-1059.
- Klaman, L.D., Boss, O., Peroni, O.D., Kim, J.K., Martino, J.L., Zabolotny, J.M., Moghal, N., Lubkin, M., Kim, Y.B., Sharpe, A.H., *et al.* (2000). Increased energy expenditure, decreased adiposity, and tissue-specific insulin sensitivity in protein-tyrosine phosphatase 1B-deficient mice. *Mol Cell Biol* 20, 5479-5489.
- Koeberl, D.D., Young, S.P., Gregersen, N.S., Vockley, J., Smith, W.E., Benjamin, D.K., Jr., An, Y., Weavil, S.D., Chaing, S.H., Bali, D., *et al.* (2003). Rare disorders of metabolism with elevated butyryl- and isobutyryl-carnitine detected by tandem mass spectrometry newborn screening. *Pediatr Res* 54, 219-223.

- Koehler, C.M., Beverly, K.N., and Leverich, E.P. (2006). Redox pathways of the mitochondrion. *Antioxid Redox Signal* 8, 813-822.
- Kovacic, P., and Somanathan, R. (2012). Redox processes in neurodegenerative disease involving reactive oxygen species. *Curr Neuropharmacol* 10, 289-302.
- Koves, T.R., Li, P., An, J., Akimoto, T., Slentz, D., Ilkayeva, O., Dohm, G.L., Yan, Z., Newgard, C.B., and Muoio, D.M. (2005). Peroxisome proliferator-activated receptor-gamma co-activator 1alpha-mediated metabolic remodeling of skeletal myocytes mimics exercise training and reverses lipid-induced mitochondrial inefficiency. *J Biol Chem* 280, 33588-33598.
- Koves, T.R., Ussher, J.R., Noland, R.C., Slentz, D., Mosedale, M., Ilkayeva, O., Bain, J., Stevens, R., Dyck, J.R., Newgard, C.B., *et al.* (2008). Mitochondrial overload and incomplete fatty acid oxidation contribute to skeletal muscle insulin resistance. *Cell Metab* 7, 45-56.
- Kumar, M., Gromiha, M.M., and Raghava, G.P. (2011). SVM based prediction of RNA-binding proteins using binding residues and evolutionary information. *J Mol Recognit* 24, 303-313.
- Kuznetsov, A.V., Tiivel, T., Sikk, P., Kaambre, T., Kay, L., Daneshrad, Z., Rossi, A., Kadaja, L., Peet, N., Seppet, E., *et al.* (1996). Striking differences between the kinetics of regulation of respiration by ADP in slow-twitch and fast-twitch muscles in vivo. *Eur J Biochem* 241, 909-915.
- Kuznetsov, A.V., Veksler, V., Gellerich, F.N., Saks, V., Margreiter, R., and Kunz, W.S. (2008). Analysis of mitochondrial function in situ in permeabilized muscle fibers, tissues and cells. *Nat Protoc* 3, 965-976.
- Lane, T., Flam, B., Lockey, R., and Kolliputi, N. (2013). TXNIP shuttling: missing link between oxidative stress and inflammasome activation. *Front Physiol* 4, 50.
- Lee, S.R., Yang, K.S., Kwon, J., Lee, C., Jeong, W., and Rhee, S.G. (2002). Reversible inactivation of the tumor suppressor PTEN by H₂O₂. *J Biol Chem* 277, 20336-20342.
- Lehninger, A.L., Sudduth, H.C., and Wise, J.B. (1960). D-beta-Hydroxybutyric dehydrogenase of mitochondria. *J Biol Chem* 235, 2450-2455.
- Lerner, A.G., Upton, J.P., Praveen, P.V., Ghosh, R., Nakagawa, Y., Igarria, A., Shen, S., Nguyen, V., Backes, B.J., Heiman, M., *et al.* (2012). IRE1alpha induces thioredoxin-

interacting protein to activate the NLRP3 inflammasome and promote programmed cell death under irremediable ER stress. *Cell Metab* 16, 250-264.

Leslie, N.R., Bennett, D., Lindsay, Y.E., Stewart, H., Gray, A., and Downes, C.P. (2003). Redox regulation of PI 3-kinase signalling via inactivation of PTEN. *Embo J* 22, 5501-5510.

Li, J.M., and Shah, A.M. (2002). Intracellular localization and preassembly of the NADPH oxidase complex in cultured endothelial cells. *J Biol Chem* 277, 19952-19960.

Li, Y., Zhu, H., Kuppusamy, P., Roubaud, V., Zweier, J.L., and Trush, M.A. (1998). Validation of lucigenin (bis-N-methylacridinium) as a chemilumigenic probe for detecting superoxide anion radical production by enzymatic and cellular systems. *J Biol Chem* 273, 2015-2023.

Lin, C.H., MacGurn, J.A., Chu, T., Stefan, C.J., and Emr, S.D. (2008). Arrestin-related ubiquitin-ligase adaptors regulate endocytosis and protein turnover at the cell surface. *Cell* 135, 714-725.

Lippolis, R., Altamura, N., and Landriscina, C. (1988). Ketone-body metabolism in hyperthyroid rats: reduced activity of D-3-hydroxybutyrate dehydrogenase in both liver and heart and of succinyl-coenzyme A: 3-oxoacid coenzyme A-transferase in heart. *Arch Biochem Biophys* 260, 94-101.

Lodish, H.F. (2003). *Molecular cell biology*, 5th edn (New York, W.H. Freeman and Company).

Loh, K., Deng, H., Fukushima, A., Cai, X., Boivin, B., Galic, S., Bruce, C., Shields, B.J., Skiba, B., Ooms, L.M., *et al.* (2009). Reactive oxygen species enhance insulin sensitivity. *Cell Metab* 10, 260-272.

Lombardo, Y.B., Serdikoff, C., Thamocharan, M., Paul, H.S., and Adibi, S.A. (1999). Inverse alterations of BCKA dehydrogenase activity in cardiac and skeletal muscles of diabetic rats. *Am J Physiol* 277, E685-692.

Luan, B., Zhao, J., Wu, H., Duan, B., Shu, G., Wang, X., Li, D., Jia, W., Kang, J., and Pei, G. (2009). Deficiency of a beta-arrestin-2 signal complex contributes to insulin resistance. *Nature* 457, 1146-1149.

Madamanchi, N.R., and Runge, M.S. (2013). Redox signaling in cardiovascular health and disease. *Free Radic Biol Med* 61C, 473-501.

- Mahadev, K., Motoshima, H., Wu, X., Ruddy, J.M., Arnold, R.S., Cheng, G., Lambeth, J.D., and Goldstein, B.J. (2004). The NAD(P)H oxidase homolog Nox4 modulates insulin-stimulated generation of H₂O₂ and plays an integral role in insulin signal transduction. *Mol Cell Biol* 24, 1844-1854.
- Mailloux, R.J., and Harper, M.E. (2010). Glucose regulates enzymatic sources of mitochondrial NADPH in skeletal muscle cells; a novel role for glucose-6-phosphate dehydrogenase. *Faseb J* 24, 2495-2506.
- Masson, E., Koren, S., Razik, F., Goldberg, H., Kwan, E.P., Sheu, L., Gaisano, H.Y., and Fantus, I.G. (2009). High beta-cell mass prevents streptozotocin-induced diabetes in thioredoxin-interacting protein-deficient mice. *Am J Physiol Endocrinol Metab* 296, E1251-1261.
- Masutani, H., Yoshihara, E., Masaki, S., Chen, Z., and Yodoi, J. (2012). Thioredoxin binding protein (TBP)-2/Txnip and alpha-arrestin proteins in cancer and diabetes mellitus. *J Clin Biochem Nutr* 50, 23-34.
- May, J.M., and de Haen, C. (1979). Insulin-stimulated intracellular hydrogen peroxide production in rat epididymal fat cells. *J Biol Chem* 254, 2214-2220.
- McGarry, J.D., Leatherman, G.F., and Foster, D.W. (1978). Carnitine palmitoyltransferase I. The site of inhibition of hepatic fatty acid oxidation by malonyl-CoA. *J Biol Chem* 253, 4128-4136.
- McKenna, M.C., Waagepetersen, H.S., Schousboe, A., and Sonnewald, U. (2006). Neuronal and astrocytic shuttle mechanisms for cytosolic-mitochondrial transfer of reducing equivalents: current evidence and pharmacological tools. *Biochem Pharmacol* 71, 399-407.
- Melov, S. (2000). Mitochondrial oxidative stress. Physiologic consequences and potential for a role in aging. *Ann N Y Acad Sci* 908, 219-225.
- Millington, D.S., Kodo, N., Norwood, D.L., and Roe, C.R. (1990). Tandem mass spectrometry: a new method for acylcarnitine profiling with potential for neonatal screening for inborn errors of metabolism. *J Inherit Metab Dis* 13, 321-324.
- Minn, A.H., Hafele, C., and Shalev, A. (2005a). Thioredoxin-interacting protein is stimulated by glucose through a carbohydrate response element and induces beta-cell apoptosis. *Endocrinology* 146, 2397-2405.

- Minn, A.H., Pise-Masison, C.A., Radonovich, M., Brady, J.N., Wang, P., Kendzioriski, C., and Shalev, A. (2005b). Gene expression profiling in INS-1 cells overexpressing thioredoxin-interacting protein. *Biochem Biophys Res Commun* 336, 770-778.
- Morel, Y., and Barouki, R. (1999). Repression of gene expression by oxidative stress. *Biochem J* 342 Pt 3, 481-496.
- Morino, K., Petersen, K.F., and Shulman, G.I. (2006). Molecular mechanisms of insulin resistance in humans and their potential links with mitochondrial dysfunction. *Diabetes* 55 Suppl 2, S9-S15.
- Mukherjee, S.P., Lane, R.H., and Lynn, W.S. (1978). Endogenous hydrogen peroxide and peroxidative metabolism in adipocytes in response to insulin and sulfhydryl reagents. *Biochem Pharmacol* 27, 2589-2594.
- Muoio, D.M. (2007). TXNIP links redox circuitry to glucose control. *Cell Metab* 5, 412-414.
- Muoio, D.M., Dohm, G.L., Tapscott, E.B., and Coleman, R.A. (1999). Leptin opposes insulin's effects on fatty acid partitioning in muscles isolated from obese ob/ob mice. *Am J Physiol* 276, E913-921.
- Muoio, D.M., and Neufer, P.D. (2012). Lipid-induced mitochondrial stress and insulin action in muscle. *Cell Metab* 15, 595-605.
- Muoio, D.M., and Newgard, C.B. (2006). Obesity-related derangements in metabolic regulation. *Annu Rev Biochem* 75, 367-401.
- Muoio, D.M., and Newgard, C.B. (2008). Mechanisms of disease: molecular and metabolic mechanisms of insulin resistance and beta-cell failure in type 2 diabetes. *Nat Rev Mol Cell Biol* 9, 193-205.
- Muoio, D.M., Noland, R.C., Kovalik, J.P., Seiler, S.E., Davies, M.N., DeBalsi, K.L., Ilkayeva, O.R., Stevens, R.D., Kheterpal, I., Zhang, J., *et al.* (2012). Muscle-specific deletion of carnitine acetyltransferase compromises glucose tolerance and metabolic flexibility. *Cell Metab* 15, 764-777.
- Nabhan, J.F., Pan, H., and Lu, Q. (2010). Arrestin domain-containing protein 3 recruits the NEDD4 E3 ligase to mediate ubiquitination of the beta2-adrenergic receptor. *EMBO Rep* 11, 605-611.

- Ngala, R.A., O'Dowd, J., Wang, S.J., Agarwal, A., Stocker, C., Cawthorne, M.A., and Arch, J.R. (2008). Metabolic responses to BRL37344 and clenbuterol in soleus muscle and C2C12 cells via different atypical pharmacologies and beta2-adrenoceptor mechanisms. *Br J Pharmacol* 155, 395-406.
- Ngala, R.A., O'Dowd, J., Wang, S.J., Stocker, C., Cawthorne, M.A., and Arch, J.R. (2009). Beta2-adrenoceptors and non-beta-adrenoceptors mediate effects of BRL37344 and clenbuterol on glucose uptake in soleus muscle: studies using knockout mice. *Br J Pharmacol* 158, 1676-1682.
- Ngala, R.A., O'Dowd, J.F., Stocker, C.J., Cawthorne, M.A., and Arch, J.R. (2013). beta-adrenoceptor agonists can both stimulate and inhibit glucose uptake in mouse soleus muscle through ligand-directed signalling. *Naunyn Schmiedebergs Arch Pharmacol*.
- Nishinaka, Y., Masutani, H., Oka, S., Matsuo, Y., Yamaguchi, Y., Nishio, K., Ishii, Y., and Yodoi, J. (2004). Importin alpha1 (Rch1) mediates nuclear translocation of thioredoxin-binding protein-2/vitamin D(3)-up-regulated protein 1. *J Biol Chem* 279, 37559-37565.
- Nishiyama, A., Masutani, H., Nakamura, H., Nishinaka, Y., and Yodoi, J. (2001). Redox regulation by thioredoxin and thioredoxin-binding proteins. *IUBMB Life* 52, 29-33.
- Nishiyama, A., Matsui, M., Iwata, S., Hirota, K., Masutani, H., Nakamura, H., Takagi, Y., Sono, H., Gon, Y., and Yodoi, J. (1999). Identification of thioredoxin-binding protein-2/vitamin D(3) up-regulated protein 1 as a negative regulator of thioredoxin function and expression. *J Biol Chem* 274, 21645-21650.
- Nivet-Antoine, V., Cottart, C.H., Lemarechal, H., Vamy, M., Margaille, I., Beaudoux, J.L., Bonnefont-Rousselot, D., and Borderie, D. (2010). trans-Resveratrol downregulates Txnip overexpression occurring during liver ischemia-reperfusion. *Biochimie* 92, 1766-1771.
- Nordberg, J., and Arner, E.S. (2001). Reactive oxygen species, antioxidants, and the mammalian thioredoxin system. *Free Radic Biol Med* 31, 1287-1312.
- Nulton-Persson, A.C., Starke, D.W., Mieyal, J.J., and Szweda, L.I. (2003). Reversible inactivation of alpha-ketoglutarate dehydrogenase in response to alterations in the mitochondrial glutathione status. *Biochemistry* 42, 4235-4242.
- Nulton-Persson, A.C., and Szweda, L.I. (2001). Modulation of mitochondrial function by hydrogen peroxide. *J Biol Chem* 276, 23357-23361.

- Odin, J.A., Huebert, R.C., Casciola-Rosen, L., LaRusso, N.F., and Rosen, A. (2001). Bcl-2-dependent oxidation of pyruvate dehydrogenase-E2, a primary biliary cirrhosis autoantigen, during apoptosis. *J Clin Invest* 108, 223-232.
- Oka, S., Liu, W., Masutani, H., Hirata, H., Shinkai, Y., Yamada, S., Yoshida, T., Nakamura, H., and Yodoi, J. (2006a). Impaired fatty acid utilization in thioredoxin binding protein-2 (TBP-2)-deficient mice: a unique animal model of Reye syndrome. *Faseb J* 20, 121-123.
- Oka, S., Liu, W., Yoshihara, E., Ahsan, M.K., Ramos, D.A., Son, A., Okuyama, H., Zhang, L., Masutani, H., Nakamura, H., *et al.* (2010). Thioredoxin binding protein-2 mediates metabolic adaptation in response to lipopolysaccharide in vivo. *Crit Care Med* 38, 2345-2351.
- Oka, S., Masutani, H., Liu, W., Horita, H., Wang, D., Kizaka-Kondoh, S., and Yodoi, J. (2006b). Thioredoxin-binding protein-2-like inducible membrane protein is a novel vitamin D3 and peroxisome proliferator-activated receptor (PPAR)gamma ligand target protein that regulates PPARgamma signaling. *Endocrinology* 147, 733-743.
- Oka, S., Yoshihara, E., Bizen-Abe, A., Liu, W., Watanabe, M., Yodoi, J., and Masutani, H. (2009). Thioredoxin binding protein-2/thioredoxin-interacting protein is a critical regulator of insulin secretion and peroxisome proliferator-activated receptor function. *Endocrinology* 150, 1225-1234.
- Osowski, C.M., Hara, T., O'Sullivan-Murphy, B., Kanekura, K., Lu, S., Hara, M., Ishigaki, S., Zhu, L.J., Hayashi, E., Hui, S.T., *et al.* (2012). Thioredoxin-interacting protein mediates ER stress-induced beta cell death through initiation of the inflammasome. *Cell Metab* 16, 265-273.
- Parikh, H., Carlsson, E., Chutkan, W.A., Johansson, L.E., Storgaard, H., Poulsen, P., Saxena, R., Ladd, C., Schulze, P.C., Mazzini, M.J., *et al.* (2007). TXNIP regulates peripheral glucose metabolism in humans. *PLoS Med* 4, e158.
- Park, C., and Marqusee, S. (2005). Pulse proteolysis: a simple method for quantitative determination of protein stability and ligand binding. *Nat Methods* 2, 207-212.
- Patwari, P., Chutkan, W.A., Cummings, K., Verstraeten, V.L., Lammerding, J., Schreiter, E.R., and Lee, R.T. (2009). Thioredoxin-independent regulation of metabolism by the alpha-arrestin proteins. *J Biol Chem* 284, 24996-25003.

- Patwari, P., Emilsson, V., Schadt, E.E., Chutkow, W.A., Lee, S., Marsili, A., Zhang, Y., Dobrin, R., Cohen, D.E., Larsen, P.R., *et al.* (2011). The arrestin domain-containing 3 protein regulates body mass and energy expenditure. *Cell Metab* 14, 671-683.
- Patwari, P., Higgins, L.J., Chutkow, W.A., Yoshioka, J., and Lee, R.T. (2006). The interaction of thioredoxin with Txnip. Evidence for formation of a mixed disulfide by disulfide exchange. *J Biol Chem* 281, 21884-21891.
- Patwari, P., and Lee, R.T. (2012). An expanded family of arrestins regulate metabolism. *Trends Endocrinol Metab* 23, 216-222.
- Pelicano, H., Xu, R.H., Du, M., Feng, L., Sasaki, R., Carew, J.S., Hu, Y., Ramdas, L., Hu, L., Keating, M.J., *et al.* (2006). Mitochondrial respiration defects in cancer cells cause activation of Akt survival pathway through a redox-mediated mechanism. *J Cell Biol* 175, 913-923.
- Perrone, L., Devi, T.S., Hosoya, K., Terasaki, T., and Singh, L.P. (2009). Thioredoxin interacting protein (TXNIP) induces inflammation through chromatin modification in retinal capillary endothelial cells under diabetic conditions. *J Cell Physiol* 221, 262-272.
- Perrone, L., Devi, T.S., Hosoya, K.I., Terasaki, T., and Singh, L.P. (2010). Inhibition of TXNIP expression in vivo blocks early pathologies of diabetic retinopathy. *Cell Death Dis* 1, e65.
- Perrone, L., Sbai, O., Nawroth, P.P., and Bierhaus, A. (2012). The Complexity of Sporadic Alzheimer's Disease Pathogenesis: The Role of RAGE as Therapeutic Target to Promote Neuroprotection by Inhibiting Neurovascular Dysfunction. *Int J Alzheimers Dis* 2012, 734956.
- Perry, C.G., Kane, D.A., Lin, C.T., Kozy, R., Cathey, B.L., Lark, D.S., Kane, C.L., Brophy, P.M., Gavin, T.P., Anderson, E.J., *et al.* (2011). Inhibiting myosin-ATPase reveals a dynamic range of mitochondrial respiratory control in skeletal muscle. *Biochem J* 437, 215-222.
- Petersen, K.F., and Shulman, G.I. (2002). Cellular mechanism of insulin resistance in skeletal muscle. *J R Soc Med* 95 *Suppl* 42, 8-13.
- Pieczenik, S.R., and Neustadt, J. (2007). Mitochondrial dysfunction and molecular pathways of disease. *Exp Mol Pathol* 83, 84-92.

- Polekhina, G., Ascher, D.B., Kok, S.F., Beckham, S., Wilce, M., and Waltham, M. (2013). Structure of the N-terminal domain of human thioredoxin-interacting protein. *Acta Crystallogr D Biol Crystallogr* 69, 333-344.
- Popolo, A., Autore, G., Pinto, A., and Marzocco, S. (2013). Oxidative stress in patients with cardiovascular disease and chronic renal failure. *Free Radic Res* 47, 346-356.
- Pospisilik, J.A., Knauf, C., Joza, N., Benit, P., Orthofer, M., Cani, P.D., Ebersberger, I., Nakashima, T., Sarao, R., Neely, G., *et al.* (2007). Targeted deletion of AIF decreases mitochondrial oxidative phosphorylation and protects from obesity and diabetes. *Cell* 131, 476-491.
- Pratley, R.E., and Weyer, C. (2001). The role of impaired early insulin secretion in the pathogenesis of Type II diabetes mellitus. *Diabetologia* 44, 929-945.
- Price, S.A., Gardiner, N.J., Duran-Jimenez, B., Zeef, L.A., Obrosova, I.G., and Tomlinson, D.R. (2006). Thioredoxin interacting protein is increased in sensory neurons in experimental diabetes. *Brain Res* 1116, 206-214.
- Quistorff, B., and Grunnet, N. (2011). The isoenzyme pattern of LDH does not play a physiological role; except perhaps during fast transitions in energy metabolism. *Aging (Albany NY)* 3, 457-460.
- Rani, S., Mehta, J.P., Barron, N., Doolan, P., Jeppesen, P.B., Clynes, M., and O'Driscoll, L. (2010). Decreasing Txnip mRNA and protein levels in pancreatic MIN6 cells reduces reactive oxygen species and restores glucose regulated insulin secretion. *Cell Physiol Biochem* 25, 667-674.
- Rauch, S., and Martin-Serrano, J. (2011). Multiple interactions between the ESCRT machinery and arrestin-related proteins: implications for PPXY-dependent budding. *J Virol* 85, 3546-3556.
- Reisch, A.S., and Elpeleg, O. (2007). Biochemical assays for mitochondrial activity: assays of TCA cycle enzymes and PDHc. *Methods Cell Biol* 80, 199-222.
- Rinaldo, P., Cowan, T.M., and Matern, D. (2008). Acylcarnitine profile analysis. *Genet Med* 10, 151-156.
- Ronnebaum, S.M., Ilkayeva, O., Burgess, S.C., Joseph, J.W., Lu, D., Stevens, R.D., Becker, T.C., Sherry, A.D., Newgard, C.B., and Jensen, M.V. (2006). A pyruvate cycling pathway involving cytosolic NADP-dependent isocitrate dehydrogenase regulates glucose-stimulated insulin secretion. *J Biol Chem* 281, 30593-30602.

Sadowska, A.M., Manuel, Y.K.B., and De Backer, W.A. (2007). Antioxidant and anti-inflammatory efficacy of NAC in the treatment of COPD: discordant in vitro and in vivo dose-effects: a review. *Pulm Pharmacol Ther* 20, 9-22.

Sakellariou, G.K., Vasilaki, A., Palomero, J., Kayani, A., Zibrik, L., McArdle, A., and Jackson, M.J. (2013). Studies of mitochondrial and nonmitochondrial sources implicate nicotinamide adenine dinucleotide phosphate oxidase(s) in the increased skeletal muscle superoxide generation that occurs during contractile activity. *Antioxid Redox Signal* 18, 603-621.

Saks, V.A., Belikova, Y.O., Kuznetsov, A.V., Khuchua, Z.A., Branishte, T.H., Semenovskiy, M.L., and Naumov, V.G. (1991). Phosphocreatine pathway for energy transport: ADP diffusion and cardiomyopathy. *Am J Physiol* 261, 30-38.

Saks, V.A., Khuchua, Z.A., Vasilyeva, E.V., Belikova, O., and Kuznetsov, A.V. (1994). Metabolic compartmentation and substrate channelling in muscle cells. Role of coupled creatine kinases in in vivo regulation of cellular respiration--a synthesis. *Mol Cell Biochem* 133-134, 155-192.

Saks, V.A., Kuznetsov, A.V., Khuchua, Z.A., Vasilyeva, E.V., Belikova, J.O., Kesvatera, T., and Tiivel, T. (1995). Control of cellular respiration in vivo by mitochondrial outer membrane and by creatine kinase. A new speculative hypothesis: possible involvement of mitochondrial-cytoskeleton interactions. *J Mol Cell Cardiol* 27, 625-645.

Saxena, G., Chen, J., and Shalev, A. (2010). Intracellular shuttling and mitochondrial function of thioredoxin-interacting protein. *J Biol Chem* 285, 3997-4005.

Schantz, P.G., Sjoberg, B., and Svedenhag, J. (1986). Malate-aspartate and alpha-glycerophosphate shuttle enzyme levels in human skeletal muscle: methodological considerations and effect of endurance training. *Acta Physiol Scand* 128, 397-407.

Schulze, P.C., De Keulenaer, G.W., Yoshioka, J., Kassik, K.A., and Lee, R.T. (2002). Vitamin D3-upregulated protein-1 (VDUP-1) regulates redox-dependent vascular smooth muscle cell proliferation through interaction with thioredoxin. *Circ Res* 91, 689-695.

Schulze, P.C., Yoshioka, J., Takahashi, T., He, Z., King, G.L., and Lee, R.T. (2004). Hyperglycemia promotes oxidative stress through inhibition of thioredoxin function by thioredoxin-interacting protein. *J Biol Chem* 279, 30369-30374.

Seay, D., Hook, B., Evans, K., and Wickens, M. (2006). A three-hybrid screen identifies mRNAs controlled by a regulatory protein. *Rna* 12, 1594-1600.

- Seo, J.H., Ahn, Y., Lee, S.R., Yeol Yeo, C., and Chung Hur, K. (2005). The major target of the endogenously generated reactive oxygen species in response to insulin stimulation is phosphatase and tensin homolog and not phosphoinositide-3 kinase (PI-3 kinase) in the PI-3 kinase/Akt pathway. *Mol Biol Cell* 16, 348-357.
- Serdikoff, C., and Adibi, S.A. (2001). Protein expressions of branched-chain keto acid dehydrogenase subunits are selectively and posttranscriptionally altered in liver and skeletal muscle of starved rats. *J Nutr* 131, 1682-1686.
- Shaked, M., Ketzinel-Gilad, M., Ariav, Y., Cerasi, E., Kaiser, N., and Leibowitz, G. (2009). Insulin counteracts glucotoxic effects by suppressing thioredoxin-interacting protein production in INS-1E beta cells and in *Psammomys obesus* pancreatic islets. *Diabetologia* 52, 636-644.
- Shea, F.F., Rowell, J.L., Li, Y., Chang, T.H., and Alvarez, C.E. (2012). Mammalian alpha arrestins link activated seven transmembrane receptors to Nedd4 family e3 ubiquitin ligases and interact with beta arrestins. *PLoS One* 7, e50557.
- Shenoy, S.K., and Lefkowitz, R.J. (2011). beta-Arrestin-mediated receptor trafficking and signal transduction. *Trends Pharmacol Sci* 32, 521-533.
- Sheth, S.S., Castellani, L.W., Chari, S., Wagg, C., Thippavong, C.K., Bodnar, J.S., Tontonoz, P., Attie, A.D., Lopaschuk, G.D., and Lusis, A.J. (2005). Thioredoxin-interacting protein deficiency disrupts the fasting-feeding metabolic transition. *J Lipid Res* 46, 123-134.
- Shim, H., Dolde, C., Lewis, B.C., Wu, C.S., Dang, G., Jungmann, R.A., Dalla-Favera, R., and Dang, C.V. (1997). c-Myc transactivation of LDH-A: implications for tumor metabolism and growth. *Proc Natl Acad Sci U S A* 94, 6658-6663.
- Shin, D., Jeon, J.H., Jeong, M., Suh, H.W., Kim, S., Kim, H.C., Moon, O.S., Kim, Y.S., Chung, J.W., Yoon, S.R., *et al.* (2008). VDUP1 mediates nuclear export of HIF1alpha via CRM1-dependent pathway. *Biochim Biophys Acta* 1783, 838-848.
- Soeters, M.R., Serlie, M.J., Sauerwein, H.P., Duran, M., Ruiten, J.P., Kulik, W., Ackermans, M.T., Minkler, P.E., Hoppel, C.L., Wanders, R.J., *et al.* (2012). Characterization of D-3-hydroxybutyrylcarnitine (ketocarnitine): an identified ketosis-induced metabolite. *Metabolism* 61, 966-973.
- Sohn, H.Y., Keller, M., Gloe, T., Crause, P., and Pohl, U. (2000). Pitfalls of using lucigenin in endothelial cells: implications for NAD(P)H dependent superoxide formation. *Free Radic Res* 32, 265-272.

- Spindel, O.N., World, C., and Berk, B.C. (2012). Thioredoxin interacting protein: redox dependent and independent regulatory mechanisms. *Antioxid Redox Signal* 16, 587-596.
- Srere, P.A. (1969). Citrate Synthase. *Methods in Enzymology* 13, 3-11.
- Stanton, R.C. (2012). Glucose-6-phosphate dehydrogenase, NADPH, and cell survival. *IUBMB Life* 64, 362-369.
- Stoltzman, C.A., Peterson, C.W., Breen, K.T., Muoio, D.M., Billin, A.N., and Ayer, D.E. (2008). Glucose sensing by MondoA:Milx complexes: a role for hexokinases and direct regulation of thioredoxin-interacting protein expression. *Proc Natl Acad Sci U S A* 105, 6912-6917.
- Suh, H.W., Yun, S., Song, H., Jung, H., Park, Y.J., Kim, T.D., Yoon, S.R., and Choi, I. (2013). TXNIP interacts with hEcd to increase p53 stability and activity. *Biochem Biophys Res Commun*.
- Summermatter, S., Santos, G., Perez-Schindler, J., and Handschin, C. (2013). Skeletal muscle PGC-1alpha controls whole-body lactate homeostasis through estrogen-related receptor alpha-dependent activation of LDH B and repression of LDH A. *Proc Natl Acad Sci U S A* 110, 8738-8743.
- Takahashi, Y., Nagata, T., Ishii, Y., Ikarashi, M., Ishikawa, K., and Asai, S. (2002). Up-regulation of vitamin D3 up-regulated protein 1 gene in response to 5-fluorouracil in colon carcinoma SW620. *Oncol Rep* 9, 75-79.
- Tan, S.M., Zhang, Y., Cox, A.J., Kelly, D.J., and Qi, W. (2011). Tranilast attenuates the up-regulation of thioredoxin-interacting protein and oxidative stress in an experimental model of diabetic nephropathy. *Nephrol Dial Transplant* 26, 100-110.
- Taylor, E.R., Hurrell, F., Shannon, R.J., Lin, T.K., Hirst, J., and Murphy, M.P. (2003). Reversible glutathionylation of complex I increases mitochondrial superoxide formation. *J Biol Chem* 278, 19603-19610.
- Thannickal, V.J., and Fanburg, B.L. (2000). Reactive oxygen species in cell signaling. *Am J Physiol Lung Cell Mol Physiol* 279, L1005-1028.
- Tomoda, K., Kubota, Y., and Kato, J. (1999). Degradation of the cyclin-dependent-kinase inhibitor p27Kip1 is instigated by Jab1. *Nature* 398, 160-165.

- Tonkonogi, M., Fernstrom, M., Walsh, B., Ji, L.L., Rooyackers, O., Hammarqvist, F., Wernerman, J., and Sahlin, K. (2003). Reduced oxidative power but unchanged antioxidative capacity in skeletal muscle from aged humans. *Pflugers Arch* 446, 261-269.
- Tonks, N.K. (2003). PTP1B: from the sidelines to the front lines! *FEBS Lett* 546, 140-148.
- Townsend, D.M. (2007). S-glutathionylation: indicator of cell stress and regulator of the unfolded protein response. *Mol Interv* 7, 313-324.
- Townsend, D.M., Findlay, V.J., Fazilev, F., Ogle, M., Fraser, J., Saavedra, J.E., Ji, X., Keefer, L.K., and Tew, K.D. (2006). A glutathione S-transferase pi-activated prodrug causes kinase activation concurrent with S-glutathionylation of proteins. *Mol Pharmacol* 69, 501-508.
- Traber, J., Suter, M., Walter, P., and Richter, C. (1992). In vivo modulation of total and mitochondrial glutathione in rat liver. Depletion by phorone and rescue by N-acetylcysteine. *Biochem Pharmacol* 43, 961-964.
- Usui, I., Imamura, T., Huang, J., Satoh, H., Shenoy, S.K., Lefkowitz, R.J., Hupfeld, C.J., and Olefsky, J.M. (2004). beta-arrestin-1 competitively inhibits insulin-induced ubiquitination and degradation of insulin receptor substrate 1. *Mol Cell Biol* 24, 8929-8937.
- Valko, M., Leibfritz, D., Moncol, J., Cronin, M.T., Mazur, M., and Telser, J. (2007). Free radicals and antioxidants in normal physiological functions and human disease. *Int J Biochem Cell Biol* 39, 44-84.
- van Greevenbroek, M.M., Vermeulen, V.M., Feskens, E.J., Evelo, C.T., Kruijshoop, M., Hoebee, B., van der Kallen, C.J., and de Bruin, T.W. (2007). Genetic variation in thioredoxin interacting protein (TXNIP) is associated with hypertriglyceridaemia and blood pressure in diabetes mellitus. *Diabet Med* 24, 498-504.
- Veksler, V.I., Kuznetsov, A.V., Sharov, V.G., Kapelko, V.I., and Saks, V.A. (1987). Mitochondrial respiratory parameters in cardiac tissue: a novel method of assessment by using saponin-skinned fibers. *Biochim Biophys Acta* 892, 191-196.
- Walsh, B., Tonkonogi, M., Soderlund, K., Hultman, E., Saks, V., and Sahlin, K. (2001). The role of phosphorylcreatine and creatine in the regulation of mitochondrial respiration in human skeletal muscle. *J Physiol* 537, 971-978.

- Wamelink, M.M., Struys, E.A., and Jakobs, C. (2008). The biochemistry, metabolism and inherited defects of the pentose phosphate pathway: a review. *J Inherit Metab Dis* 31, 703-717.
- Wang, H.J., Pan, Y.X., Wang, W.Z., Zucker, I.H., and Wang, W. (2009). NADPH oxidase-derived reactive oxygen species in skeletal muscle modulates the exercise pressor reflex. *J Appl Physiol* 107, 450-459.
- Wang, X., Gargalovic, P., Wong, J., Gu, J.L., Wu, X., Qi, H., Wen, P., Xi, L., Tan, B., Gogliotti, R., *et al.* (2004). Hyplip2, a new gene for combined hyperlipidemia and increased atherosclerosis. *Arterioscler Thromb Vasc Biol* 24, 1928-1934.
- Wang, Y., De Keulenaer, G.W., and Lee, R.T. (2002). Vitamin D(3)-up-regulated protein-1 is a stress-responsive gene that regulates cardiomyocyte viability through interaction with thioredoxin. *J Biol Chem* 277, 26496-26500.
- Wang, Z., Rong, Y.P., Malone, M.H., Davis, M.C., Zhong, F., and Distelhorst, C.W. (2006). Thioredoxin-interacting protein (txnip) is a glucocorticoid-regulated primary response gene involved in mediating glucocorticoid-induced apoptosis. *Oncogene* 25, 1903-1913.
- Wolterbeek, H.T., and van der Meer, A.J. (2005). Optimization, application, and interpretation of lactate dehydrogenase measurements in microwell determination of cell number and toxicity. *Assay Drug Dev Technol* 3, 675-682.
- World, C., Spindel, O.N., and Berk, B.C. (2011). Thioredoxin-interacting protein mediates TRX1 translocation to the plasma membrane in response to tumor necrosis factor-alpha: a key mechanism for vascular endothelial growth factor receptor-2 transactivation by reactive oxygen species. *Arterioscler Thromb Vasc Biol* 31, 1890-1897.
- Wu, N., Zheng, B., Shaywitz, A., Dagon, Y., Tower, C., Bellinger, G., Shen, C.H., Wen, J., Asara, J., McGraw, T.E., *et al.* (2013). AMPK-dependent degradation of TXNIP upon energy stress leads to enhanced glucose uptake via GLUT1. *Mol Cell* 49, 1167-1175.
- Wu, X., Zhu, L., Zilbering, A., Mahadev, K., Motoshima, H., Yao, J., and Goldstein, B.J. (2005). Hyperglycemia potentiates H(2)O(2) production in adipocytes and enhances insulin signal transduction: potential role for oxidative inhibition of thiol-sensitive protein-tyrosine phosphatases. *Antioxid Redox Signal* 7, 526-537.
- Xu, W., Ngo, L., Perez, G., Dokmanovic, M., and Marks, P.A. (2006). Intrinsic apoptotic and thioredoxin pathways in human prostate cancer cell response to histone deacetylase inhibitor. *Proc Natl Acad Sci U S A* 103, 15540-15545.

- Yamaguchi, F., Takata, M., Kamitori, K., Nonaka, M., Dong, Y., Sui, L., and Tokuda, M. (2008). Rare sugar D-allose induces specific up-regulation of TXNIP and subsequent G1 cell cycle arrest in hepatocellular carcinoma cells by stabilization of p27kip1. *Int J Oncol* 32, 377-385.
- Yamanaka, H., Maehira, F., Oshiro, M., Asato, T., Yanagawa, Y., Takei, H., and Nakashima, Y. (2000). A possible interaction of thioredoxin with VDUP1 in HeLa cells detected in a yeast two-hybrid system. *Biochem Biophys Res Commun* 271, 796-800.
- Yamawaki, H., Pan, S., Lee, R.T., and Berk, B.C. (2005). Fluid shear stress inhibits vascular inflammation by decreasing thioredoxin-interacting protein in endothelial cells. *J Clin Invest* 115, 733-738.
- Yang, S., Madyastha, P., Bingel, S., Ries, W., and Key, L. (2001). A new superoxide-generating oxidase in murine osteoclasts. *J Biol Chem* 276, 5452-5458.
- Yarian, C.S., Toroser, D., and Sohal, R.S. (2006). Aconitase is the main functional target of aging in the citric acid cycle of kidney mitochondria from mice. *Mech Ageing Dev* 127, 79-84.
- Yoshihara, E., Fujimoto, S., Inagaki, N., Okawa, K., Masaki, S., Yodoi, J., and Masutani, H. (2010). Disruption of TBP-2 ameliorates insulin sensitivity and secretion without affecting obesity. *Nat Commun* 1, 127.
- Yoshioka, J., Chutkow, W.A., Lee, S., Kim, J.B., Yan, J., Tian, R., Lindsey, M.L., Feener, E.P., Seidman, C.E., Seidman, J.G., *et al.* (2012). Deletion of thioredoxin-interacting protein in mice impairs mitochondrial function but protects the myocardium from ischemia-reperfusion injury. *J Clin Invest* 122, 267-279.
- Yoshioka, J., Imahashi, K., Gabel, S.A., Chutkow, W.A., Burds, A.A., Gannon, J., Schulze, P.C., MacGillivray, C., London, R.E., Murphy, E., *et al.* (2007). Targeted deletion of thioredoxin-interacting protein regulates cardiac dysfunction in response to pressure overload. *Circ Res* 101, 1328-1338.
- Yu, C.X., Li, S., and Whorton, A.R. (2005). Redox regulation of PTEN by S-nitrosothiols. *Mol Pharmacol* 68, 847-854.
- Yu, F.X., Chai, T.F., He, H., Hagen, T., and Luo, Y. (2010). Thioredoxin-interacting protein (Txnip) gene expression: sensing oxidative phosphorylation status and glycolytic rate. *J Biol Chem* 285, 25822-25830.

- Yu, F.X., Goh, S.R., Dai, R.P., and Luo, Y. (2009). Adenosine-containing molecules amplify glucose signaling and enhance txnip expression. *Mol Endocrinol* 23, 932-942.
- Zhang, P., Wang, C., Gao, K., Wang, D., Mao, J., An, J., Xu, C., Wu, D., Yu, H., Liu, J.O., *et al.* (2010). The ubiquitin ligase itch regulates apoptosis by targeting thioredoxin-interacting protein for ubiquitin-dependent degradation. *J Biol Chem* 285, 8869-8879.
- Zhao, J., and Pei, G. (2013). Arrestins in metabolic regulation. *Prog Mol Biol Transl Sci* 118, 413-427.
- Zhou, R., Tardivel, A., Thorens, B., Choi, I., and Tschopp, J. (2010). Thioredoxin-interacting protein links oxidative stress to inflammasome activation. *Nat Immunol* 11, 136-140.
- Zhou, R., Yazdi, A.S., Menu, P., and Tschopp, J. (2011). A role for mitochondria in NLRP3 inflammasome activation. *Nature* 469, 221-225.
- Zhuang, L.N., Hu, W.X., Xin, S.M., Zhao, J., and Pei, G. (2011a). Beta-arrestin-1 protein represses adipogenesis and inflammatory responses through its interaction with peroxisome proliferator-activated receptor-gamma (PPARgamma). *J Biol Chem* 286, 28403-28413.
- Zhuang, L.N., Hu, W.X., Zhang, M.L., Xin, S.M., Jia, W.P., Zhao, J., and Pei, G. (2011b). Beta-arrestin-1 protein represses diet-induced obesity. *J Biol Chem* 286, 28396-28402.
- Zhuo de, X., Niu, X.H., Chen, Y.C., Xin, D.Q., Guo, Y.L., and Mao, Z.B. (2010). Vitamin D3 up-regulated protein 1(VDUP1) is regulated by FOXO3A and miR-17-5p at the transcriptional and post-transcriptional levels, respectively, in senescent fibroblasts. *J Biol Chem* 285, 31491-31501.

Biography

Karen Lynn DeBalsi

Born to Raffaele and Cecilia DeBalsi on November 1, 1966 in New Bedford, MA.

Education:

- Duke University, Durham, NC, August 2006 to September 2013.
 - Doctor of Philosophy in Pharmacology with a Certificate in Cell & Molecular Biology
- Bridgewater State College, Bridgewater, MA, January 2006.
 - Bachelor of Science in Biology and Chemistry, summa cum laude with departmental honors
 - Concentrations: Molecular Biology and Biochemistry
- Boston University, Boston, MA, January 1998.
 - Master of Science in Occupational Therapy
- Quincy College, Quincy, MA, June 1994.
 - Bachelor Certificate in Business Administration, with high honors
 - Concentrations: Management and Marketing
- Boston University, Boston, MA, May 1988.
 - Bachelor of Arts in Psychology, cum laude

Publications:

- **DeBalsi KL**, Wong KE, Koves TR, Slentz DH, Seiler SE, Wittmann AH, Ilkayeva OR, Stevens RD, Perry CGR, Gilliam LA, Hui ST, Szweda L, Neuffer, PD, Muoio DM. Targeted metabolomics connects TXNIP to adaptive fuel selection and regulation of specific mitochondrial oxidoreductase enzymes in skeletal muscle. In revision at *J Biol Chem* as of September 2013.
- Seiler SE, Martin O, Noland RC, Slentz DH, **DeBalsi KL**, Ilkayeva OR, An J, Newgard CB, Koves TR, Muoio DM. Obesity and lipid exposure inhibit carnitine acetyltransferase activity. Submitted to *J Lipid Res* in August 2013.
- Seiler SE, Koves TR, Gooding J, Wong KE, **DeBalsi KL**, Davies MV, Stevens RD, Ilkayeva OR, Muoio DM. Carnitine acetyltransferase offsets energy stress and delays muscle fatigue during strenuous exercise. In preparation.

- Koves TR, Sparks LM, Kovalik JP, Mosedale M, Arumugam R, **DeBalsi KL**, Everingham K, Thorne L, Phielix E, Meex RC, Kien CL, Hesselink MK, Schrauwen P, Muoio DM. (2013). PPAR γ coactivator-1 α contributes to exercise-induced regulation of intramuscular lipid droplet programming in mice and humans. *J Lipid Res.* 54: 522-534.
- Muoio DM*, Noland RC*, Kovalik J-P, Seiler SE, Davies MN, **DeBalsi KL**, Ilkayeva OR, Stevens RD, Kheterpal I, Zhang J, Kraus W, Koves TR, Mynatt RL. (2012). Muscle-specific deficiency of carnitine acetyltransferase compromises glucose tolerance and metabolic flexibility. *Cell Metab.* 15: 764-777. *Equal work.
- Lum H, Koves TR, **DeBalsi KL**, Stevens R, Muoio DM. Alterations in whole body and mitochondrial fuel metabolism in mice with reduced manganese superoxide dismutase (SOD2). In preparation.

Honors and Awards:

- Duke University:
 - Keystone Symposia on Type 2 Diabetes, Insulin Resistance and Metabolic Dysfunction and Obesity, Scholarship for conference assistant, 2011.
 - Department of Pharmacology and Cancer Biology Fitzgerald Scholar for outstanding poster, DUMC, Department of Pharmacology and Cancer Biology Annual Retreat, 2009.
- Bridgewater State College:
 - Dr. William J. Wall Memorial Award in Biological Sciences, 2004.
 - $\beta\beta\beta$, National Biology Honors Society, 2004-2006.
 - The Northeastern Section of the American Chemical Society Grants-in-Aid Program for Undergraduate Researchers, 2004.
 - The Bridgewater State College Honors Program, Departmental Honors, 2003-2004 and 2004-2005.
 - The Cottrell College Science Award, sponsored by the Research Corporation, Summer 2003.
 - The Adrian Tinsley Program for Undergraduate Research, Awards/Semester Grants: Fall 2001, Spring 2002, Fall 2002, Fall 2003, Spring 2004, and Summer 2004.
 - Dean's List, 2001-2002.

- Boston University:
 - Dean's List, 1986-1988.
 - Psi Chi, National Psychology Honors Society, Boston University, 1987-1988.